In presenting the dissertation as a partial fulfillment of the requirements for an advanced degree from the Georgia Institute of Technology, I agree that the Library of the Institute shall make it available for inspection and circulation in accordance with its regulations governing materials of this type. I agree that permission to copy from, or to publish from, this dissertation may be granted by the professor under whose direction it was written, or, in his absence, by the Dean of the Graduate Division when such copying or publication is solely for scholarly purposes and does not involve potential financial gain. It is understood that any copying from, or publication of, this dissertation which involves potential financial gain will not be allowed without written permission.

7/25/68

AN ANALYTICAL STUDY OF THE INTERIOR BALLISTICS PROBLEM, INCLUDING MOVEMENT OF SOLIDS AND WALL HEAT TRANSFER

A THESIS

Presented to

The Faculty of the Division of Graduate

Studies and Research

by

Pradip Saha

In Partial Fulfillment

of the Requirements for the Degree

Master of Science in Mechanical Engineering

Georgia Institute of Technology

September, 1971

AN ANALYTICAL STUDY OF THE INTERIOR BALLISTICS PROBLEM, INCLUDING MOVEMENT OF SOLIDS AND WALL HEAT TRANSFER

Approved:

_____

Chairman

_____

_____

Date approved by Chairman Aug. 23 71

ACKNOWLEDGMENTS

The author is deeply indebted to his faculty advisor, Dr. S. V. Shelton, for suggesting the problem and for continuous guidance and encouragement without which this work could not be finished.

It gives the author a great pleasure to thank Drs. C. W. Gorton and A. E. Bergles for their sincere interest and constructive suggestions in course of reviewing this work. The comments made by Dr. P. V. Desai on the boundary layer analysis are also appreciated.

The author is grateful to the U. S. Air Force for financial aid and a few experimental data of great help.

Many other persons, too numerous to list, helped the author both directly and indirectly during the period of execution of this work. Special thanks are to Mr. P. K. Raut for his help in various stages of computer programming.

The author would like to dedicate this work to his parents for their immeasurable love, training and constant encouragement in continuation of his education.

TABLE OF CONTENTS

TABLE OF CONTENTS (continued)

LIST OF TABLES

LIST OF FIGURES

LIST OF FIGURES (continued)

LIST OF FIGURES (continued)

NOMENCLATURE

English notations

A	coefficient in wall sheat stress expression (2.59)
A_p	cross-sectional area of tube
a	sonic velocity in gas media
a_p	piston acceleration
B	exponent of Reynolds number in (2.59)
B_I	function defined by Equation (2.11)
B_{II}	function defined by Equation (2.38)
C_1	ratio of boundary layer thickness and momentum thickness, δ/δ^*
C_I	function defined by Equation (2.12)
C_{II}	function defined by Equation (2.39)
C_f	local wall friction coefficient
c_s	specific heat of solids
c_p	specific heat of gas at constant pressure
c_v	specific heat of gas at constant volume
D	tube inside diameter
D_1'	function defined by Equation (2.78)
D_2'	function defined by Equation (2.79)
D_3'	function defined by Equation (3.21)
E_I	function defined by Equation (2.13)
E_{II}	function defined by Equation (2.40)
E'	function defined by Equation (2.77)

NOMENCLATURE (continued)

English notations

e	internal energy per unit mass
G'	function defined by Equation (2.83)
H	profile shape factor, δ^*/θ
H'_I	function defined by Equation (2.84)
H'_{II}	function defined by Equation (2.94)
h	enthalpy per unit mass film heat transfer coefficient
h_m	mean heat transfer coefficient at the inner surface, $(h_{ij}^{n} + h_{ij}^{n+1})/2$
J	mechanical equivalent of heat
j	axial position of a nodal point in finite difference grid
L_o	initial piston distance from tube head end
L_p	piston distance from tube head end at any instant
L_t	tube length
M	molecular weight of gas
M_p	piston mass
m_{s_i}	initial charge of propellant
n	time in finite difference grid reciprocal of exponent in power-law velocity profile
P	pressure
Pr	Prandtl number
$\dot{q}''$	heat flux per unit area
R	tube inside radius

NOMENCLATURE (continued)

English notations

R_o	tube outside radius
R_g	gas constant, R_u/M
R_u	universal gas constant
Re_θ	Reynolds number based on momentum thickness, $(\frac{\rho_f U\theta}{\mu_f})$
r	radial distance from tube axis
r_b	linear speed of burning
S_{b_t}	total burning surface
St	Stanton number, $(\frac{h}{\rho_f U c_p})$
s	entropy
T	one-dimensional gas temperature
T_o	explosion temperature
T_w	tube wall temperature
T_∞	free stream gas temperature
T_f	film temperature, $(T_\infty + T_{w,i})/2$
$T_{w,i}$	inner surface temperature of tube wall
t	time
U	one-dimensional velocity
U_p	piston velocity
U_∞	free stream velocity
u	velocity within boundary layer
v	specific volume
V_o	initial chamber volume
$\dot{v}_{d_s}$	volume rate of decrease of solids

NOMENCLATURE (continued)

English notations

W	potential of propellant per unit mass, $\frac{R_g T_o}{(\gamma-1)}$
w_{s_i}	initial web thickness of a solid particle
x	axial distance from tube head end

Greek notations

α	thermal diffusivity
β	coefficient of thermal expansion
γ	ratio of specific heats, c_p/c_v
ΔE	additional energy available per unit mass during conversion of solids into gases
Δf	change of function f
δ	boundary layer thickness
δ^*	displacement thickness
η	covolume in Equation of state (2.6)
η, ξ	characteristic directions corresponding to positive and negative value of λ respectively
Θ	function defined by Equation (2.61)
θ	momentum thickness
κ	thermal conductivity
λ	arbitrary multiplier to determine η, ξ characteristics
μ	viscosity
ν_s	volume fraction of solids
ρ_g	one-dimensional gas density
ρ_s	density of propellant material

NOMENCLATURE (continued)

Greek notations

ρ_f	gas density at film temperature T_f
ρ_m	mixture density, $[\nu_s\rho_s + (1-\nu_s)\rho_g]$
τ_w	wall shear stress
ζ	characteristic direction along a particle path

Subscripts

f	value at film temperature T_f
g	value for gas
i	value at inner surface of tube wall
o	initial value
p	value at piston base
s	value for solids
w	value for wall material
∞	free stream value

Superscripts

'	corresponding non-dimensional form

Special notations

$(\tilde{})$	first estimated value of a function after time $\Delta t'$
$(\tilde{\tilde{}})$	second estimated value of a function after time $\Delta t'$
$(\ )_j^n$	value at node n,j in time-space finite difference grid
$\frac{D}{Dt}$	$\frac{\partial}{\partial t} + U\frac{\partial}{\partial x}$

SUMMARY

The objective of this thesis is to provide a mathematical model that can be used to predict the performance of devices, such as guns, which produce high pressure in an enclosed, but expanding volume by burning solid propellant. The propellant is assumed to be in the form of solid particles and is burned in a closed cylindrical tube with a sliding piston at one end. Due to the complexity in estimating the relative velocity between the gas phase and solid phase, two limiting cases of solids velocity are examined in the present work. These are: (a) assume the solids have the same velocity as the gases around the particle and (b) assume the solids have zero velocity, i.e. the solids remaining stationary at their initial positions.

For both cases, the conservation of mass, momentum and energy results in a set of four coupled partial differential equations expressing volume fraction of solids, gas density, velocity and pressure as a function of axial distance from the tube head end and time. The equation of state of Noble and Abel, with constant covolume, is used for the combustion gas. The heat transfer to the tube wall and pressure drop due to skin friction have also been taken into consideration.

A boundary layer analysis is carried out by deriving the boundary layer momentum integral equation for a non-steady, non-uniform, developing flow in a tube. The profile shape factor (ratio of displacement thickness and momentum thickness) is introduced and the Ludwieg-Tillmann friction coefficient is used. As a first approximation, the shape factor is

assumed to be constant and, as the flow is in the high Reynolds number region, the usual approximation of a thin boundary layer is made.

The conservation equations together with the boundary layer equation are written in finite difference form and the MacCormack version of the Lax-Wendroff method is used to calculate all the ballistic properties, i.e. gas velocity, density, pressure, temperature, volume fraction of solids and boundary layer thickness at each of the interior points in the axial direction at every time step. For the two end points, namely the tube head end and the piston end, the method of characteristics is used. The film heat transfer coefficient is obtained by using Colburn's analogy between heat and momentum transfer. The wall temperature is also completely determined by solving the unsteady heat conduction equation for the tube wall with appropriate boundary conditions. The calculation procedure is repeated until the piston reaches the end of the tube.

Results are obtained for a set of "standard conditions," for both of the limiting cases of solids velocity. Although the final piston velocity and time of travel are very close in both cases, the peak pressure in the case of stationary solid is approximately 10 to 15 per cent higher than the corresponding value in the case of moving solids. There is also a large pressure gradient along the length of the tube and at the peak condition, the tube head end pressure can be 30 to 40 per cent higher than the piston base pressure.

The maximum boundary layer displacement thickness is less than three per cent of the tube radius in the typical case with the shape factor equal to 1.2857, i.e. with the one-seventh velocity profile.

Average values of the heat transfer coefficient and heat flux per unit surface area are found to be 50 kcal/m^2-sec-^oK and 50,000 kcal/m^2-sec respectively. The tube inner surface temperature can reach a peak value of 800-1000^oC during the first operation in an initially cold tube. The total heat loss to the tube wall is found to be five to six per cent of the input energy and has insignificant effect on the ballistic performance of the device.

A study of parameter variation shows that the initial chamber pressure, i.e. the "piston start pressure," has little effect on the ballistic solution. An increase in propellant charge or piston mass, or a reduction in initial web thickness of the solids can improve the ballistic efficiency of the device; but there is always an adverse effect of higher peak pressure and higher wall temperature which put a limit on such attempts. Therefore, a great deal of judgment and care is needed to determine the optimum condition for a particular application.

CHAPTER I

INTRODUCTION

Definition of the Problem

Devices which produce high pressure in an enclosed but expanding volume by burning combustible mixture of gases or solid propellant with the objective of performing work are common in practice. Internal ballistics of these devices, for example the problem of the gun, have been solved experimentally since fourteenth century when gunpowder first came into use [1]*. But surprisingly enough, an analytical solution which may be used to accurately predict the performance of such devices is yet to come. This lack of a mathematical model compels a designer to choose the comparatively expensive path of experimentation, although only limited information can be obtained from these experiments. Moreover, a large number of experiments have to be performed before a set of optimum design parameters can be determined for a particular purpose, and still the final result remains in question as to whether a truly optimum condition has been achieved.

The problem of internal ballistics requires a modeling of the fluid flow phenomena and heat transfer to the wall inside the expanding volume. For simplicity, throughout this work we shall restrict ourselves to the special geometry of a closed cylindrical tube with a sliding piston

---

*Number in [ ] refers to the references in Bibliography.

at one end as shown in Figure 1. The combustible mixture is burnt inside the enclosed volume whereby the pressure is increased and the piston is set into motion. The products of combustion which flow down the cylinder behind the piston impart a considerable amount of its energy to the piston and a fraction is lost to the tube wall. This cools the combustion gases and modifies the pressure and flow conditions.

While heat transfer has some effect on the ballistic properties, this is probably more important with respect to the material properties of the tube. Since the combustion gases are usually at a temperature of 2000-3000^{o}K, after repeated use of the device at high frequency the wall temperature of the tube may reach a value high enough to cause appreciable wear as the piston slides down the tube. A model of heat transfer, which can be used to predict the wall temperature, will help a designer to choose the optimum design parameters which will minimize the erosion rate.

The purpose of the present research is, therefore, to provide a working analytical model which shall be able to predict all the ballistic properties, namely velocity, pressure, temperature and density of the combustion gas mixture as a function of space and time. The heat loss to the tube wall shall be considered and the temperature distribution at the wall shall be determined. This model will then allow study and optimization of various parameters without expensive trial and error experimentation.

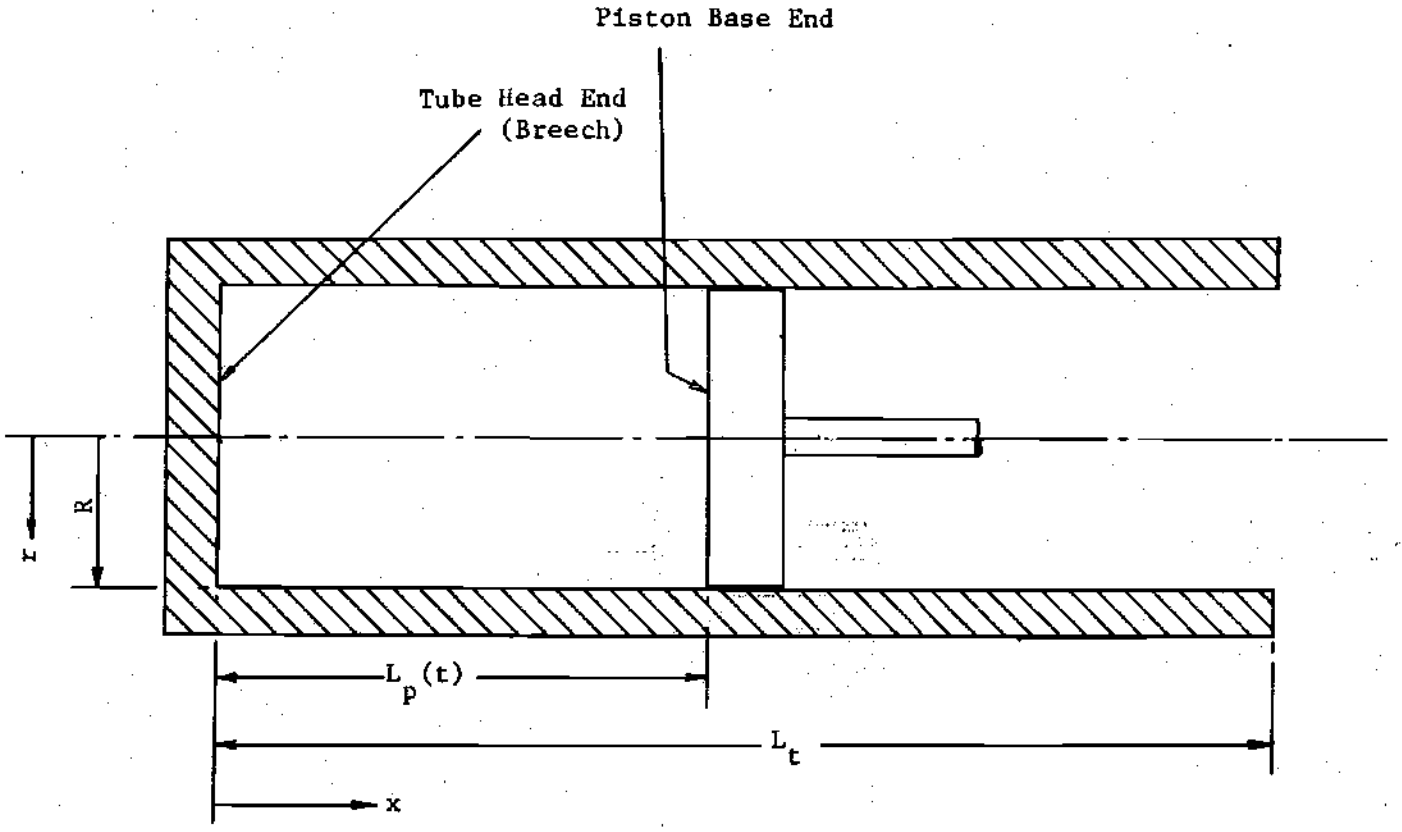

Figure 1. Schematic of the Piston-Cylinder Arrangement.

Related Work

Theoretical solutions to the problem of interior ballistics have been attempted since the days of Lagrange who in 1793 first tried to determine the spatial distribution of pressure, density and gas velocity in the tube at all times after the combustion. The work available until now can be divided into two broad categories:

1) Semiempirical solutions which may have practical utility in the study of familiar devices.

2) Exact theories which attempt to include the predominate phenomena up to a certain order of magnitude by formulating a simple mathematical model of the flow.

Semiempirical Solutions

The major works in this area with special application to the guns using solid propellant are described in references [1] and [2]. The main purpose of these works is to obtain a solution which matches with the experimental values of peak chamber pressure and muzzle velocity of the projectile. Only a few of the number of solutions shall be discussed here.

Isothermal Solution. The solution as described by Corner [2] is based on the following assumptions:

1) The propellant stays in the chamber burning under the tube head end (breech) pressure and the rate of burning is proportional to that pressure.

2) During the period of burning of the propellant, the progressive cooling of the combustion gases due to the work done on the projectile can be approximated by taking a mean gas temperature over this time

interval, corresponding to an effective mean force constant λ.

3) Uniform gas density and linear velocity distribution in the space between the tube head end and piston base.

4) Resistance to motion of the projectile can be taken into account by introducing an increased effective projectile mass instead of actual mass.

5) The covolume η (volume correcting term in the equation of state of the combustion gas) is equal to the specific volume of the propellant material.

The expressions for breech pressure P, projectile velocity V, and projectile distance from breech face x, are given as a function of "convenient variable" f, the form factor θ, the force constant λ, burning rate β, and central ballistic parameter M. The central ballistic parameter M itself is a function of λ, β, initial mass and web size of propellant, effective projectile mass, and tube diameter. The form factor θ depends on the geometrical shape of the propellant and the variable "f" goes from one to zero as the propellant is burnt. Other parameters, namely λ, M and β are chosen following a trial and error procedure until good agreement is obtained with the experimental values of peak pressure and muzzle velocity. The solution, however, does not take into account the heat loss to the tube wall.

Coppock's Solution [2]. This is an extension to the isothermal solution described above with the following modifications:

1) Instead of taking a mean gas temperature during burning, the analysis takes into account the kinetic energy of the projectile and that of the gases, assuming that the combustion gases are uniform in density

between the breech and the projectile and that their velocity at any point is proportional to the distance from the breech face. The total heat loss to the tube wall up to a particular instance of time is assumed to be a certain fraction of the total kinetic energy of the projectile and the gases at that instant. In practice, the effect of heat loss is incorporated in the energy equation by a proper choice of γ (ratio of specific heats at constant pressure and constant volume).

2) The gases have a constant covolume η, not necessarily equal to the specific volume of the propellant material.

From the observed peak pressure it is possible to back-calculate the central ballistic parameter M, and thence the burning rate β.

The solution is superior to the isothermal solution because there is only one arbitrary parameter, namely the burning rate β, whose value is selected so that the peak pressure matches the experimental data. Moreover, the model takes into account the heat loss to the tube wall, though in a crude fashion.

Goldie's Solution [2]. The solution follows Coppock's solution described above with the only modification that the projectile is assumed to be motionless until a "shot-start pressure" is produced inside the chamber. If there is any resistance to motion at later times, the effect is simulated by a change in effective shot weight.

Apart from these solutions, there are solutions which attempt to use a better relationship between the burning rate and the corresponding pressure. But the solutions still need trial and error of one or more variables to match experimental data. Besides, there is no guarantee as to how good the solutions will be when prediction of performance of

a new device is desired. Also, no information regarding the ballistic properties in between the breech face and the projectile is available from any of these models. Even a recent publication [3] fails to provide such informations.

Exact Theories

As mentioned earlier, Lagrange took the initiative to solve the one-dimensional problem of interior ballistics in 1793. He introduced the "Lagrange approximation" which assumes that the gas velocity at any instant increases linearly with distance along the tube, from zero at the tube head end to the full projectile velocity at the back of the piston. It is further assumed that all the propellant charge is in gaseous form from the start and at any time the gas density is the same at all points. It can be shown from the equation of continuity that if gas density is independent of position, the velocity distribution is linear; but the converse is not necessarily true.

In other work, Hugoniot in 1889 used the theory of waves of finite amplitude developed by Riemann in 1858, with the assumption that all the propellant was completely burnt when the piston began to move. He followed the resulting wave of rarefaction on its journey to the tube head end. The method was extended by Gossot and Liouville to follow the wave as it travels back to the piston after being reflected from the tube head end. Finally, Love [4] carried the analysis as far as the third wave traveling toward the breech and Pidduck [4] applied Love's solution in the special case of internal ballistics. But all these solutions, though completely analytical, hold good under two important assumptions:

a) Instantaneous combustion.

b) Adiabatic expansion of each element of gas.

The assumptions may be applicable for the devices which use gaseous fuel as propellant, say automobile engines, but for the devices using solid propellant the assumptions are far from the real situation. In this case, gradual burning of the propellant must be considered.

Analytical work based on most realistic assumptions has been done by Carriere [5]. For simplicity he assumed the propellant to be stationary in the combustion chamber at the time of burning which is a good assumption for cast propellant in a rocket-motor. From the basic concept of conservation of mass, momentum and energy, he derived three partial differential equations expressing gas density, gas velocity and entropy as a function of time and distance. He transformed those equations into three ordinary differential equations along three characteristic directions in the time-space co-ordinate. Then with proper choice of the equation of state for the combustion gas, he followed what is commonly known as the "method of characteristics" to determine the gas properties at any time and position. The effect of frictional losses and heat loss to the tube wall were disregarded in the analysis.

The problem of heat loss to the tube wall has been studied by Hicks and Thornhill in England. A fairly elaborate description of their method has been given in both references [1] and [2]. This work is also based on the Lagrange approximation of linear velocity distribution and uniform gas density in between the breech face and the piston.

It can be shown that at high velocity, heat is mainly transferred to the tube wall by convection. It is also evident that a boundary layer

is formed at the inner surface of the tube. The heat transfer rate per unit area through the boundary layer can be given as $h(T_g-T_s)$, where h, T_g and T_s are the film heat transfer coefficient, temperature of the gas, and temperature of the inner surface of the tube respectively. All three quantities depend on time as well as position along the tube.

Hicks and Thornhill considered the flow in the boundary layer to be the same as the flow over a flat plate. In internal ballistic applications the flow is in the turbulent region most of the time. Therefore, they used the analogy solution, as extended by Von Karman to cover Prandtl number other than unity, to obtain a relation between the heat transfer coefficient h and wall shear stress τ_w. To get the wall shear stress they first found a "best" power law for the velocity profile (non-dimensionalized with respect to the shear velocity $\sqrt{\tau_w/\rho}$) inside the boundary layer which was capable of giving the local wall shear stress τ_w within three per cent of the value that could be obtained by using more rigorous logarithmic form of the velocity profile when applied to steady and uniform flow situations. Then they used the boundary layer momentum integral, including the terms due to non-steady and non-uniform nature of the flow, and used the "best" power law found earlier to obtain the local wall shear stress at all points. The heat transfer coefficient h is then easily calculated from the analogy solution. They, however, omitted one boundary condition that the boundary layer thickness at the base of the piston be zero at all times.

The heat transfer in the tube wall has been calculated by using the differential equation for unsteady heat conduction with proper boundary conditions. For the case studied by Hicks and Thornhill, i.e.

the first round of firing from a cold gun, the curvature effect of the wall was neglected as the temperature rise was confined within one millimeter of the inside surface. Consequently, there was no heat loss from the outer surface of the tube which remained at ambient temperature. The heat conduction along the length of the barrel was also neglected. Knowing the tube material properties, namely thermal conductivity and diffusivity, it was possible to obtain the temperature distribution at the inner surface of the tube along the length at all times. The free stream values of the gas velocity, density and temperature were taken from the one-dimensional ballistic solution.

It has been indicated in reference [2] that frictional pressure drop is small compared to the inertia pressure drop needed to accelerate the gas. But no analysis until now indicate quantitatively the effect of skin friction on the ballistic properties. Even the heat transfer solution has not been fed back to study its effect on the one-dimensional solution.

Present Investigation

In the light of available theories, it is clear that a good one-dimensional solution is first required to replace the Lagrange approximation, or at least check its validity for the particular problem. The first and most formidable difficulty in writing down the one-dimensional continuity, momentum and energy equations during the burning of the solid propellant is due to the uncertainty of the relative velocity between the gas phase and the solid phase. It is extremely difficult to estimate the drag exerted on the burning solid particles by the accelerating

combustion gases. Therefore, two limiting cases of the solids velocity have been considered in the present work:

Case I. The solid particles move at the same velocity as the gas phase.

Case II. The solid particles remain at their initial positions throughout the period of burning.

For both cases the conservation of mass, momentum and energy results in four coupled partial differential equations expressing volume fraction of solid ν_s, gas density ρ_g, gas velocity U, and pressure P as a function of axial distance x and time t. The heat release due to gradual burning of the propellant is taken into account. A special propellant geometry, namely a hollow cylinder, is considered whereby the total burning surface remains constant, although this assumption is not essential.

The ballistic properties at the internal points are calculated from these equations after writing the same in finite difference form. But to obtain the properties at the two ends, namely the tube head end and the piston base, the equations are transformed into ordinary differential equations along the characteristic directions. The covolume of the gas is assumed to be constant, and experimental data for burning rate is used. As one of the initial conditions, it is assumed that the piston does not start until a certain specified pressure is reached inside the chamber and thereafter the piston does not experience any resistance to motion.

The boundary layer momentum integral for a non-steady, non-uniform, developing flow inside a tube is derived. The profile shape factor H

(ratio between the displacement thickness δ^* and momentum thickness θ) is introduced and the Ludwieg-Tillmann [6] friction factor is used. As a first approximation, the shape factor is assumed to be constant in the present work. The flow is in the high Reynolds number region for which the boundary layer thickness is small compared to the tube radius. It is therefore legitimate to replace the free stream values of gas density and velocity by the values obtained from the one-dimensional solution neglecting the boundary layer thickness.

The local heat transfer coefficient h is calculated by using Colburn's analogy [7] between heat and momentum transfer. It covers Prandtl numbers other than unity and is simple to use. The values of viscosity and gas density at the film temperature are used. The heat transfer in the tube wall is computed from the unsteady one-dimensional (radial) heat conduction equation with appropriate boundary conditions. The wall temperature is also found as a function of axial distance and time.

The heat loss term is entered into the one-dimensional energy equation and a comparison of ballistic properties is made with the solution without heat loss. Effect of wall shear stress is also included. The ballistic efficiency of the piston-cylinder arrangement is compared by varying different design parameters.

CHAPTER II

MATHEMATICAL ANALYSIS

The mathematical analysis consists of two major parts:

1) One-dimensional analysis with gradual burning of the solid propellant, including the effect of heat transfer and skin friction.
2) Formulation of the boundary layer problem and determination of heat transfer to the tube wall.

As outlined in the previous chapter, the present analysis is carried out for two extreme cases of solid velocity. In the first case, it is assumed that a burning solid particle moves with the same velocity as the combustion gases. In the second case, however, the solid particles are assumed to be stationary at their initial positions throughout the period of burning. Henceforth these two cases are referred as Case I and Case II, respectively.

One-Dimensional Analysis Including Heat Transfer and Skin Friction

Case I

The assumptions, other than that regarding the solids velocity, which are made to simplify the model are as follows:

1) At any instance of time, the linear speed of burning r_b is same for all the solid particles and it is a function of the

average pressure in the chamber (space in between the tube head end and the piston base).

2) The solid propellants are single perforated circular cylinders in shape whereby the total burning surface remains constant during the whole period of burning.

3) The burning rate is fast enough to consider that the temperature of the remaining solids at any instance of time remains constant at the initial temperature.

4) The propellant material is incompressible and its coefficient of thermal expansion is negligible.

5) The piston starts to move only when the chamber pressure reaches a certain value P_o, and thereafter the resistance to its motion is negligible compared to the pressure force exerted on it by the combustion gases in the chamber.

The conservation equations are as follows (for derivation see Appendix A):

Solid continuity:

$$\frac{\partial \nu_s}{\partial t} + U\frac{\partial \nu_s}{\partial x} + \nu_s \frac{\partial U}{\partial x} + \dot{v}_{d_s} = 0 \qquad (2.1)$$

Gas continuity:

$$\frac{\partial \rho_g}{\partial t} + U\frac{\partial \rho_g}{\partial x} + \frac{\rho_g}{(1-\nu_s)} \frac{\partial U}{\partial x} = \frac{(\rho_s - \rho_g)}{(1-\nu_s)} \dot{v}_{d_s} \qquad (2.2)$$

Momentum:

$$\frac{\partial U}{\partial t} + U \frac{\partial U}{\partial x} = - \frac{1}{\rho_m} \frac{\partial P}{\partial x} - \frac{2\tau_w}{\rho_m R} \tag{2.3}$$

Energy:

$$\nu_s \rho_s \frac{Dh_s}{Dt} + (1-\nu_s)\, \rho_g \frac{Dh_g}{Dt} - \frac{DP}{Dt}$$

$$= \rho_s (W + \frac{P}{\rho_s} - h_g) \dot{v}_{d_s} - \frac{2h_i}{R}(T-T_{w,i}) + \frac{2\tau_w U}{R} \tag{2.4}$$

where $\dot{v}_{d_s}$ is the volume rate of decrease of solids per unit cylinder volume and is given by:

$$\dot{v}_{d_s}(x,t) = (\frac{S_b}{A_p}) \frac{\nu_s(x,t) r_b}{\int_o^{L_p} \nu_s(x,t)\, dx} \tag{2.5}$$

The equation of state of the gas is:

$$P(v_g - \eta) = R_g T$$

or,

$$P(\frac{1}{\rho_g} - \eta) = R_g T \tag{2.6}$$

where the gas constant R_g is obtained from the ratio of the universal gas constant R_u and the molecular weight of the gas M.

It has been shown in Appendix A that under assumptions three and four as stated earlier, the differential of enthalpy of solids per unit

mass h_s and the differential of enthalpy of gases per unit mass h_g can be given by:

$$dh_s = \frac{1}{\rho_s} dP \tag{2.7}$$

$$dh_g = \frac{(\gamma-\eta\rho_g)}{\rho_g(\gamma-1)} dP - \frac{\gamma P}{(\gamma-1)\rho_g^2} d\rho_g \tag{2.8}$$

Substituting equations (2.7) and (2.8) into the energy equation (2.4):

$$\frac{(1-\nu_s)(1-\eta\rho_g)}{(\gamma-1)} \frac{DP}{Dt} - \frac{(1-\nu_s)\gamma P}{(\gamma-1)\rho_g} \frac{D\rho_g}{Dt}$$

$$= \rho_s(W + \frac{P}{\rho_s} - h_g)\dot{v}_{d_s}$$

$$- \frac{2h_i}{R}(T-T_{w,i}) + \frac{2\tau_w U}{R} \tag{2.9}$$

Using gas continuity, i.e. equation (2.2) to replace $\frac{D\rho_g}{Dt}$ in equation (2.9) the final form of the energy equation becomes:

$$\frac{(1-\nu_s)(1-\eta\rho_g)}{(\gamma-1)} \frac{DP}{Dt} + \frac{\gamma P}{(\nu-1)} \frac{\partial U}{\partial x} - \frac{\gamma P(\rho_s-\rho_g)}{(\gamma-1)\rho_g} \dot{v}_{d_s}$$

$$= \rho_s(W + \frac{P}{\rho_s} - h_g)\dot{v}_{d_s} - \frac{2h_i}{R}(T-T_{w,i})$$

$$+ \frac{2\tau_w U}{R}$$

or,

$$\frac{\partial P}{\partial t} + U\frac{\partial P}{\partial x} + B_I \frac{\partial U}{\partial x} = C_I \dot{v}_{d_s} - E_I \frac{2h_i}{R}(T-T_{w,i}) + E_I \frac{2\tau_w U}{R} \tag{2.10}$$

where

$$B_I = \frac{\gamma P}{(1-\nu_s)(1-\eta\rho_g)} \tag{2.11}$$

$$C_I = \frac{\gamma P(\rho_s-\rho_g) + (\gamma-1)\rho_s\rho_g(W + \frac{P}{\rho_s} - h_g)}{\rho_g\{(1-\nu_s)(1-\eta\rho_g)\}} \tag{2.12}$$

$$E_I = \frac{(\gamma-1)}{(1-\nu_s)(1-\eta\rho_g)} \tag{2.13}$$

The initial conditions of the conservation equations are:

Position of the piston, $L_p(0) = L_o$

$$U(x,0) = 0 \;;\quad P(x,0) = P_o \;;\quad T(x,0) = T_o \;;\quad \rho_g(x,0) = \rho_{g_o}$$

and $\nu_s(x,0) = \nu_{s_o}$ at $0 \leq x \leq L_o$ (2.14)

where P_o is the pressure at which the piston starts to move, and T_o is the explosion temperature of the propellant. By knowing P_o and T_o it is possible to determine ρ_{g_o} from the equation of state (2.6):

$$\rho_{g_o} = \frac{1}{\frac{R_g T_o}{P_o} + \eta} \tag{2.15}$$

Neglecting the initial mass of air in the chamber, a mass balance gives:

$$m_{s_i} = \nu_{s_o} V_o \rho_s + (1-\nu_{s_o}) V_o \rho_{g_o}$$

or,

$$\nu_{s_o} = \frac{(m_{s_i}/V_o) - \rho_{g_o}}{\rho_s - \rho_{g_o}} \tag{2.16}$$

(m_{s_i}/V_o) is called the "loading density."

The boundary conditions are:

$$\text{at } x = 0, \qquad U(0,t) = 0$$

and (2.17)

$$\text{at } x = L_p, \qquad U(L_p,t) = U_p(t)$$

The piston velocity $U_p(t)$ is obtained from the equation of motion of the piston, which under the assumption five takes the following form:

$$\frac{dU_p}{dt} = a_p = \frac{P_p A_p}{M_p} \tag{2.18}$$

The position of the piston is obtained from:

$$\frac{d^2x_p}{dt^2} = a_p \tag{2.19}$$

The unknowns, and the corresponding equations from which they can be calculated are listed below:

Unknown	Equation
Volume fraction of solids, ν_s	Solid continuity, (2.1)
Gas density, ρ_g	Gas continuity, (2.2)
Velocity, U	Momentum equation, (2.3)
Pressure, P	Energy equation, (2.10)
Gas temperature, T	Equation of state, (2.6)

The conservation equations, i.e. (2.1), (2.2), (2.3) and (2.10) are written in finite difference form, and a numerical scheme which takes into account both forward and backward space derivatives are used to calculate the corresponding unknowns, i.e. ν_s, ρ_g, U and P, at all the interior points at an advanced time by knowing the present values at and around those points. The gas temperature, T, is then calculated from the equation of state (2.6). The details of the solution technique shall be discussed in Chapter III.

The above solution technique, however, is not applicable to the boundary points, i.e. the piston base end and the tube head end, as space derivatives on both sides of these two points are not available. This necessitates the transformation of the conservation equations to ordinary differential equations along characteristic directions, i.e. to follow the "method of characteristics" [8].

P-U Characteristic. The energy equation (2.10) is:

$$\frac{\partial P}{\partial t} + U\frac{\partial P}{\partial x} + B_I \frac{\partial U}{\partial x} = C_I \dot{v}_{d_s} - E_I \frac{2h_i}{R} (T-T_{w,i})$$

$$+ E_I \frac{2\tau_w U}{R}$$

Multiplying the momentum equation (2.3) by an arbitrary constant λ:

$$\lambda\frac{\partial P}{\partial x} + \lambda\rho_m \frac{\partial U}{\partial t} + \lambda\rho_m U\frac{\partial U}{\partial x} = - \lambda \frac{2\tau_w}{R} \qquad (2.20)$$

Adding equation (2.20) to equation (2.10):

$$\left[\frac{\partial P}{\partial t} + (U+\lambda) \frac{\partial P}{\partial x}\right] + \left[\lambda\rho_m \frac{\partial U}{\partial t} + (B_I + \lambda\rho_m U)\frac{\partial U}{\partial x}\right]$$

$$= C_I \dot{v}_{d_s} - E_I \frac{2h_i}{R} (T-T_{w,i})$$

$$+ \frac{2\tau_w}{R} \left[E_I U - \lambda\right] \qquad (2.21)$$

To obtain the characteristic directions, the value of λ shall be such that:

$$\frac{dt}{dx} = \frac{1}{U+\lambda} = \frac{\lambda\rho_m}{B_I+\lambda\rho_m U}$$

$$\lambda_{1,2} = \pm \sqrt{B_I/\rho_m} \qquad (2.22)$$

Dividing equation (2.21) by $\sqrt{1+(U+\lambda)^2}$ and using

$$\frac{1}{\sqrt{1+(U+\lambda)^2}}\frac{\partial}{\partial t}+\frac{(U+\lambda)}{\sqrt{1+(U+\lambda)^2}}\frac{\partial}{\partial x}=\frac{d}{d\eta,\xi}$$

where η corresponds to λ_1 i.e. +ve sign of λ

and ξ corresponds to λ_2 i.e. -ve sign of λ

the equation (2.21) becomes:

$$\frac{dP}{d\eta,\xi}+\lambda_{1,2}\rho_m\frac{dU}{d\eta,\xi}=\frac{1}{\sqrt{1+(U+\lambda)^2}}\left[C_I\dot{v}_{d_s}-E_I\frac{2h_i}{R}(T-T_{w,i})+\frac{2\tau_w}{R}(E_IU-\lambda)\right] \quad (2.23)$$

Now,

$$\Delta\eta,\xi=\sqrt{(\Delta x)^2+(\Delta t)^2}=\Delta t\sqrt{1+(U+\lambda)^2} \quad (2.24)$$

Therefore, along η-characteristic, i.e. $\frac{dt}{dx}=\frac{1}{U+\sqrt{B_I/\rho_m}}$:

$$\Delta P+\rho_m\sqrt{B_I/\rho_m}\,\Delta U=\left[C_I\dot{v}_{d_s}-E_I\frac{2h_i}{R}(T-T_{w,i})+\frac{2\tau_w}{R}(E_IU-\sqrt{B_I/\rho_m})\right]\Delta t \quad (2.25)$$

and along ξ-characteristic, i.e. $\frac{dt}{dx}=\frac{1}{U-\sqrt{B_I/\rho_m}}$:

$$\Delta P - \rho_m \sqrt{B_I/\rho_m}\,\Delta U = \left[C_I \dot{v}_{d_s} - E_I \frac{2h_i}{R}(T-T_{w,i}) + \frac{2\tau_w}{R}(E_I U + \sqrt{B_I/\rho_m})\right] \Delta t \qquad (2.26)$$

P-ρ_g Characteristic. By rearranging equation (2.9),

$$\frac{\partial \rho_g}{\partial t} + U\frac{\partial \rho_g}{\partial x} = \frac{\rho_g(1-\eta\rho_g)}{\gamma P}\left[\frac{\partial P}{\partial t} + U\frac{\partial P}{\partial x}\right] + \frac{(\gamma-1)\rho_s\rho_g\left(h_g - \frac{P}{\rho_s} - W\right)}{(1-\nu_s)\gamma P}\dot{v}_{d_s} + \frac{(\gamma-1)\rho_g}{(1-\nu_s)\gamma P}\left[\frac{2h_i}{R}(T-T_{w,i}) - \frac{2\tau_w U}{R}\right] \qquad (2.27)$$

Dividing this equation by $\sqrt{1+U^2}$ and using,

$$\frac{1}{\sqrt{1+U^2}}\frac{\partial}{\partial t} + \frac{U}{\sqrt{1+U^2}}\frac{\partial}{\partial x} = \frac{d}{d\zeta}$$

and

$$\Delta\zeta = \sqrt{(\Delta x)^2+(\Delta t)^2} = \Delta t\,\sqrt{1+U^2}$$

along a particle path, i.e. $\frac{dt}{dx} = \frac{1}{U}$:

$$\Delta\rho_g = \frac{\rho_g(1-\eta\rho_g)}{\gamma P}\Delta P + \frac{(\gamma-1)\rho_s\rho_g\left(h_g - \frac{P}{\rho_s} - W\right)}{(1-\nu_s)\gamma P}\dot{v}_{d_s}\Delta t + \frac{(\gamma-1)\rho_g}{(1-\nu_s)\gamma P}\left[\frac{2h_i}{R}(T-T_{w,i}) - \frac{2\tau_w}{R}U\right]\Delta t \qquad (2.28)$$

ν_s-ρ_g Characteristic. From equation (2.2):

$$\frac{\partial U}{\partial x} = -\frac{(1-\nu_s)}{\rho_g}\left[\frac{\partial \rho_g}{\partial t} + U\frac{\partial \rho_g}{\partial x}\right] + \frac{(\rho_s-\rho_g)}{\rho_g}\dot{v}_{d_s} \qquad (2.29)$$

Substituting this expression for $\frac{\partial U}{\partial x}$ in solid continuity (2.1):

$$\frac{\partial \nu_s}{\partial t} + U\frac{\partial \nu_s}{\partial x} - \frac{\nu_s(1-\nu_s)}{\rho_g}\left[\frac{\partial \rho_g}{\partial t} + U\frac{\partial \rho_g}{\partial x}\right] + \left[\frac{\nu_s\rho_s+(1-\nu_s)\rho_g}{\rho_g}\right]\dot{v}_{d_s} = 0 \qquad (2.30)$$

Proceeding in the same fashion as for the P-ρ_g characteristic, one obtains:

Along a particle path, i.e. $\frac{dt}{dx} = \frac{1}{U}$:

$$\Delta\nu_s = \frac{\nu_s(1-\nu_s)}{\rho_g}\Delta\rho_g - \frac{\rho_m}{\rho_g}\dot{v}_{d_s}\Delta t \qquad (2.31)$$

The procedure of solving the above characteristic equations are discussed in Chapter III.

Case II

In this case the solid propellant particles are assumed to be stationary at their initial positions throughout the period of burning. The linear speed of burning r_b, is same for all the solid particles and is a function of the average pressure in the space between the tube head end and the initial position of the piston L_o. The rest of the assumptions are the same as those for Case I.

The conservation equations in this case are (See Appendix A for derivation):

Solid continuity:

$$\frac{\partial \nu_s}{\partial t} + \dot{v}_{d_s} = 0 \tag{2.32}$$

Gas continuity:

$$\frac{\partial \rho_g}{\partial t} + U\frac{\partial \rho_g}{\partial x} + \rho_g \frac{\partial U}{\partial x} = \frac{(\rho_s - \rho_g)}{(1-\nu_s)} \dot{v}_{d_s} + \frac{\rho_g U}{(1-\nu_s)} \frac{\partial \nu_s}{\partial x} \tag{2.33}$$

Momentum:

$$\frac{\partial U}{\partial t} + U\frac{\partial U}{\partial x} = -\frac{1}{\rho_g}\frac{\partial P}{\partial x} - \frac{\rho_s U}{(1-\nu_s)\rho_g}\dot{v}_{d_s} - \frac{2\tau_w}{(1-\nu_s)\rho_g R} \tag{2.34}$$

Energy:

$$(1-\nu_s)\rho_g \frac{Dh_g}{Dt} - (1-\nu_s)\frac{DP}{Dt} = \rho_s\left(W + \frac{P}{\rho_s} + \frac{U^2}{2} - h_g\right)\dot{v}_{d_s}$$

$$- \frac{2h_i}{R}(T - T_{w,i}) + \frac{2\tau_w U}{R} \tag{2.35}$$

As none of the solid particles moves beyond L_o, $\dot{v}_{d_s}$ can be expressed as:

$$\dot{v}_{d_s} = \left(\frac{S_b t}{A_p}\right) \frac{\nu_s r_b}{\int_0^{L_o} \nu_s dx} \tag{2.36}$$

The same equation of state, i.e. equation (2.6), is used and by successive use of equation (2.8) and (2.33) the final form of the energy equation (2.35) becomes:

$$\frac{\partial P}{\partial t} + U\frac{\partial P}{\partial x} + B_{II}\frac{\partial U}{\partial x} = C_{II}\dot{v}_{d_s} + \frac{B_{II}U}{(1-\nu_s)}\frac{\partial \nu_s}{\partial x}$$

$$- E_{II}\frac{2h_i}{R}(T-T_{w,i}) + E_{II}\frac{2\tau_w U}{R} \qquad (2.37)$$

where

$$B_{II} = \frac{\gamma P}{(1-\eta\rho_g)} \qquad (2.38)$$

$$C_{II} = \frac{\gamma P(\rho_s-\rho_g) + (\gamma-1)\rho_s\rho_g\left(W + \frac{P}{\rho_s} + \frac{U^2}{2} - h_g\right)}{\rho_g\{(1-\nu_s)(1-\eta\rho_g)\}} \qquad (2.39)$$

$$E_{II} = E_I = \frac{(\gamma-1)}{(1-\nu_s)(1-\eta\rho_g)} \qquad (2.40)$$

The initial and boundary conditions are the same as those for Case I. The characteristic equations are also required to calculate the ballistic properties at the two ends.

P-U Characteristic. The procedure is exactly same as Case I. Multiplying the momentum equation (2.34) by an arbitrary constant λ, and adding to the energy equation (2.37) one obtains:

$$\left[\frac{\partial P}{\partial t} + (U+\lambda)\frac{\partial P}{\partial x}\right] + \left[\lambda\rho_g \frac{\partial U}{\partial t} + (B_{II}+\lambda\rho_g U)\frac{\partial U}{\partial x}\right]$$

$$= C_{II}\dot{v}_{d_s} + \frac{B_{II}U}{(1-\nu_s)}\frac{\partial \nu_s}{\partial x} - \lambda\frac{\rho_s U}{(1-\nu_s)}\dot{v}_{d_s}$$

$$- E_{II}\frac{2h_i}{R}(T-T_{w,i}) + \frac{2\tau_w}{R}\left[E_{II}U - \frac{\lambda}{(1-\nu_s)}\right] \quad (2.41)$$

The characteristic directions are such that:

$$\frac{dt}{dx} = \frac{1}{U+\lambda} = \frac{\lambda\rho_g}{B_{II}+\lambda\rho_g U}$$

$$\therefore \quad \lambda_{1,2} = \pm\sqrt{\frac{B_{II}}{\rho_g}} = \pm\sqrt{\frac{\gamma P}{\rho_g(1-\eta\rho_g)}} = \pm a \quad (2.42)$$

From solid continuity, i.e. equation (2.32)

$$\frac{\partial \nu_s}{\partial t} = -\dot{v}_{d_s} \quad (2.43)$$

By adding and substracting $\frac{B_{II}U}{(1-\nu_s)(U+\lambda)}\frac{\partial \nu_s}{\partial t}$ on the right hand side of equation (2.41):

$$\left[\frac{\partial P}{\partial t} + (U+\lambda)\frac{\partial P}{\partial x}\right] + \lambda\rho_g\left[\frac{\partial U}{\partial t} + (U+\lambda)\frac{\partial U}{\partial x}\right]$$

$$= \frac{B_{II}U}{(1-\nu_s)(U+\lambda)}\left[\frac{\partial \nu_s}{\partial t} + (U+\lambda)\frac{\partial \nu_s}{\partial x}\right] - \frac{B_{II}U}{(1-\nu_s)(U+\lambda)}\frac{\partial \nu_s}{\partial t}$$

$$+ C_{II}\dot{v}_{d_s} - \lambda\frac{\rho_s U}{(1-\nu_s)}\dot{v}_{d_s} - E_{II}\frac{2h_i}{R}(T-T_{w,i}) + \frac{2\tau_w}{R}\left[E_{II}U\frac{\lambda}{(1-\nu_s)}\right]$$

(2.44)

Dividing equation (2.44) by $\sqrt{1+(U+\lambda)^2}$ and using

$$\frac{1}{\sqrt{1+(U+\lambda)^2}}\frac{\partial}{\partial t}+\frac{(U+\lambda)}{\sqrt{1+(U+\lambda)^2}}\frac{\partial}{\partial x}=\frac{d}{d\eta,\xi}$$

yields the relation:

$$\frac{dP}{d\eta,\xi}+\lambda_{1,2}\rho_g\frac{dU}{d\eta,\xi}=\frac{B_{II}U}{(1-\nu_s)(U+\lambda)}\frac{d\nu_s}{d\eta,\xi}$$

$$+\frac{1}{\sqrt{1+(U+\lambda)^2}}\left[\{C_{II}-\frac{\rho_s U\lambda}{(1-\nu_s)}+\frac{B_{II}U}{(1-\nu_s)(U+\lambda)}\}\dot{v}_{d_s}\right.$$

$$\left.-E_{II}\frac{2h_i}{R}(T-T_{w,i})+\frac{2\tau_w}{R}\{E_{II}U-\frac{\lambda}{(1-\nu_s)}\}\right] \qquad (2.45)$$

Therefore, along η-characteristic, i.e. $\frac{dt}{dx}=\frac{1}{U+a}$:

$$\Delta P+\rho_g\, a\,\Delta U=\frac{B_{II}U}{(1-\nu_s)(U+a)}\Delta\nu_s$$

$$+\left[C_{II}-a\frac{\rho_s U}{(1-\nu_s)}+\frac{B_{II}U}{(1-\nu_s)(U+a)}\right]\dot{v}_{d_s}\,\Delta t$$

$$-E_{II}\frac{2h_i}{R}(T-T_{w,i})\Delta t+\frac{2\tau_w}{R}\left[E_{II}U-\frac{a}{(1-\nu_s)}\right]\Delta t \qquad (2.46)$$

and along ξ-characteristic, i.e. $\frac{dt}{dx}=\frac{1}{U-a}$:

$$\Delta P - \rho_g \, a \, \Delta U = \frac{B_{II} U}{(1-\nu_s)(U-a)} \Delta \nu_s$$

$$+ \left[C_{II} + a\frac{\rho_s U}{(1-\nu_s)} + \frac{B_{II} U}{(1-\nu_s)(U-a)} \right] \dot{v}_{d_s} \Delta t$$

$$- E_{II} \frac{2h_i}{R}(T-T_{w,i})\Delta t + \frac{2\tau_w}{R}\left[E_{II} U + \frac{a}{(1-\nu_s)} \right] \Delta t \qquad (2.47)$$

P-ρ_g Characteristic. Using equation (2.8) in equation (2.35), an alternative form of energy equation is:

$$\frac{\partial \rho_g}{\partial t} + U\frac{\partial \rho_g}{\partial x} = \frac{\rho_g(1-\eta\rho_g)}{\gamma P}\left[\frac{\partial P}{\partial t} + U\frac{\partial P}{\partial x} \right]$$

$$+ \frac{(\gamma-1)\rho_s\rho_g(h_g - W - \frac{P}{\rho_s} - \frac{U^2}{2})}{(1-\nu_s)\gamma P}\dot{v}_{d_s}$$

$$+ \frac{(\gamma-1)\rho_g}{(1-\nu_s)\gamma P}\left[\frac{2h_i}{R}(T-T_{w,i}) - \frac{2\tau_w U}{R} \right] \qquad (2.48)$$

Proceeding in exactly the same manner as for Case I, along a particle path, i.e. $\frac{dt}{dx} = \frac{1}{U}$:

$$\Delta\rho_g = \frac{\rho_g(1-\eta\rho_g)}{\gamma P}\Delta P + \frac{(\gamma-1)\rho_s\rho_g(h_g - W - \frac{P}{\rho_s} - \frac{U^2}{2})}{(1-\nu_s)\gamma P}\dot{v}_{d_s}\Delta t$$

$$+ \frac{(\gamma-1)\rho_g}{(1-\nu_s)\gamma P}\left[\frac{2h_i}{R}(T-T_{w,i}) - \frac{2\tau_w U}{R} \right]\Delta t \qquad (2.49)$$

v_s at the piston base is always zero after the piston starts moving and v_s at the tube head end can be obtained from equation (2.32) alone.

Boundary Layer Analysis

The boundary layer part of the entire analysis did not receive much attention in the past because of the nonsteady and nonuniform nature of the free stream flow. The flow is generally in the turbulent region with pressure gradient in the direction of the flow and a large temperature difference across the boundary layer. Also, in Case I a gas-solid mixture flows down the tube; hence the analysis is more complicated. A number of attempts [9, 10, 11, 12] have been made in the past to model the mechanism of heat transfer in a gas-solid mixture with various solid particle sizes and loading ratios (w_s/w_g). It has been found that the effect of the solids on heat transfer is prominent for micron-size particles whereas for millimeter size the effect is not appreciable. The present problem deals with the solid propellant of millimeter size and most of the time it burns out completely long before the piston reaches the end of the tube. It has also been found from the study of Hicks and Thornhill [2] that the boundary layer thickness is small compared to the tube radius. Therefore, to simplify the model, it is assumed that the solids always stay in the core of the flow and never enter into the thin boundary layer at the wall.

In the present study, an integral approach is preferred to a differential approach to keep the model relatively simple and traceable. The boundary layer momentum integral for the nonsteady and nonuniform compressible flow inside a tube as derived in Appendix B is:

$$\frac{\partial}{\partial t}\left[\int_{R-\delta}^{R}\rho(U_\infty-u)r\,dr\right]+\frac{\partial}{\partial x}\left[\int_{R-\delta}^{R}\rho u(U_\infty-u)r\,dr\right]+\int_{R-\delta}^{R}\rho(U_\infty-u)r\,dr\;\frac{\partial U_\infty}{\partial x}$$

$$=\left(R\delta-\frac{\delta^2}{2}\right)\left[\frac{\partial P}{\partial x}+\rho_f\frac{\partial U_\infty}{\partial t}+\rho_f U_\infty\frac{\partial U_\infty}{\partial x}\right]$$

$$+\tau_w R \qquad (2.50)$$

Defining δ^* = Displacement thickness

and θ = Momentum thickness

such that,

$$\rho_f U_\infty\int_{R-\delta^*}^{R}2\pi r\,dr=\int_{R-\delta}^{R}\rho 2\pi r(U_\infty-u)dr$$

or,

$$\rho_f U_\infty R\delta^*\left(1-\frac{\delta^*}{2R}\right)=\int_{R-\delta}^{R}\rho r(U_\infty-u)dr \qquad (2.51)$$

and

$$\rho_f U_\infty^2\int_{R-\theta}^{R}2\pi r\,dr=\int_{R-\delta}^{R}\rho\;2\pi r\;u(U_\infty-u)dr$$

or,

$$\rho_f U_\infty^2 R\theta\left(1-\frac{\theta}{2R}\right)=\int_{R-\delta}^{R}\rho\;u\;r(U_\infty-u)dr \qquad (2.52)$$

and using the definition of the profile shape factor $H=\frac{\delta^*}{\theta}$, and for a thin boundary layer $\frac{\delta}{2R}\ll 1$, $\frac{\delta^*}{2R}\ll 1$, $\frac{\theta}{2R}\ll 1$, the momentum integral equation (2.50) becomes,

$$\frac{\partial}{\partial t}\left[\rho_f U_\infty RH\theta\right] + \frac{\partial}{\partial x}\left[\rho_f U_\infty^2 R\theta\right] + (\rho_f U_\infty RH\theta)\frac{\partial U_\infty}{\partial x}$$

$$= R\delta\left[\frac{\partial P}{\partial x} + \rho_f \frac{\partial U_\infty}{\partial t} + \rho_f U_\infty \frac{\partial U_\infty}{\partial x}\right] + \tau_w R$$

or,

$$\rho_f U_\infty RH\frac{\partial \theta}{\partial t} + \rho_f U_\infty R\theta\frac{\partial H}{\partial t} + \rho_f RH\theta\frac{\partial U_\infty}{\partial t} + U_\infty RH\theta\frac{\partial \rho_f}{\partial t} + \rho_f U_\infty^2 R\frac{\partial \theta}{\partial x}$$

$$+ 2\rho_f U_\infty R\theta\frac{\partial U_\infty}{\partial x} + U_\infty^2 R\theta\frac{\partial \rho_f}{\partial x} + \rho_f U_\infty RH\theta\frac{\partial U_\infty}{\partial x}$$

$$= R\delta\left[\frac{\partial P}{\partial x} + \rho_f \frac{\partial U_\infty}{\partial t} + \rho_f U_\infty\frac{\partial U_\infty}{\partial x}\right] + \tau_w R \qquad (2.53)$$

Dividing equation (2.53) by $\rho_f U_\infty RH\theta$:

$$\frac{1}{\theta}\frac{\partial \theta}{\partial t} + \frac{1}{H}\frac{\partial H}{\partial t} + \frac{1}{U_\infty}\frac{\partial U_\infty}{\partial t} + \frac{1}{\rho_f}\frac{\partial \rho_f}{\partial t} + \frac{U_\infty}{H\theta}\frac{\partial \theta}{\partial x} + \frac{2}{H}\frac{\partial U_\infty}{\partial x} + \frac{U_\infty}{\rho_f H}\frac{\partial \rho_f}{\partial x} + \frac{\partial U_\infty}{\partial x}$$

$$= \frac{\delta}{\rho_f U_\infty H\theta}\left[\frac{\partial P}{\partial x} + \rho_f \frac{\partial U_\infty}{\partial t} + \rho_f U_\infty \frac{\partial U_\infty}{\partial x}\right] + \frac{\tau_w}{\rho_f U_\infty H\theta} \qquad (2.54)$$

From the study of steady compressible turbulent boundary layers by Reshotko and Tucker [13], it is likely that for moderate Mach number flow encountered in this problem ($M < 1.5$), the percentage change in the shape factor, i.e. $\frac{1}{H}\frac{\partial H}{\partial t}$, is small compared to the percentage change in momentum thickness, $\frac{1}{\theta}\frac{\partial \theta}{\partial t}$. As a first approximation, therefore, the shape factor, H, is assumed to be a constant. A more rigorous approach would be to derive another auxiliary equation, say moment of momentum

integral [14] to obtain an expression for $\frac{\partial H}{\partial t}$. However, derivation of such an equation for the nonsteady case is extremely complicated and therefore neglected in the present work.

For thin boundary layers, $U_\infty \approx U$; $T_\infty \approx T$ and the film temperature,

$$T_f = \frac{T+T_{w,i}}{2} \tag{2.55}$$

The gas density at the film temperature, ρ_f, can be evaluated from the equation of state (2.6), and the final form is:

$$\rho_f = \frac{(\frac{T}{T_f})\rho_g}{\left[1 + \eta\rho_g(\frac{T}{T_f} - 1)\right]} \tag{2.56}$$

Equation (2.54) finally becomes:

$$\frac{\partial\theta}{\partial t} = -\frac{U}{H}\frac{\partial\theta}{\partial x} + \frac{\tau_w}{\rho_f UH} - \theta\left[\frac{1}{\rho_f}\frac{\partial\rho_f}{\partial t} + \frac{U}{\rho_f H}\frac{\partial\rho_f}{\partial x} + \frac{1}{U}\frac{\partial U}{\partial t} + \frac{(H+2)}{H}\frac{\partial U}{\partial x}\right]$$

$$+ \frac{\delta}{\rho_f UH}\left[\frac{\partial P}{\partial x} + \rho_f\frac{\partial U}{\partial t} + \rho_f U\frac{\partial U}{\partial x}\right] \tag{2.57}$$

The initial condition is: $\theta(x,0) = 0$.

The boundary condition at the piston end is $\theta(L_p,t) = 0$, which is obvious from the fact that all the particles at the piston base are at the full piston velocity all the time. The condition at the tube head end shall be established later.

It is assumed that the entire flow is in the turbulent region and the wall shear stress can be obtained from the Ludwieg-Tillmann

friction factor [6], which was developed from a series of experiments with all types of pressure gradients. The original expression which holds good for incompressible flow with small temperature differences across the boundary layer is:

$$C_f = \frac{\tau_w}{\frac{1}{2}\rho_\infty U_\infty^2} = 0.246 \times 10^{-0.678H} \left(\frac{\rho_\infty U_\infty \theta}{\mu_\infty}\right)^{-0.268} \qquad (2.58)$$

In the present work, the expression is slightly modified by using the fluid properties (ρ, μ) at the film temperature, T_f, instead of the free stream temperature, T_∞, to take into account the effect of property variation across the boundary layer. The expressions for local friction coefficient, C_f, and local shear stress at the tube wall, τ_w, used in the present work are:

$$C_f = 2A \frac{1}{(Re_\theta)^B}$$

$$\tau_w = A \rho_f U^2 \frac{1}{(Re_\theta)^B} \qquad (2.59)$$

where

$$A = \frac{0.123}{10^{0.678H}} \quad ; \qquad B = 0.268; \qquad Re_\theta = \frac{\rho_f U \theta}{\mu_f}$$

Using the above expression for wall shear stress in equation (2.57), and multiplying equation (2.57) by $(1+B)\theta^B$:

$$\frac{\partial \Theta}{\partial t} = -\frac{U}{H}\frac{\partial \Theta}{\partial x} + (1+B)\frac{A}{H}\frac{\mu_f^B}{\rho_f^B}U^{(1-B)}$$

$$-(1+B)\Theta\left[\frac{1}{\rho_f}\frac{\partial \rho_f}{\partial t} + \frac{U}{\rho_f H}\frac{\partial \rho_f}{\partial x} + \frac{1}{U}\frac{\partial U}{\partial t} + \frac{(H+2)}{H}\frac{\partial U}{\partial x}\right]$$

$$+(1+B)\,C_1\,\Theta\left[\frac{1}{\rho_f U}\frac{\partial P}{\partial x} + \frac{1}{U}\frac{\partial U}{\partial t} + \frac{\partial U}{\partial x}\right] \qquad (2.60)$$

where

$$\Theta = \theta^{(1+B)} \qquad \text{or,} \quad \theta = \Theta^{\frac{1}{(1+B)}} \qquad (2.61)$$

and,

$$C_1 = \frac{\delta}{\delta^*}$$

At the tube head end, U = 0 and the equation (2.60) becomes:

$$\frac{\partial \Theta}{\partial t} = -(1+B)\,\Theta\left[\frac{1}{\rho_f}\frac{\partial \rho_f}{\partial t} + \frac{U}{\rho_f H}\frac{\partial \rho_f}{\partial x} + \frac{1}{U}\frac{\partial U}{\partial t} + \frac{(H+2)}{H}\frac{\partial U}{\partial x}\right]$$

$$+(1+B)\,\Theta\,C_1\left[\frac{1}{\rho_f U}\frac{\partial P}{\partial x} + \frac{1}{U}\frac{\partial U}{\partial t} + \frac{\partial U}{\partial x}\right] \qquad (2.62)$$

and at t = 0, Θ = 0. This implies that at the tube head end, θ, i.e. momentum thickness or boundary layer thickness is zero at all times.

The equation (2.60) is applicable to both Case I and II for computing momentum thickness θ, and thence the friction coefficient,

C_f, at each station in the axial direction at each time step.

Heat Transfer Analysis

As the flow is in the turbulent region, the analogy between the momentum transfer and the heat transfer provides the easiest way to determine the heat transfer coefficient, h_i, at the tube wall. Because of its simplicity, Colburn's analogy [7] has been used for Prandtl numbers other than unity as follows:

$$St\ Pr^{2/3} = \frac{C_f}{2}$$

or,

$$h_i = \rho_f U c_p \left(\frac{C_f}{2}\right) / Pr^{2/3} \tag{2.63}$$

where $Pr = \left(\frac{\mu_g c_p}{\kappa_g}\right)$.

The heat transfer in the tube wall is considered as a one-dimensional (radial) unsteady heat conduction problem in a hollow cylinder. Longitudinal heat conduction is neglected because the temperature gradient in the radial direction is expected to be steeper by several order of magnitude than in the axial direction. The differential equation can be written as [15]:

$$\frac{\partial T_w}{\partial t} = \alpha_w \left[\frac{\partial^2 T_w}{\partial r^2} + \frac{1}{r}\frac{\partial T_w}{\partial r}\right] \tag{2.64}$$

The boundary conditions are:

$$\text{at} \quad r = R, \quad \dot{q}_i'' = h_i(T_\infty - T_{w,i}) = -\kappa_w \left.\frac{\partial T_w}{\partial r}\right|_{r=R}$$

$$\text{at} \quad r = R_o, \quad \dot{q}_o'' = h_o(T_{w,o} - T_{amb}) = -\kappa_w \left.\frac{\partial T_w}{\partial r}\right|_{r=R_o} \qquad (2.65)$$

$$\text{at} \quad t = 0, \quad T(r) = T_{amb}$$

It is possible to solve equation (2.64) numerically and obtain the temperature at the inner surface of the tube $T_{w,i}$ at each station along the length of the tube at each time step. The local heat transfer rate to the wall per unit surface area is given by $h_i(T-T_{w,i})$, and integrating over the entire surface and the time, the total heat transfer to the tube wall can be determined. The values of local wall shear stress τ_w, heat transfer coefficient h_i, and inner surface temperature $T_{w,i}$ as calculated from (2.59), (2.63) and (2.64) are used in the one-dimensional analysis for the subsequent time step.

Non-dimensionalization

Before proceeding to the solution technique that can be applied to solve the equations derived so far, it is advantageous to non-dimensionalize the equations to obtain a general solution for the geometrically similar devices with the same initial conditions. The non-dimensionalized parameters are:

Axial distance, $x' = \frac{x}{L_t}$

Pressure, $P' = P/P_o$

Temperature, $T' = T/T_o$

Density, $\rho' = \rho/\rho_{g_o}$

Velocity, $U' = U/U_o \qquad U_o = \sqrt{P_o/\rho_{g_o}}$

Time, $t' = \frac{U_o t}{L_t}$

Linear speed of burning, $r_b' = r_b/U_o$ (2.66)

It can be noted that:

$$\dot{v}_{d_s} = \frac{U_o}{L_t}\left[\left(\frac{S_{b_t}}{Ap}\right)\frac{\nu_s r_b'}{\int_o^{L_p'} \nu_s dx'}\right] = \frac{U_o}{L_t}\ \dot{v}_{d_s}' \tag{2.67}$$

$$h_g = \frac{P_o}{\rho_{g_o}}\left[\frac{P'(\gamma - n\rho_{g_o}\rho_g')}{\rho_g'(\gamma-1)}\right] = \frac{P_o}{\rho_{g_o}}\ h_g' \tag{2.68}$$

$$W = \frac{R_g T_o}{(\gamma-1)} = \frac{P_o}{\rho_{g_o}}\left[\frac{\rho_{g_o}}{P_o}\ \frac{R_g T_o}{(\gamma-1)}\right] = \frac{P_o}{\rho_{g_o}}\ W' \tag{2.69}$$

$$\tau_w = A\,\rho_f U^2 \frac{1}{(Re_\theta)^B} = P_o\ A\rho_f' U'^2 \frac{1}{(Re_\theta)^B} \tag{2.70}$$

and, $n\rho_{g_o}$ is a constant non-dimensional quantity.

Finally, non-dimensional form of the conservation equations are:

Case I

Continuity of solids:

$$\frac{\partial \nu_s}{\partial t'} + U'\frac{\partial \nu_s}{\partial x'} + \nu_s \frac{\partial U'}{\partial x'} + \dot{v}_{d_s}' = 0 \tag{2.71}$$

Continuity of gases:

$$\frac{\partial \rho_g'}{\partial t'} + U' \frac{\partial \rho_g'}{\partial x'} + \frac{\rho_g'}{(1-\nu_s)} \frac{\partial U'}{\partial x'} = \frac{(\rho_s'-\rho_g')}{(1-\nu_s)} \dot{v}_{d_s}' \tag{2.72}$$

Momentum:

$$\frac{\partial U'}{\partial t'} + U' \frac{\partial U'}{\partial x'} = - \frac{1}{\rho_m'} \frac{\partial P'}{\partial x'} - D_1' \frac{\rho_f' U'^2}{\rho_m'} \frac{1}{(Re_\theta)^B} \tag{2.73}$$

Energy:

$$\frac{\partial P'}{\partial t'} + U' \frac{\partial P'}{\partial x'} + B_I' \frac{\partial U'}{\partial x'} = C_I' \dot{v}_{d_s}'$$

$$- D_2' E' h_i (T-T_{w,i}) + D_1' E' \frac{\rho_f' U'^3}{(Re_\theta)^B} \tag{2.74}$$

where,

$$B_I' = \frac{\gamma P'}{(1-\nu_s)(1-\eta \rho_{g_o} \rho_g')} \tag{2.75}$$

$$C_I' = \frac{\gamma P' (\rho_s'-\rho_g') + (\gamma-1)\rho_s' \rho_g' (W' + \frac{P'}{\rho_s'} - h_g')}{\rho_g' \{(1-\nu_s)(1-\eta \rho_{g_o} \rho_g')\}} \tag{2.76}$$

$$E' = \frac{(\gamma-1)}{(1-\nu_s)(1-\eta \rho_{g_o} \rho_g')} \tag{2.77}$$

$$D_1' = 2A(\frac{L_t}{R}) \tag{2.78}$$

$$D_2' = 2(\frac{L_t}{R}) \frac{J}{P_o U_o} \tag{2.79}$$

Equation of state:

$$T' = \frac{P'}{\rho_g'} \frac{(1-\eta\rho_{g_o}\rho_g')}{(1-\eta\rho_{g_o})} \tag{2.80}$$

Characteristic equations:

Along η', ξ' characteristic, i.e. $\frac{dt'}{dx'} = \frac{1}{U' \pm \sqrt{B_I'/\rho_m'}}$,

$$\Delta P' \pm \rho_m'\sqrt{B_I'/\rho_m'}\ \Delta U' = C_I'\dot{v}_{d_s}'\ \Delta t - D_2'E'h_i(T-T_{w,i})\Delta t'$$

$$+ D_1'\left[E'U' \mp \sqrt{B_I'/\rho_m'}\right]\frac{\rho_f'U'^2}{(Re_\theta)^B}\Delta t' \tag{2.81}$$

Along a particle path, i.e. $\frac{dt'}{dx'} = \frac{1}{U'}$,

$$\Delta\rho_g' = G'\Delta P' + H_I'\dot{v}_{d_s}'\Delta t' + D_2'\left[\frac{(\gamma-1)\rho_g'}{(1-\nu_s)\gamma P'}\right]h_1(T-T_{w,i})\Delta t'$$

$$- D_1'\left[\frac{(\gamma-1)\rho_g'}{(1-\nu_s)\gamma P'}\right]\frac{\rho_g'U'^3}{(Re_\theta)^B}\Delta t' \tag{2.82}$$

where,

$$G' = \frac{\rho_g'(1-\eta\rho_{g_o}\rho_g')}{\gamma P'} \tag{2.83}$$

$$H_I' = \frac{(\gamma-1)\rho_s'\rho_g'(h_g' - W' - \frac{P'}{\rho_s'})}{(1-\nu_s)\gamma P'} \tag{2.84}$$

Again along a particle path, i.e. $\frac{dt'}{dx'} = \frac{1}{U'}$,

$$\Delta\nu_s = \frac{\nu_s(1-\nu_s)}{\rho_g'}\ \Delta\rho_g' - \frac{\rho_m'}{\rho_g'}\ \dot{v}_{d_s}'\Delta t' \qquad (2.85)$$

Case II

Continuity of solids:

$$\frac{\partial\nu_s}{\partial t'} + \dot{v}_{d_s}' = 0 \qquad (2.86)$$

Continuity of gases:

$$\frac{\partial\rho_g'}{\partial t'} + U'\frac{\partial\rho_g'}{\partial x'} + \rho_g'\frac{\partial U'}{\partial x'} = \frac{(\rho_s'-\rho_g')}{(1-\nu_s)}\ \dot{v}_{d_s}' + \frac{\rho_g'U'}{(1-\nu_s)}\ \frac{\partial\nu_s}{\partial x'} \qquad (2.87)$$

Momentum:

$$\frac{\partial U'}{\partial t'} + U'\frac{\partial U'}{\partial x'} = -\frac{1}{\rho_g'}\ \frac{\partial P'}{\partial x'} - \frac{\rho_s'U'}{(1-\nu_s)\rho_g'}\ \dot{v}_{d_s}' - D_1'\frac{\rho_f'U'^2}{(1-\nu_s)\rho_g'(Re_\theta)^B} \qquad (2.88)$$

Energy:

$$\frac{\partial P'}{\partial t'} + U'\frac{\partial P'}{\partial x'} + B_{II}'\frac{\partial U'}{\partial x'} = C_{II}'\dot{v}_{d_s}' + \frac{B_{II}'U'}{(1-\nu_s)}\ \frac{\partial\nu_s}{\partial x'}$$

$$- D_2'E'h_i(T-T_{w,i}) + D_1'E'\frac{\rho_f'U'^3}{(Re_\theta)^B} \qquad (2.89)$$

where,

$$B_{II}' = \frac{\gamma P'}{(1-\eta\rho_{g_o}\rho_g')} \tag{2.90}$$

$$C_{II}' = \frac{\gamma P'(\rho_s'-\rho_g') + (\gamma-1)\rho_s'\rho_g'(W' + \frac{P'}{\rho_s'} + \frac{U'^2}{2} - h_g')}{\rho_g'\{(1-\nu_s)(1-\eta\rho_{g_o}\rho_g')\}} \tag{2.91}$$

E', D_1', and D_2' are given by equations (2.77), (2.78), (2.79), respectively. The equation of state for the gas is also same as equation (2.80).

Characteristic equations:

Along η', ξ' characteristic, i.e. $\frac{dt'}{dx'} = \frac{1}{U' \pm \sqrt{B_{II}'/\rho_g'}}$,

$$\Delta P' \pm \rho_g' \sqrt{B_{II}'/\rho_g'}\,\Delta U' = \frac{B_{II}'U'}{(1-\nu_s)(U' \pm \sqrt{B_{II}'/\rho_g'})}\Delta\nu_s$$

$$+ \left[C_{II}' \mp \sqrt{B_{II}/\rho_g'}\,\frac{\rho_s'U'}{(1-\nu_s)} + \frac{B_{II}'U'}{(1-\nu_s)(U' \pm \sqrt{B_{II}'/\rho_g'})}\right]\dot{v}_{d_s}'\Delta t'$$

$$- D_2'E'h_i(T-T_{w,i})\Delta t'$$

$$+ D_1'\left[E'U' \mp \frac{1}{(1-\nu_s)}\sqrt{B_{II}'/\rho_g'}\right]\frac{\rho_f'U'^2}{(Re_\theta)^B}\Delta t' \tag{2.92}$$

Along a particle path, i.e. $\frac{dt'}{dx'} = \frac{1}{U'}$,

$$\Delta\rho_g' = G'\,\Delta P' + H_{II}'\,\dot{v}_{d_s}'\,\Delta t' + D_2'\left[\frac{(\gamma-1)\rho_g'}{(1-\nu_s)\gamma P'}\right] h_i(\dot{T}-T_{w,i})\Delta t'$$

$$- D_1'\left[\frac{(\gamma-1)\rho_g'}{(1-\nu_s)\gamma P'}\right]\frac{\rho_g' U'^3}{(Re_\theta)^B}\,\Delta t' \qquad (2.93)$$

where

$$H_{II}' = \frac{(\gamma-1)\rho_s'\rho_g'(h_g' - W' - \frac{P'}{\rho_s'} - \frac{U'^2}{2})}{(1-\nu_s)\gamma P'} \qquad (2.94)$$

Boundary Layer Equation

Using the non-dimensional momentum thickness, $\theta' = \frac{\theta}{R}$ and all the non-dimensionalized parameters listed in (2.66), the boundary layer equation (2.60) becomes:

$$\frac{\partial\Theta'}{\partial t'} = -\frac{U'}{H}\frac{\partial\Theta'}{\partial x'} + (1+B)\frac{A}{H}\left(\frac{L_t}{R}\right)\left(\frac{\mu_f}{\rho_{g_o} U_o R}\right)^B \frac{U'^{(1-B)}}{\rho_f'^B}$$

$$- (1+B)\Theta'\left[\frac{1}{\rho_f'}\frac{\partial\rho_f'}{\partial t'} + \frac{U'}{\rho_f' H}\frac{\partial\rho_f'}{\partial x'} + \frac{1}{U'}\frac{\partial U'}{\partial t'} + \frac{H+2}{H}\frac{\partial U'}{\partial x'}\right]$$

$$+ (1+B)C_1\Theta'\left[\frac{1}{\rho_f' U'}\frac{\partial P'}{\partial x'} + \frac{1}{U'}\frac{\partial U'}{\partial t'} + \frac{\partial U'}{\partial x'}\right] \qquad (2.95)$$

where

$$\Theta' = \theta'^{(1+B)} \qquad \text{or} \qquad \theta' = \Theta'^{\frac{1}{1+B}} \qquad (2.96)$$

Now U', ρ_g' and P' are taken from the one-dimensional solution and ρ_f' is obtained from the non-dimensional form of equation (2.56), i.e.:

$$\rho_f' = \frac{(\frac{2T}{T+T_{w,i}})\rho_g'}{\left[1+n\rho_{g_o}\rho_g'(\frac{2T}{T+T_{w,l}} - 1)\right]} \qquad (2.97)$$

CHAPTER III

SOLUTION PROCEDURE

Solution of Interior Points

As there is no analytical solution to the set of coupled non-linear partial differential equations derived in the previous chapter, numerical techniques have been used to solve the conservation equations along with the boundary layer momentum integral equation and the equation of state of the combustion gas. The differential equations are written in finite difference form and MacCormack's version [16] of Lax-Wendroff two step method [17] is followed. The procedure is shown by an example below:

Let,

$$\frac{\partial u}{\partial t} = -c \frac{\partial u}{\partial x} \tag{3.1}$$

where c is a constant.

Equation (3.1) can be written as,

$$\begin{aligned} \tilde{u}_j^{n+1} &= u_j^n - c \frac{\Delta t}{\Delta x} (u_{j+1}^n - u_j^n) \\ \bar{u}_j^{n+1} &= u_j^n - c \frac{\Delta t}{\Delta x} (\tilde{u}_j^{n+1} - \tilde{u}_{j-1}^{n+1}) \end{aligned} \tag{3.2}$$

and finally,

$$u_j^{n+1} = \tfrac{1}{2} \left[\tilde{u}_j^{n+1} + \bar{u}_j^{n+1} \right]$$

where $\tilde{u}_j^{n+1}$ and $\bar{u}_j^{n+1}$ are the first and second estimated value of u_j^{n+1}. The integer n, and j denote the time and axial position of a nodal point shown in Figure 2. If c is a variable, i.e. c(u), $\tilde{c}(\tilde{u})_j^{n+1}$ is used in the second estimation of u_j^{n+1}. It can be recognized that both forward and backward space derivatives have been taken into account.

Case I

Using the MacCormack scheme, the non-dimensionalized conservation equations, i.e. (2.71) through (2.74) can be written as:

$$\tilde{\nu}_{s_j}^{n+1} = \nu_{s_j}^{n} - U'^{n}_{j} \frac{\Delta t'}{\Delta x'_o} (\nu_{s_{j+1}}^{n} - \nu_{s_j}^{n}) - \nu_{s_j}^{n} \frac{\Delta t'}{\Delta x'_o} (U'^{n}_{j+1} - U'^{n}_{j}) - \left[\dot{v}_{d_s}'\right]_j^n \Delta t' \tag{3.3}$$

$$\tilde{\rho}_{g_j}'^{n+1} = \rho_{g_j}'^{n} - U'^{n}_{j} \frac{\Delta t'}{\Delta x'_o} (\rho_{g_{j+1}}'^{n} - \rho_{g_j}'^{n}) - \frac{\rho_{g_j}'^{n}}{(1-\nu_{s_j}^{n})} \frac{\Delta t'}{\Delta x'_o} (U'^{n}_{j+1} - U'^{n}_{j}) + \frac{(\rho_s' - \rho_{g_j}'^{n})}{(1-\nu_{s_j}^{n})} \left[\dot{v}_{d_s}'\right]_j^n \Delta t' \tag{3.4}$$

$$\tilde{U}'^{n+1}_{j} = U'^{n}_{j} - U'^{n}_{j} \frac{\Delta t'}{\Delta x'_o} (U'^{n}_{j+1} - U'^{n}_{j}) - \frac{1}{\rho_{m_j}'^{n}} \frac{\Delta t'}{\Delta x'_o} (P'^{n}_{j+1} - P'^{n}_{j}) - ULF_j^n \Delta t' \tag{3.5}$$

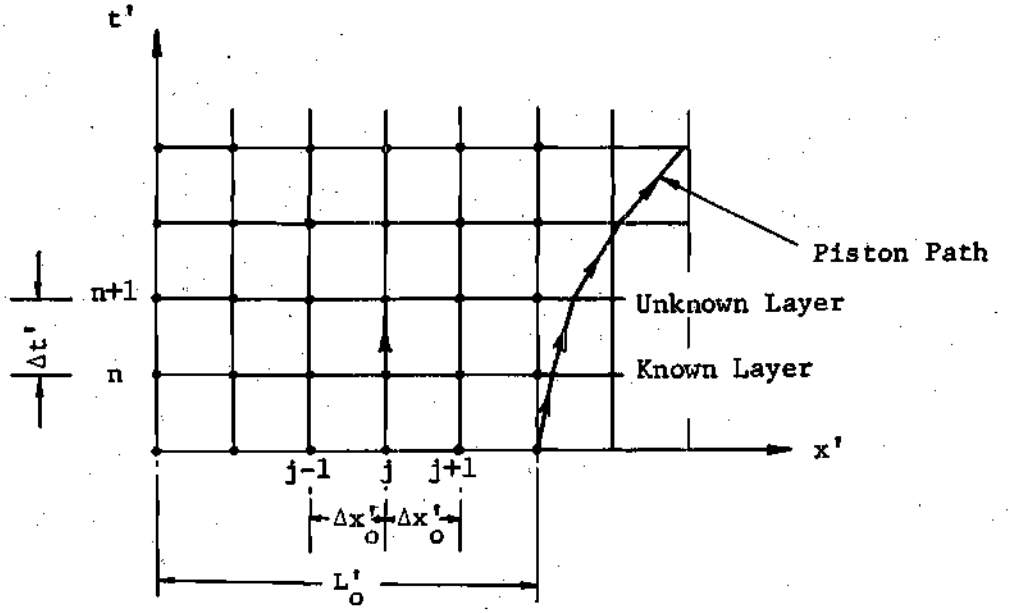

Figure 2. Numerical Scheme for Interior Points

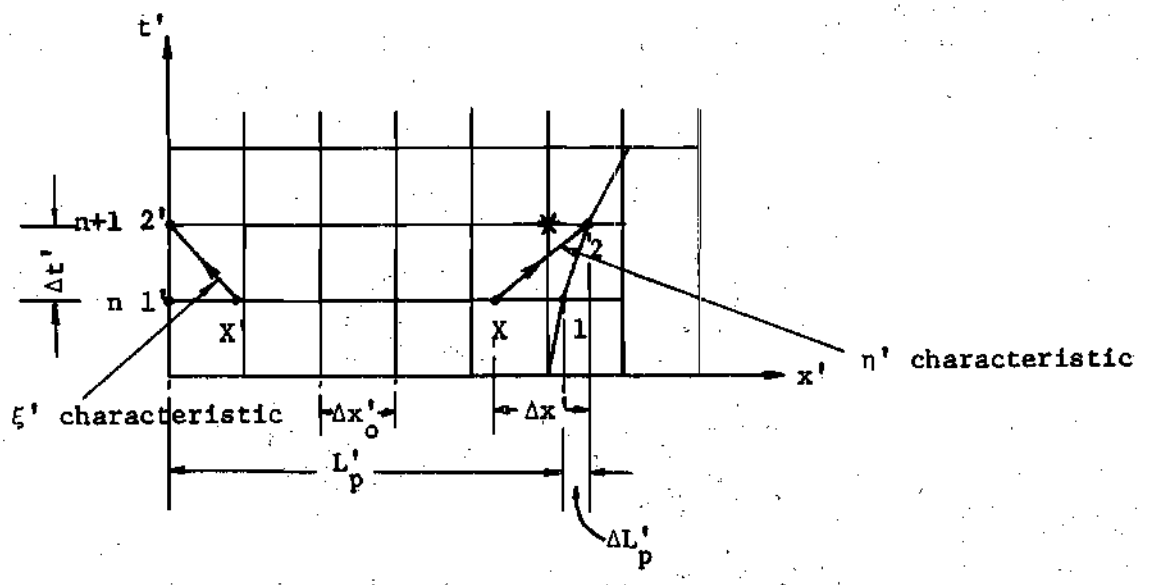

Figure 3. Scheme for End Points.

$$\tilde{P}'^{n+1}_j = P'^{n}_j - U'^{n}_j \frac{\Delta t'}{\Delta x'_o} (P'^{n}_{j+1} - P'^{n}_j) - B'^{n}_{I\,j} \frac{\Delta t'}{\Delta x'_o} (U'^{n}_{j+1} - U'^{n}_j)$$

$$+ C'^{n}_{I\,j} \dot{v}'^{n}_{d_s\,j} \Delta t' - E'^{n}_j D'_2 \dot{q}''^{n}_j \Delta t'$$

$$+ E'^{n}_j PGF^{n}_j \Delta t' \qquad (3.6)$$

where,

$$\dot{v}'_{d_s} = \frac{S_{b_t}}{A_p} \frac{\nu_s r'_b}{\int_o^{L'_p} \nu_s dx'} \qquad (3.7)$$

$$\dot{q}'' = h_i (T - T_{w,i}) \qquad (3.8)$$

$$ULF = D'_1 \frac{\rho'_f U'^2}{\rho'_m} \frac{1}{(Re_\theta)^B} \qquad (3.9)$$

$$PGF = D'_1 \frac{\rho'_f U'^3}{(Re_\theta)^B} \qquad (3.10)$$

Thus, for all the nodal points (except the last point adjacent to the piston base) the first estimation regarding the ballistic properties after a time increment $\Delta t'$ is made by knowing the present values of the properties at the point of interest and at its forward nodal point. The second estimation is done as follows:

$$\tilde{\tilde{\nu}}_{s_j}^{n+1} = \nu_{s_j}^{n} - \tilde{U}'^{,n+1}_{j} \frac{\Delta t'}{\Delta x'_o} (\tilde{\nu}_{s_j}^{n+1} - \tilde{\nu}_{s_{j-1}}^{n+1})$$

$$- \tilde{\nu}_{s_j}^{n+1} \frac{\Delta t'}{\Delta x'_o} (\tilde{U}'^{,n+1}_{j} - \tilde{U}'^{,n+1}_{j-1}) - \dot{v}'^{\,n}_{d_{s_j}} \Delta t' \qquad (3.11)$$

$$\tilde{\tilde{\rho}}'^{,n+1}_{g_j} = \rho'^{,n}_{g_j} - \tilde{U}'^{,n+1}_{j} \frac{\Delta t'}{\Delta x'_o} (\tilde{\rho}'^{,n+1}_{g_j} - \tilde{\rho}'^{,n+1}_{g_{j-1}})$$

$$- \frac{\tilde{\rho}'^{,n+1}_{g_j}}{(1-\tilde{\nu}_{s_j}^{n+1})} \frac{\Delta t'}{\Delta x'_o} (\tilde{U}_j^{n+1} - \tilde{U}'^{,n+1}_{j-1}) + \frac{(\rho'_s - \tilde{\rho}'^{,n+1}_{g_j})}{(1-\tilde{\nu}_{s_j}^{n+1})} \dot{v}'^{\,n}_{d_{s_j}} \Delta t' \qquad (3.12)$$

$$\tilde{\tilde{U}}'^{,n+1}_{j} = U'^{,n}_{j} - \tilde{U}'^{,n+1}_{j} \frac{\Delta t'}{\Delta x'_o} (\tilde{U}'^{,n+1}_{j} - \tilde{U}'^{,n+1}_{j-1})$$

$$- \frac{1}{\tilde{\rho}'^{,n+1}_{m_j}} \frac{\Delta t'}{\Delta x'_o} (\tilde{P}'^{,n+1}_{j} - \tilde{P}'^{,n+1}_{j-1}) - ULF_j^{n} \Delta t' \qquad (3.13$$

$$\tilde{\tilde{P}}'^{,n+1}_{j} = P'^{,n}_{j} - \tilde{U}'^{,n+1}_{j} \frac{\Delta t'}{\Delta x'_o} (\tilde{P}'^{,n+1}_{j} - \tilde{P}'^{,n+1}_{j-1})$$

$$- \tilde{B}'^{\,n+1}_{I_j} \frac{\Delta t'}{\Delta x'_o} (\tilde{U}'^{,n+1}_{j} - \tilde{U}'^{,n+1}_{j-1}) + \tilde{C}'^{\,n+1}_{I_j} \dot{v}'^{\,n}_{d_{s_j}} \Delta t'$$

$$- \tilde{E}'^{\,n+1}_{j} D'_2 \dot{q}''^{\,n}_{j} \Delta t' + \tilde{E}'^{\,n+1}_{j} PGF_j^{n} \Delta t' \qquad (3.14)$$

and finally,

$$\nu_{s_j}^{n+1} = \tfrac{1}{2}\left[\tilde{\nu}_{s_j}^{n+1} + \tilde{\tilde{\nu}}_{s_j}^{n+1}\right] \qquad (3.15)$$

$$\rho'^{n+1}_{g_j} = \tfrac{1}{2}\left[\tilde{\rho}'^{n+1}_{g_j} + \rho'^{n+1}_{g_j}\right] \tag{3.16}$$

$$U'^{n+1}_{j} = \tfrac{1}{2}\left[\tilde{U}'^{n+1}_{j} + \tilde{U}'^{n+1}_{j}\right] \tag{3.17}$$

$$P'^{n+1}_{j} = \tfrac{1}{2}\left[\tilde{P}'^{n+1}_{j} + \tilde{P}'^{n+1}_{j}\right] \tag{3.18}$$

From the equation of state (2.80):

$$T'^{n+1}_{j} = \frac{P'^{n+1}_{j}}{\rho'^{n+1}_{g_j}} \frac{(1-\eta\rho_{g_o}\rho'^{n+1}_{g_j})}{(1-\eta\rho_{g_o})} \tag{3.19}$$

Similarly, to calculate the momentum thickness at a nodal point after increment $\Delta t'$, equation (2.95) is written as:

$$\tilde{\theta}'^{n+1}_{j} = \theta'^{n}_{j} - \frac{U'^{n}_{j}}{H}\frac{\Delta t'}{\Delta x'_o}(\theta'^{n}_{j+1} - \theta'^{n}_{j}) + D'_3 \frac{\left[U'^{n}_{j}\right]^{(1-B)}}{\left[\rho'^{n}_{f_j}\right]^{B}}\Delta t'$$

$$- (1+B)\,\theta'^{n}_{j}\left[\frac{1}{\rho'^{n}_{f_j}}(\tilde{\rho}'^{n+1}_{f_j} - \rho'^{n}_{f_j}) + \frac{U'^{n}_{j}}{H\rho'^{n}_{f_j}}\frac{\Delta t'}{\Delta x'_o}(\rho'^{n}_{f_{j+1}} - \rho'^{n}_{f_j})\right.$$

$$\left. + \frac{(1-C_1)}{U'^{n}_{j}}(\tilde{U}'^{n+1}_{j} - U'^{n}_{j}) + \left(\frac{H+2}{H} - C_1\right)\frac{\Delta t'}{\Delta x'_o}(U'^{n}_{j+1} - U'^{n}_{j})\right]$$

$$+ (1+B)\,\theta'^{n}_{j}\frac{C_1}{\rho'^{n}_{f_j}U'^{n}_{j}}\frac{\Delta t'}{\Delta x'_o}(P'^{n}_{j+1} - P'^{n}_{j}) \tag{3.20}$$

where

$$D_3' = (1+B)\frac{A}{H}\left(\frac{L_t}{R}\right)\left(\frac{\mu_{f_j}^{n}}{\rho_{g_o} U_o R}\right)^{B} \tag{3.21}$$

taking

$$\mu_f = \mu_{g_o}\left(\frac{T_f}{T_o}\right)^{m}, \tag{3.22}$$

m being a suitable constant.

The densities $\tilde{\rho}_{f_j}^{',n}$ and $\tilde{\rho}_{f_j}^{',n+1}$ are calculated from equation (2.97) with the assumption,

$$\left(\frac{\tilde{T}}{T_f}\right)_j^{n+1} \simeq \left(\frac{T}{T_f}\right)_j^{n}$$

again,

$$\begin{aligned}
\tilde{\tilde{\Theta}}_j^{',n+1} = \Theta_j^{',n} &- \frac{\tilde{U}_j^{',n+1}}{H}\frac{\Delta t'}{\Delta x_o'}\left(\tilde{\Theta}_j^{',n+1} - \tilde{\Theta}_{j-1}^{',n+1}\right) + D_3'\frac{\left(\tilde{U}_j^{',n+1}\right)^{(1-B)}}{\left(\tilde{\rho}_{f_j}^{',n+1}\right)^{B}}\Delta t' \\
&- (1+B)\,\tilde{\Theta}_j^{',n+1}\left[\frac{1}{\tilde{\rho}_{f_j}^{',n+1}}\left(\tilde{\rho}_{f_j}^{',n+1} - \rho_{f_j}^{',n}\right) + \frac{\tilde{U}_j^{',n+1}}{H\tilde{\rho}_{f_j}^{',n+1}}\frac{\Delta t'}{\Delta x_o'}\left(\tilde{\rho}_{f_j}^{',n+1} - \tilde{\rho}_{f_{j-1}}^{',n+1}\right)\right. \\
&\left. + \frac{(1-C_1)}{\tilde{U}_j^{',n+1}}\left(\tilde{\tilde{U}}_j^{',n+1} - U_j^{',n}\right) + \left\{\frac{H+2}{H} - C_1\right\}\frac{\Delta t'}{\Delta x_o'}\left(\tilde{U}_j^{',n+1} - \tilde{U}_{j-1}^{',n+1}\right)\right] \\
&+ (1+B)\,\tilde{\Theta}_j^{',n+1}\frac{C_1}{\tilde{\rho}_{f_j}^{',n+1}\tilde{U}_j^{',n+1}}\frac{\Delta t'}{\Delta x_o'}\left(\tilde{P}_j^{',n+1} - \tilde{P}_{j-1}^{',n+1}\right)
\end{aligned} \tag{3.23}$$

finally,

$$\theta'^{n+1}_j = \tfrac{1}{2}\left[\tilde{\theta}'^{n+1}_j + \tilde{\tilde{\theta}}'^{n+1}_j\right] \tag{3.24}$$

and,

$$\theta'^{n+1}_j = \left[\Theta'^{n+1}_j\right]^{\frac{1}{(1+B)}} \tag{3.25}$$

The heat transfer coefficient after time $\Delta t'$, $h_{i_j}^{n+1}$ can be calculated using equation (2.59) and (2.63). The new inner surface temperature T_{w,i_j}^{n+1} is obtained from the solution of equation (2.64) using the mean heat transfer coefficient,

$$h_m = \frac{h_{i_j}^{n} + h_{i_j}^{n+1}}{2}$$

The same procedure is followed for Case II starting with appropriate conservation equations, namely equations (2.86) through (2.89), same equation of state (2.80) and boundary layer momentum equation (2.95). The only points of differences are: (1) no solid particles beyond L'_o and (2) the burning rate r_b is chosen corresponding to the average pressure in the space between the tube head end and L_o.

Solution for Boundary Points

It has been stated earlier that to calculate the ballistic properties at the tube head end and at the piston base end, one needs the characteristic equations. Typical characteristic directions are shown in Figure 3. Let, at any time t', the piston be at position 1 with

velocity $U'_{p,1}$. Its position and velocity after time $\Delta t'$ can be calculated by using equations (2.18) and (2.19) as follows:

$$U'_{p,2} = U'_{p,1} + \frac{1}{U_o} (a_p \, \Delta t)$$

and

$$\Delta L'_p = \frac{1}{L_t} \left[U_{p,1} \, \Delta t + \tfrac{1}{2} a_p \, (\Delta t)^2 \right] \tag{3.26}$$

where,

$$a_p = \frac{P_{p,m} \, A_p}{M_p} \qquad (P_{p,m} \text{ is mean of } P_1 \text{ and } P_2)$$

Then the η'-characteristic is traced back using the appropriate expression:

$$\begin{aligned} &\text{for Case I:} \quad \Delta x' = (U' + \sqrt{B'_I/\rho'_m}) \, \Delta t' \\ &\text{for Case II:} \quad \Delta x' = (U' + \sqrt{B'_{II}/\rho'_g}) \, \Delta t' \end{aligned} \tag{3.27}$$

The point X is thus determined and all the properties are interpolated between the nodal points in each side. Pressure at point 2 is calculated by applying equation (2.81) for Case I, and equation (2.92) for Case II,

$$\text{for Case I,} \quad P'_2 = P'_X - \rho'_m \sqrt{\frac{B'_I}{\rho'_m}} \, (U'_{P,2} - U'_X) + C'_I \, \dot{v}'_{d_s} \, \Delta t'$$

$$- D'_2 E' h_i (T - T_{w,i}) \Delta t' + D'_1 \left[E' U' - \sqrt{B'_I/\rho'_m} \right] \frac{\rho'_f U'^2}{(Re_\theta)^B} \, \Delta t' \tag{3.28}$$

for Case II, $P_2' = P_X' - \rho_g' \sqrt{B_{II}'/\rho_g'}\,(U_{p,2}'-U_X')$

$$+ \frac{B_{II}'U'}{(1-\nu_s)(U'+\sqrt{B_{II}'/\rho_g'})}(\nu_{s,2}-\nu_{s,X})$$

$$+ \left[C_{II}' - \sqrt{B_{II}'/\rho_g'}\,\frac{\rho_s'U'}{(1-\nu_s)} + \frac{B_{II}'U'}{(1-\nu_s)(U'+\sqrt{B_{II}'/\rho_g'})}\right]\dot{v}_{d_s}'\Delta t'$$

$$- D_2'E'h_i(T-T_{w,i})\Delta t' + D_1'\left[E'U' - \frac{1}{(1-\nu_s)}\sqrt{B_{II}'/\rho_g'}\right]$$

$$\frac{\rho_f'U'^2}{(Re_\theta)^B}\Delta t' \qquad (3.29)$$

The gas density and volume fraction of solids at the new base point 2 are determined from characteristic equations along a particle path as follows:

for Case I and II,

$$\rho_{g,2}' = \rho_{g,1}' + G'(P_2'-P_1') + H_{I,II}'\dot{v}_{d_s}'\Delta t' \qquad (3.30)$$

for Case I,

$$\nu_{s,2} = \nu_{s,1} + \frac{\nu_s(1-\nu_s)}{\rho_g'}(\rho_{g,2}'-\rho_{g,1}') - \frac{\rho_m'}{\rho_g'}\dot{v}_{d_s}'\Delta t' \qquad (3.31)$$

for Case II,

$$\nu_{s,2} = 0 \qquad (3.32)$$

For both points 1 and 2, the momentum thickness is zero, which implies that both friction factor and film heat transfer coefficient at point 1 and 2 are infinitely large. Therefore, the last two terms of equations (2.82) and (2.93) have been deleted while writing the equation (3.30). For the same reason, in equations (3.28) and (3.29) the values for $h_i(T-T_{w,i})$ and $\frac{\rho_f' U'^2}{(Re_\theta)^B}$ are taken corresponding to the nodal point adjacent to the first base point 1. All the coefficients used in equations (3.27) through (3.31) are mean values between point 2 and X or point 2 and 1 depending on the characteristic used. The properties at point 2 are first assumed to be the same as point 1 and then iteration is carried on until the values converge within the specified limit.

For the tube head end,

$$U_1' = U_2' = 0 \tag{3.33}$$

and the momentum thickness and heat transfer coefficient are also zero.

The ξ'-characteristic is traced by using,

$$\begin{aligned} &\text{for Case I:} \quad \Delta x' = (U' - \sqrt{B_I'/\rho_m'})\,\Delta t' \\ &\text{for Case II:} \quad \Delta x' = (U' - \sqrt{B_{II}'/\rho_g'})\,\Delta t' \end{aligned} \tag{3.34}$$

By knowing the properties at X' and 1', properties at point 2' are obtained in the following manner:

Case I

$$P'_{2'} = P'_{X'} + \rho'_m \sqrt{B'_I/\rho'_m}\,(0 - U'_{X'}) + C'_I\,\dot{v}_{d_s}{}'\,\Delta t' - D'_2 E'\,h_i(T-T_{w,i})\Delta t'$$

$$+ D'_1\left[E'U' + \sqrt{B'_I/\rho'_m}\right]\frac{\rho'_f U'^2}{(Re_\theta)^B}\,\Delta t' \qquad (3.35)$$

$$\rho'_{g,2'} = \rho'_{g,1'} + G'\,(P'_{2'} - P'_{1'}) + H'_I\,\dot{v}_{d_s}{}'\,\Delta t' \qquad (3.36)$$

$$\nu_{s,2'} = \nu_{s,1'} + \frac{\nu_s(1-\nu_s)}{\rho'_g}\,(\rho'_{g,2'}-\rho'_{g,1'}) - \frac{\rho'_m}{\rho'_g}\,\dot{v}_{d_s}{}'\,\Delta t' \qquad (3.37)$$

Case II

$$P'_{2'} = P'_{X'} + \rho'_g\sqrt{B'_{II}/\rho'_g}\,(0-U'_{X'}) + \frac{B'_{II}U'}{(1-\nu_s)(U'-\sqrt{B'_{II}/\rho'_g})}\,(\nu_{s,2'}-\nu_{s,1'})$$

$$+ \left[C'_{II} + \sqrt{B'_{II}/\rho'_g}\,\frac{\rho'_s U'}{(1-\nu_s)} + \frac{B'_{II}U'}{(1-\nu_s)(U'-\sqrt{B'_{II}/\rho'_g})}\right]\dot{v}_{d_s}{}'\,\Delta t'$$

$$- D'_2 E' h_i(T-T_{w,i})\Delta t' + D'_1\left[E'U' + \frac{1}{(1-\nu_s)}\sqrt{B'_{II}/\rho'_g}\right]\frac{\rho'_f U'^2}{(Re_\theta)^B}\,\Delta t' \qquad (3.38)$$

and from (2.86),

$$\nu_{s,2'} = \nu_{s,1'} - \dot{v}_{d_s}{}'\,\Delta t' \qquad (3.39)$$

The expression for $\rho'_{g,2'}$ is obtained by replacing H'_I by H'_{II} in equation (3.36).

The iteration procedure for the tube head end is the same as that for the piston base end stated earlier.

The properties at the nodal point(s) adjacent to the base point (shown by * in Figure 3), which cannot be calculated from the Lax-Wendroff method are determined by linear interpolation between the piston base point and the nearest point where properties have been calculated from the Lax-Wendroff method.

It is noted that the spatial interval $\Delta x_o'$ is fixed for the entire solution and can be chosen arbitrarily depending upon the desired accuracy. But, for the stability of the Law-Wendroff solution, the time interval $\Delta t'$ must be chosen such that $\frac{\Delta t'}{\Delta x_o'}$ nowhere exceeds the slope of any characteristic [17]. This implies that at every time step,

$$\Delta t' \leq \frac{\Delta x_o'}{|U'| + \sqrt{B_I'/\rho_m'}} \qquad \text{for Case I}$$

$$\Delta t' \leq \frac{\Delta x_o'}{|U'| + \sqrt{B_{II}'/\rho_g'}} \qquad \text{for Case II} \tag{3.40}$$

Therefore, before selecting a new time interval, the right hand side of (3.40) is calculated at each nodal point (including the end points) and then the lowest value is chosen as the next time step.

Determination of Wall Temperature

The differential equation (2.64) in finite difference form can be written as (see Figure 4 for notations):

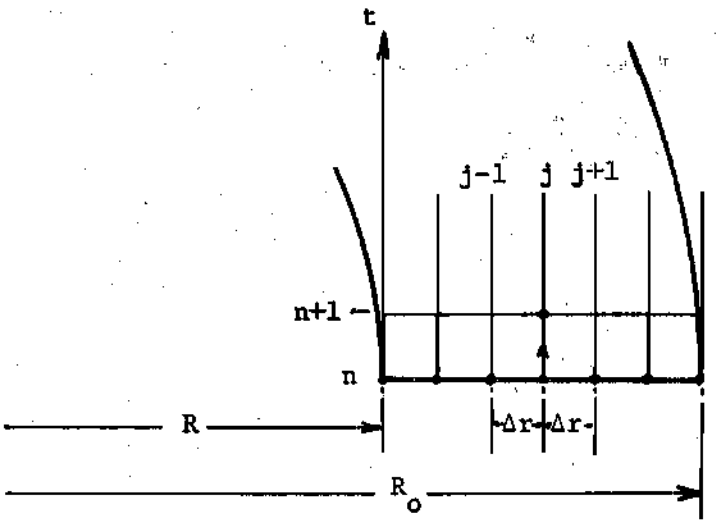

Figure 4. Numerical Scheme for Determination of Tube Wall Temperature.

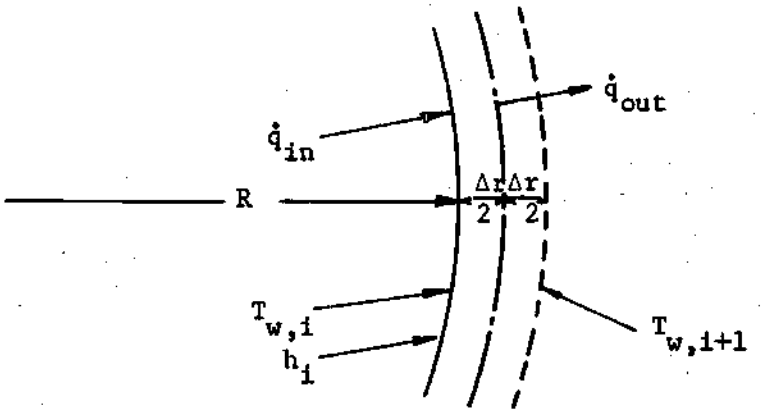

Figure 5. Heat Balance for a Thin Circular Element at the Inside Surface of the Tube

$$\frac{T^{n+1}_{w,j} - T^{n}_{w,j}}{\Delta t} = \alpha_w \left[\frac{T^{n}_{w,j+1} + T^{n}_{w,j-1} - 2T^{n}_{w,j}}{(\Delta r)^2} + \frac{1}{r_j} \frac{T^{n}_{w,j+1} - T^{n}_{w,j-1}}{2\Delta r} \right]$$

or,

$$T^{n+1}_{w,j} = \left[1 - \frac{2\alpha_w \Delta t}{(\Delta r)^2} \right] T^{n}_{w,j} + \frac{2\alpha_w \Delta t}{(\Delta r)^2} \left[\tfrac{1}{2} + \frac{\Delta r}{4r_j} \right] T^{n}_{w,j+1}$$

$$+ \frac{2\alpha_w \Delta t}{(\Delta r)^2} \left[\tfrac{1}{2} - \frac{\Delta r}{4r_j} \right] T^{n}_{w,j-1} \qquad (3.41)$$

Therefore, the temperature at any interior point in the tube wall after a time interval Δt can be calculated from the knowledge of present temperatures at and around the point of interest. For boundary points, however, a heat balance as described below is required:

Inner Surface: With reference to the Figure 5:

$$2\pi R \frac{\Delta r}{2} \rho_w c_w \frac{\partial T_{w,i}}{\partial t} = 2\pi R\, h_i (T_\infty - T_{w,i}) - 2\pi \left(R + \frac{\Delta r}{2}\right) \left(-\kappa_w \frac{\partial T_w}{\partial r} \right)\Bigg|_{r=R+\frac{\Delta r}{2}}$$

or,

$$\frac{\partial T_{w,i}}{\partial t} = \frac{2h_i}{\rho_w c_w \Delta r} (T_\infty - T_{w,i}) + \frac{2\kappa_w}{\rho_w c_w R \Delta r} \left(R + \frac{\Delta r}{2}\right) \frac{\partial T_w}{\partial r}\Bigg|_{r=R+\frac{\Delta r}{2}}$$

In finite difference form,

$$T_{w,j}^{n+1} = \left[1 - \frac{2\alpha_w \Delta t}{(\Delta r)^2}\left(\frac{h_m \Delta r}{\kappa_w} + 1 + \frac{\Delta r}{2R}\right)\right] T_{w,i}^{n}$$

$$+ \frac{2\alpha_w \Delta t}{(\Delta r)^2}\left(\frac{h_m \Delta r}{\kappa_w}\right) T_{\infty}^{n} + \frac{2\alpha_w \Delta t}{(\Delta r)^2}\left(1 + \frac{\Delta r}{2R}\right) T_{w,i+1}^{n} \qquad (3.42)$$

Similarly, for the outer surface,

$$T_{w,o}^{n+1} = \left[1 - \frac{2\alpha_w \Delta t}{(\Delta r)^2}\left(\frac{h_o \Delta r}{\kappa_w} + 1 - \frac{\Delta r}{2R_o}\right)\right] T_{w,o}^{n}$$

$$+ \frac{2\alpha_w \Delta t}{(\Delta r)^2}\left(\frac{h_o \Delta r}{\kappa_w}\right) T_{amb} + \frac{2\alpha_w \Delta t}{(\Delta r)^2}\left(1 - \frac{\Delta r}{2R_o}\right) T_{w,o-1}^{n} \qquad (3.43)$$

The stability conditions [18, 19] for the equations (3.41) through (3.43) are, respectively:

$$\Delta t \leq \frac{(\Delta r)^2}{2\alpha_w} \qquad (3.44)$$

$$\Delta t \leq \frac{(\Delta r)^2}{2\alpha_w\left[\frac{h_m \Delta r}{K_w} + 1 + \frac{\Delta r}{2R}\right]} \qquad (3.45)$$

and

$$\Delta t \leq \frac{(\Delta r)^2}{2\alpha_w\left[\frac{h_o \Delta r}{K_w} + 1 - \frac{\Delta r}{2R_o}\right]} \qquad (3.46)$$

Very small values of Δr (0.05 millimeter) are taken, and the selected Δt is the least of the values calculated from the right hand side of (3.44), (3.45), and (3.46).

For a thick wall and initially cold tube, the temperature wave does not generally reach the outer surface and, therefore, equation (3.43) can be disregarded.

Summary of the Procedure

Once the piston-cylinder arrangement, the initial conditions and all other input parameters are chosen, the solution proceeds according to the following steps:

1) The time interval $\Delta t'$ is determined in accordance with expression (3.40) and the burning rate is taken corresponding to the average burning pressure.

2) The new piston position and its velocity are calculated, and using the appropriate characteristic equations as indicated earlier the new ballistic properties at both the piston base end and the tube head end are determined.

3) The interior points are solved either by the Lax-Wendroff method or by linear interpolation as discussed earlier.

4) The new heat transfer coefficient is determined from the new ballistic properties and the momentum thickness at all the nodal points. The new wall temperature is also calculated using the mean heat transfer coefficient.

5) All the calculated values are stored as the present values and reused for the next time step.

Thus the solution proceeds until the piston reaches the desired position. A computer program for the entire solution procedure was written in FORTRAN V and was run to obtain all of the results presented in the following chapter. The flow chart for the program has been shown in Appendix C. The computation time is approximately four minutes for the typical cases run in UNIVAC 1108 machine.

CHAPTER IV

RESULTS AND DISCUSSION

Standard Conditions

A set of realistic, but somewhat arbitrary, conditions is chosen as the input data to the computer program, and results are obtained for both cases of solid velocities. These conditions will be referred to as "standard conditions." They are:

Tube length, L_t	2 m
Tube inside diameter, D	3 cm
Piston mass, M_p	0.326 kg

Initial conditions:

Piston position, L_o	25 cm
Chamber pressure (piston start pressure), P_o	200 atm
Gas temperature (explosion temperature), T_o	3000°K
Charge of propellant, m_{s_i}	0.172 kg

Propellant properties:

Density, ρ_s	1670 Kg/m^3
Initial web thickness, w_{s_i}	0.711 mm
Type:	M-10, single perforated

Gas properties:

Molecular weight, M	24
Ratio of specific heats, γ	1.252

Covolume, η	0.00095 m^3/kg.
Specific heat at constant pressure, c_p	0.412 kcal/kg-^oK
Viscosity (at 3000^oK), μ_{g_o}	0.00007 kg/m-sec
Thermal conductivity (at 3000^oK), κ_{g_o}	0.000034 kcal/m-sec-^oK

Tube material properties:

Thermal diffusivity, α_w	0.126 cm^2/sec
Thermal conductivity, κ_w	0.0138 kcal/m-sec-^oK
Initial tube temperature, T_{amb}	300^oK

The initial gas density ρ_{g_o} as calculated from equation (2.15) is 19.14 kg/m^3 and the potential of the propellant is:

$$W = \frac{R_g T_o}{(\gamma-1)} = 985.66 \text{ kcal/kg}$$

The burning rate versus pressure data for the propellant has been taken from reference [20] and is presented in Table 1. Linear interpolation is used to determine the burning rate at the desired pressure. To ensure the convergence of the solution, a single iteration on the burning rate is performed in each time step as shown in the flow diagram in Appendix C.

For Case I, the solid particles are initially assumed to be evenly distributed in the chamber. But, in Case II, a specific initial distribution, namely a constant value up to the second nodal point from the piston and then linearly to zero at the piston base, is chosen to avoid the discontinuity at x equal to L_o. This has been shown in Figure 6.

Table 1. Pressure vs Burning Rate Data for the Propellant.

Pressure X 10^{-5} Newton/m^2	Burning rate, r_b m/sec
20.68	0.00330
34.46	0.00508
48.25	0.00711
68.93	0.00965
103.39	0.01320
137.86	0.01727
172.32	0.02057
206.78	0.02438
275.71	0.03048
344.64	0.03683
413.57	0.04369
551.43	0.05588
689.28	0.06858
1378.57	0.11684
2067.86	0.17018
2757.14	0.21082
3446.43	0.24384
4825.00	0.30988
6892.86	0.40132
13785.71	0.63500

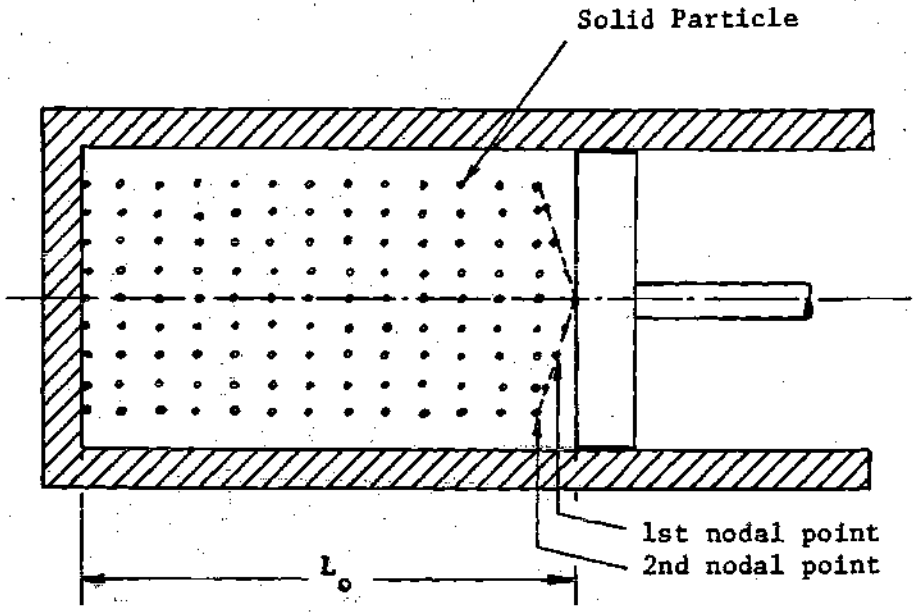

Figure 6. Assumed Initial Distribution of Solid Particles in Case II.

The general power-law velocity profile, i.e. $\frac{u}{U_\infty} = (\frac{y}{\delta})^{\frac{1}{n}}$ yields the following relationships [21]:

$$\frac{\delta}{\delta^*} = n+1 \quad ; \quad \frac{\delta}{\theta} = \frac{(n+1)(n+2)}{n} \tag{4.1}$$

and shape factor, $H = \frac{n+2}{n}$

The one-seventh profile has been used quite extensively in the past to compute the turbulent boundary layers with favorable pressure gradients [22, 23]. The same profile is assumed under the "standard conditions" and the corresponding value for the shape factor, i.e. 1.2857, is taken for the boundary layer computation.

The viscosity of the combustion gas is assumed to be proportional to the square root of the absolute temperature which implies that the value of m in (3.22) is 0.5. The same relation is assumed between the gas conductivity and its absolute temperature. These yield a constant value of 0.8482 for the Prandtl number of the gas.

One-Dimensional Solution

Case I. The results of the one-dimensional analysis have been presented in Figures 7 through 14. Comparison with the solution neglecting the heat transfer and skin friction shows insignificant effect of these phenomena on the ballistic properties of the piston-cylinder arrangement. But the following observations can be made from these results:

1) The Lagrange approximation of linear velocity distribution and constant gas density is not a good approximation of the real situation. It can be noted from Figure 10 that a considerable amount of time

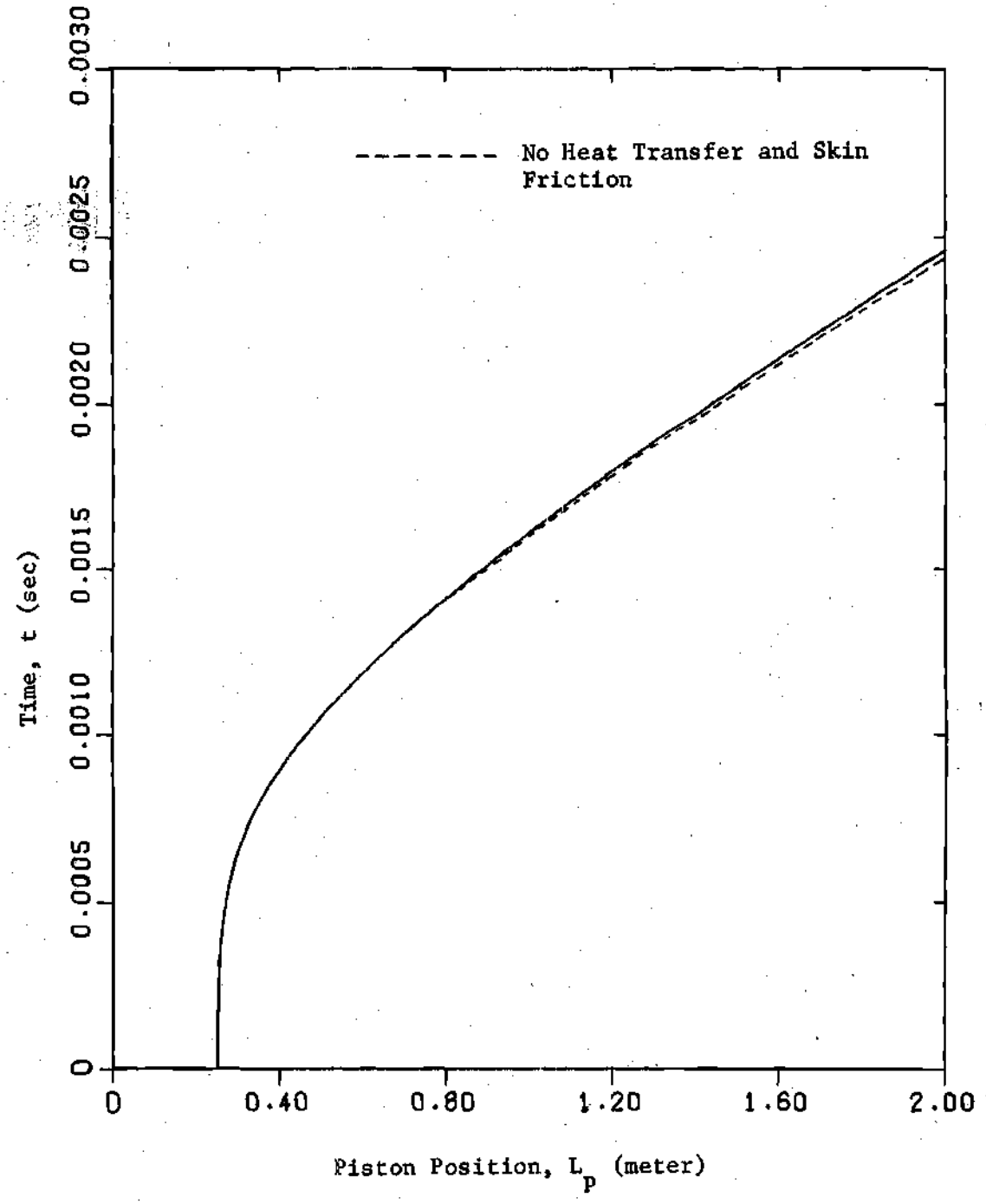

Figure 7. Piston Path for Case I.

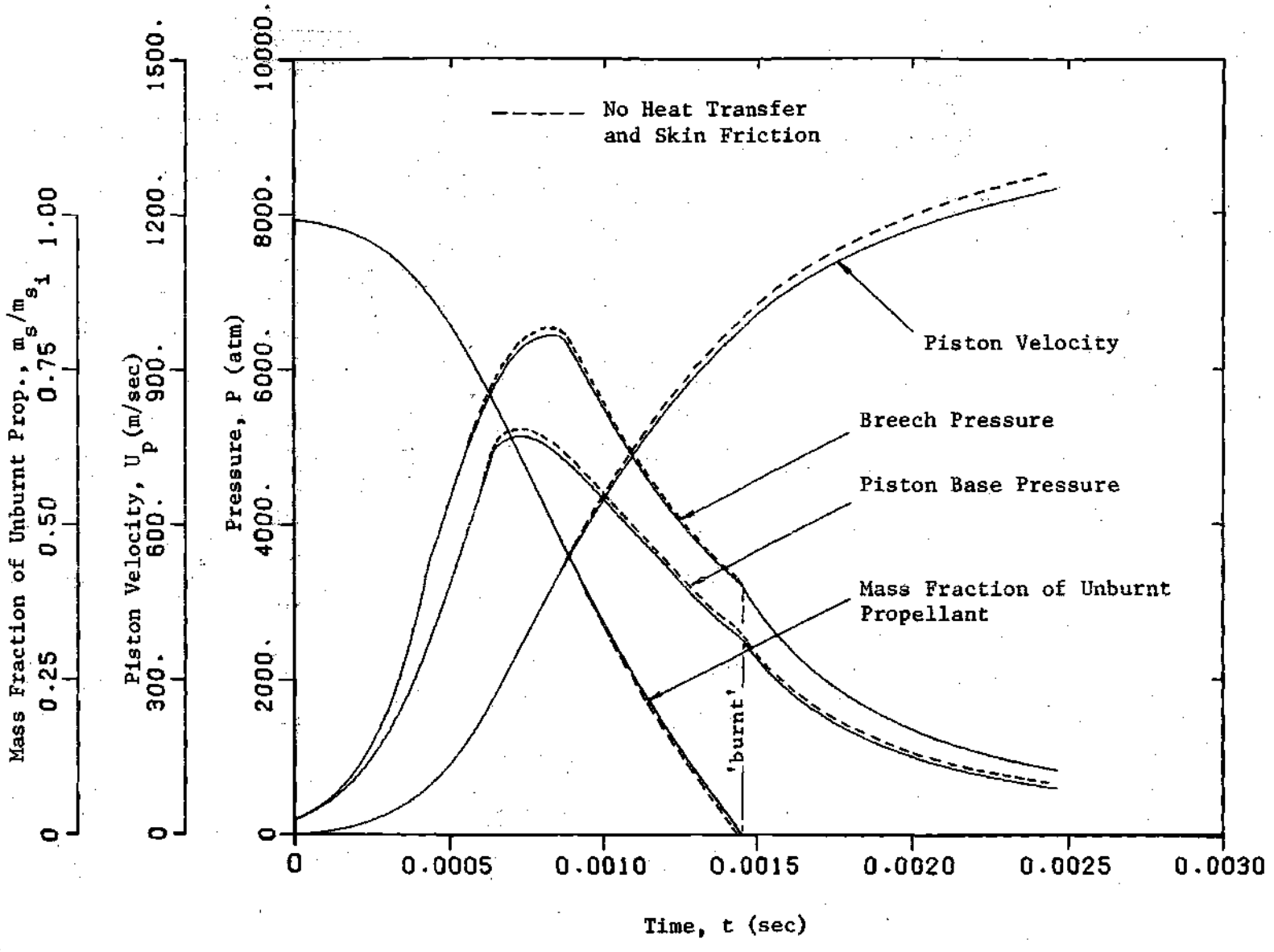

Figure 8. Variation of End Pressures, Piston Velocity and Mass Fraction of Solids with Time (Case I).

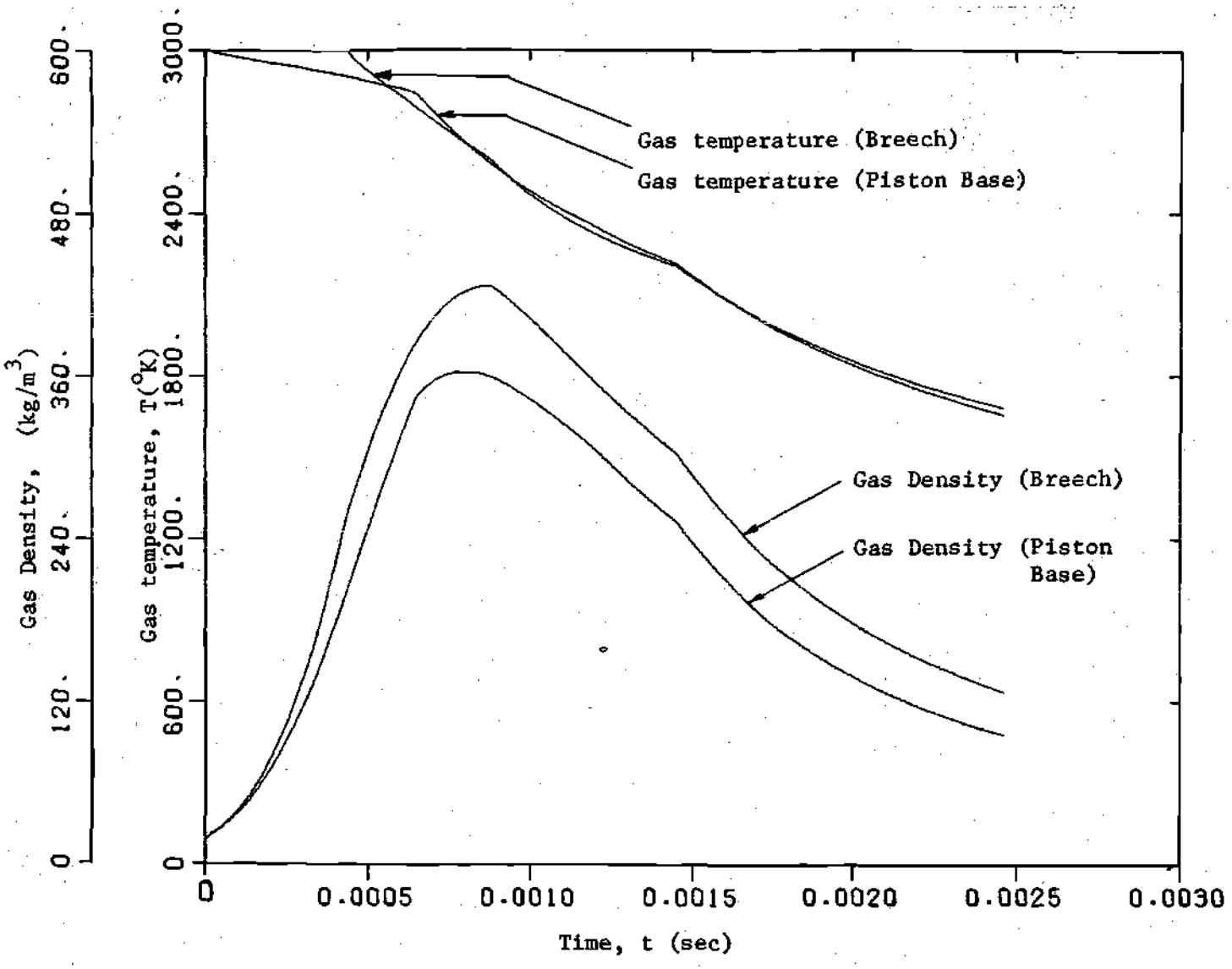

Figure 9. Variation of Gas Densities and Temperatures at the Breech and Piston Base End with Time (Case I).

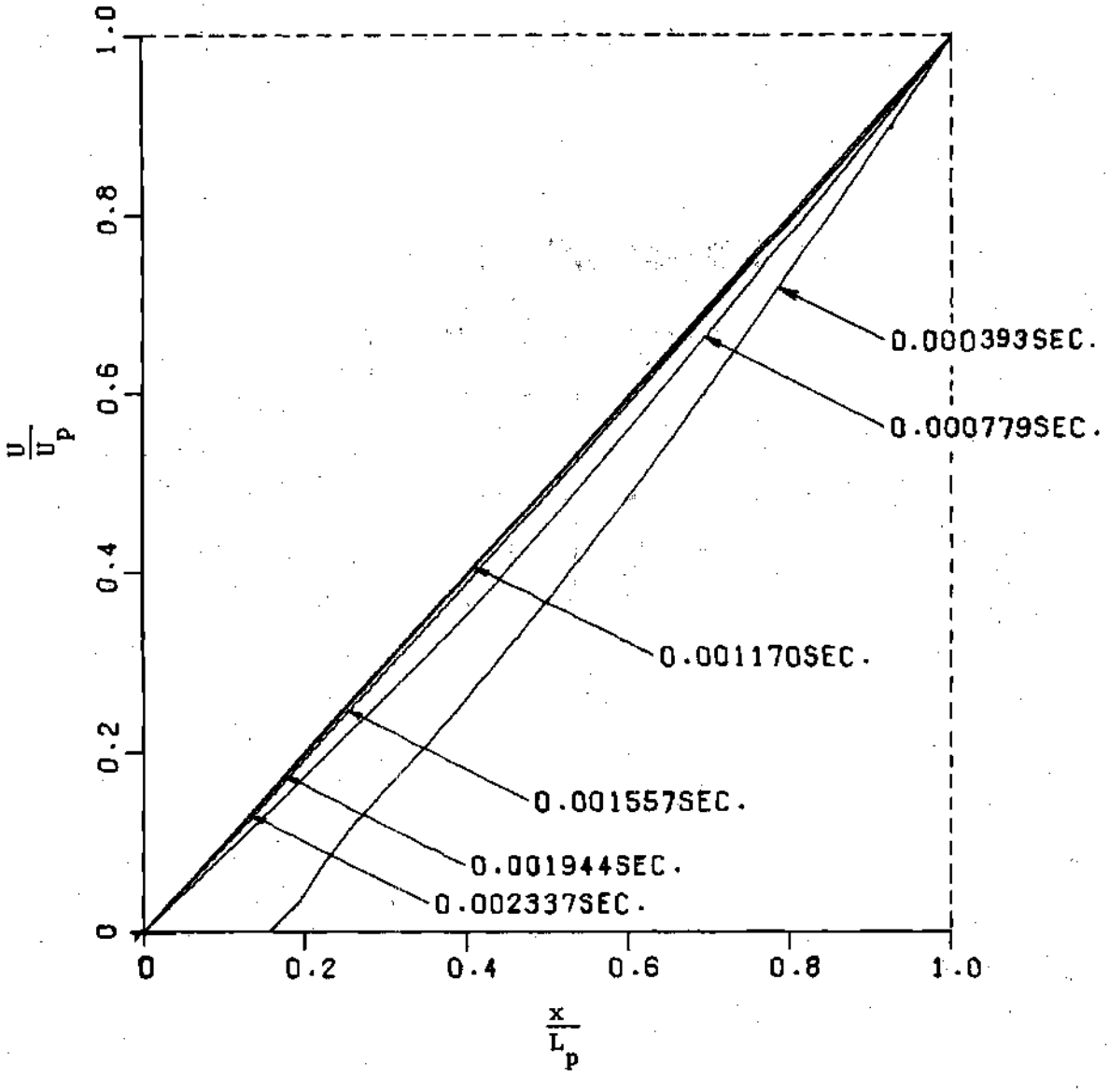

Figure 10. Spacewise Distribution of Velocity at Various Times (Case I).

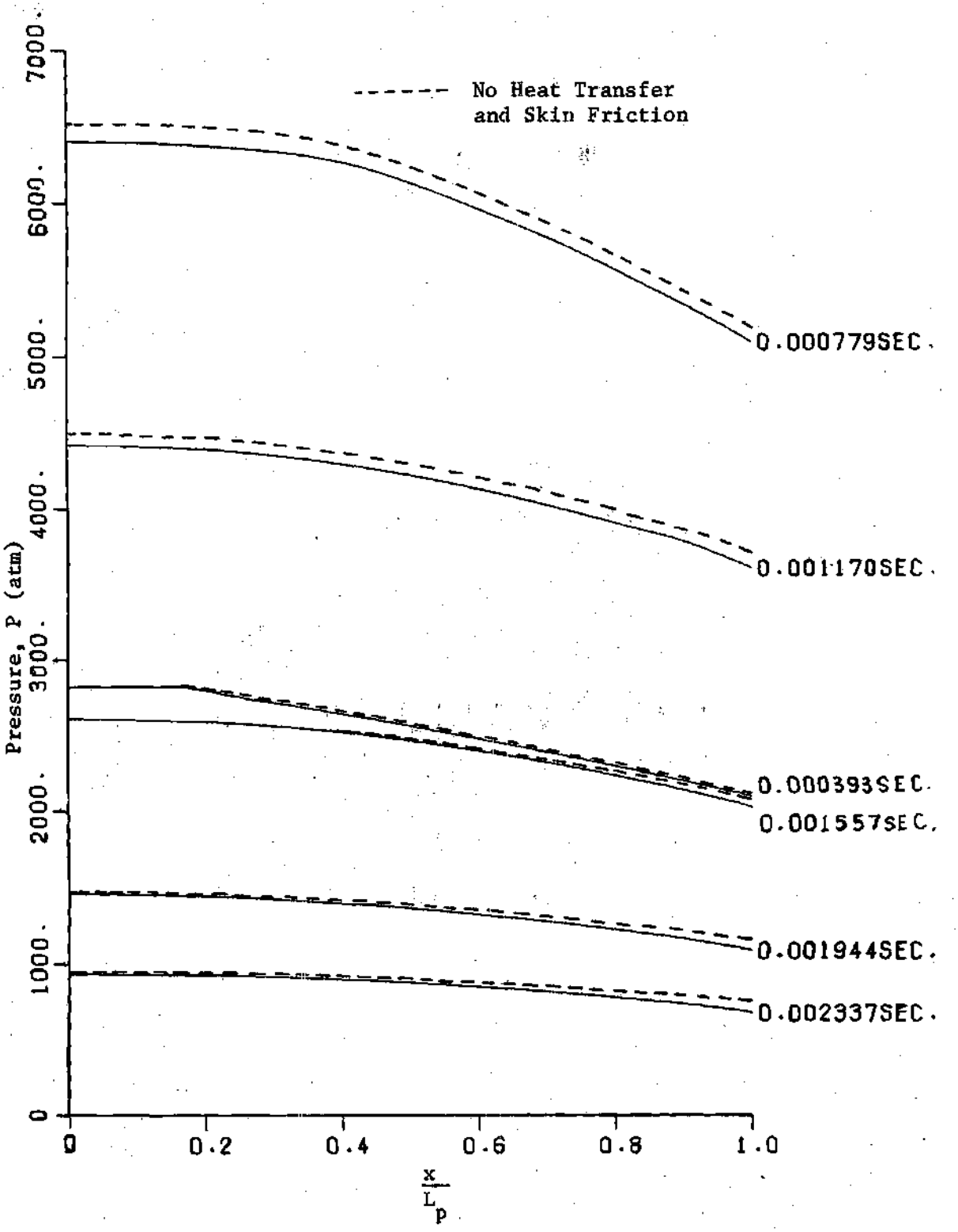

Figure 11. Spacewise Distribution of Pressure at Various Times (Case I).

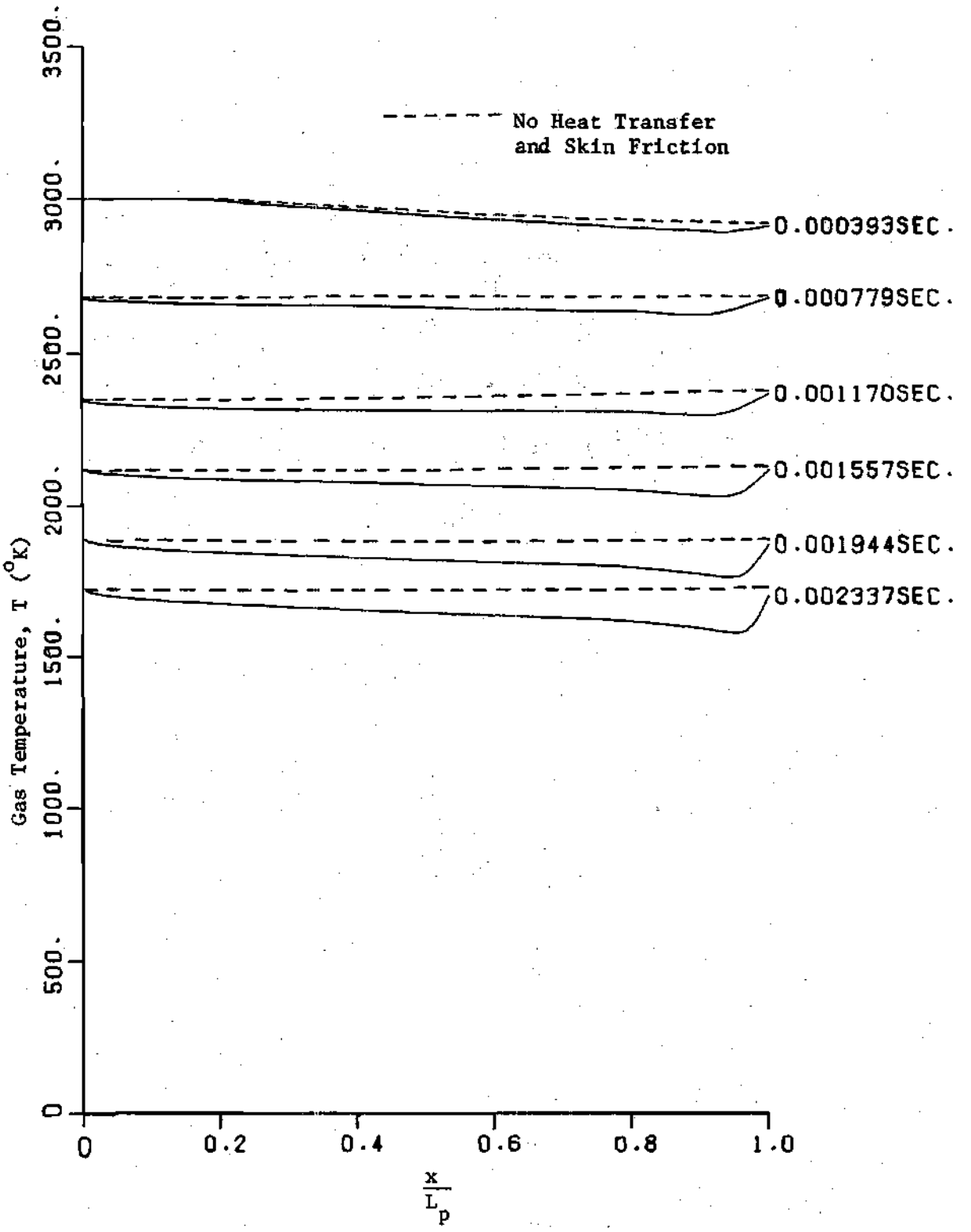

Figure 12. Spacewise Distribution of Gas Temperature at Various Times (Case I).

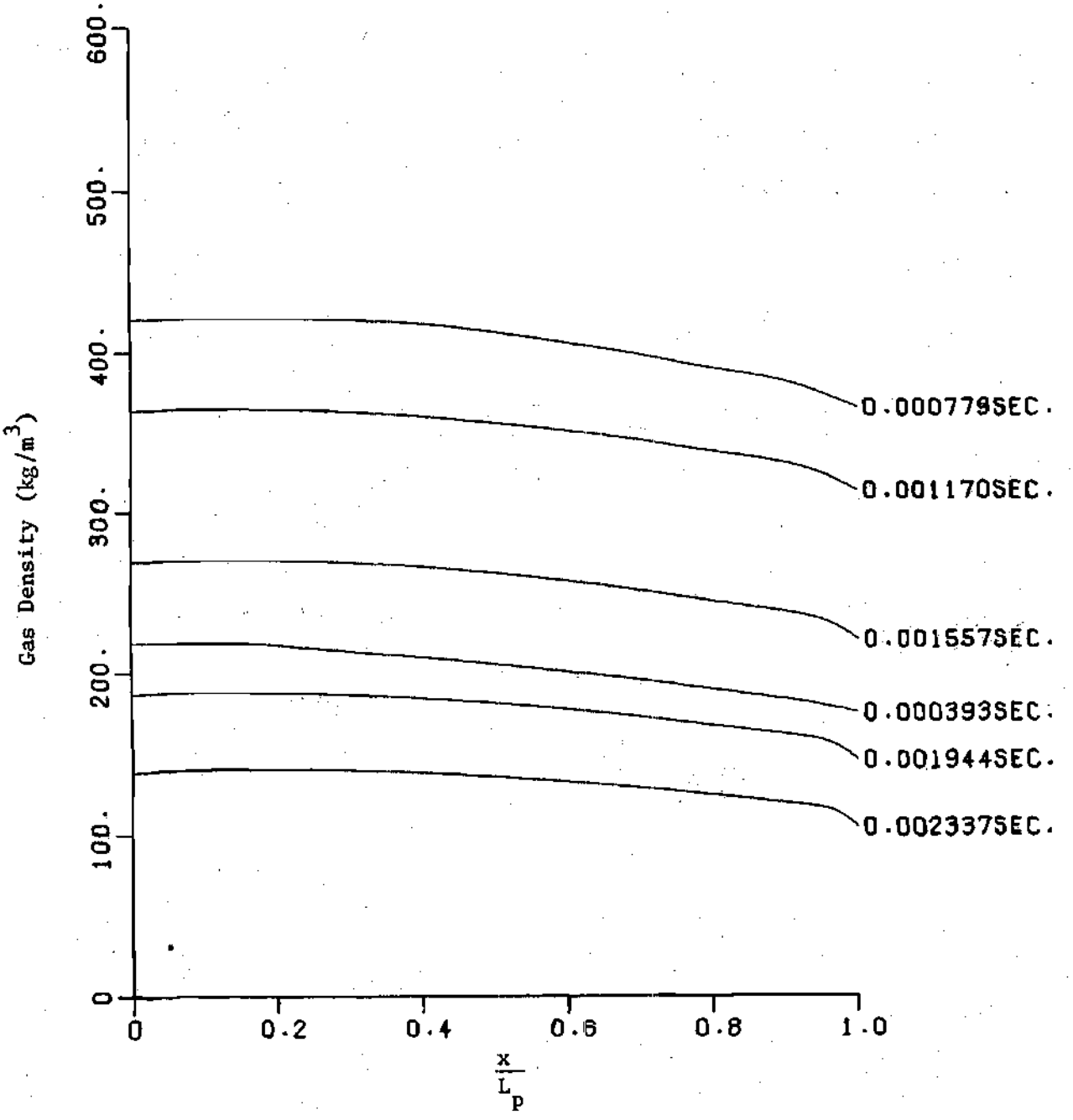

Figure 13. Spacewise Distribution of Gas Density at Various Times (Case I).

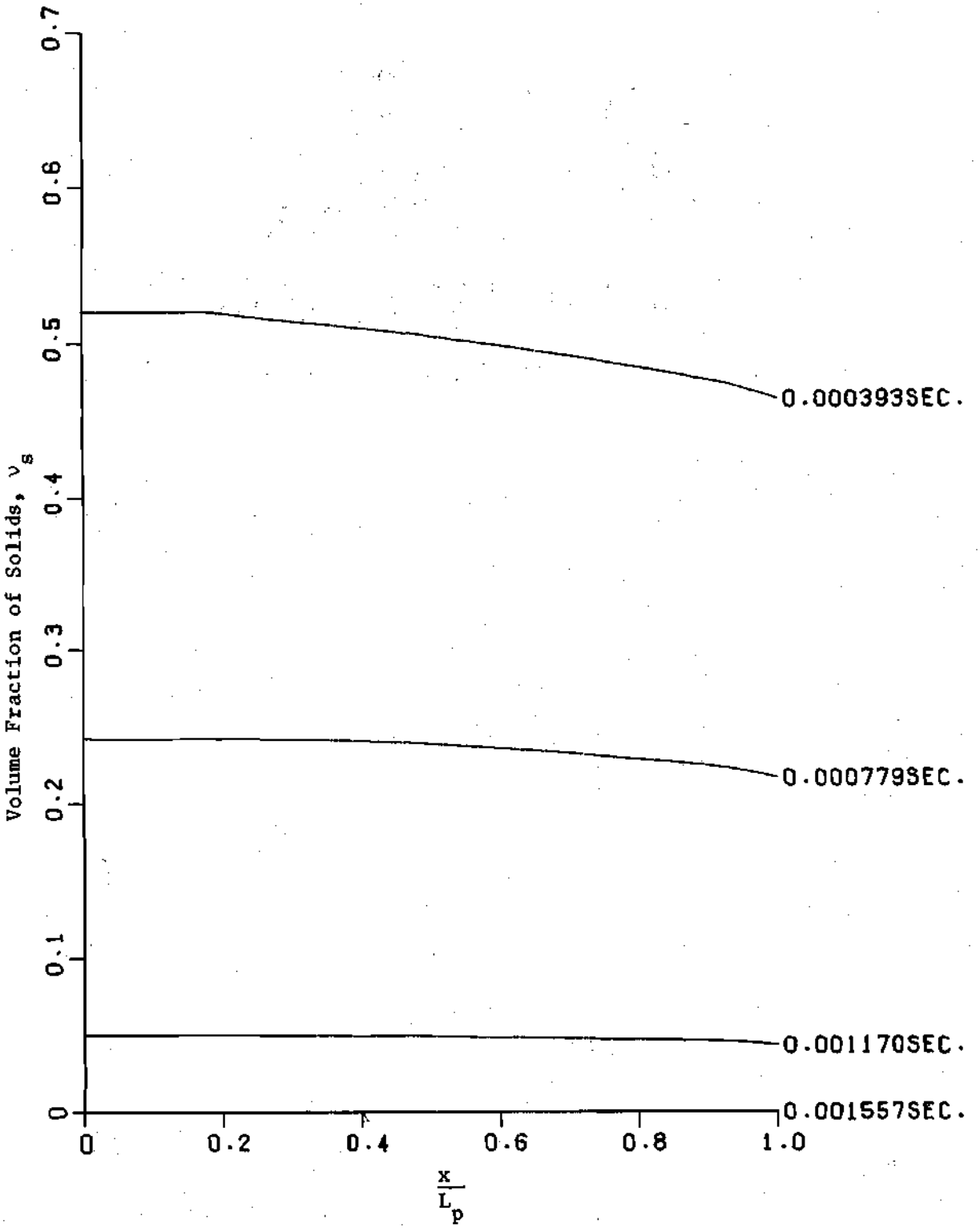

Figure 14. Spacewise Distribution of Volume Fraction of Solids at Various Times (Case I).

(approximately one-third of the total time) is elapsed before the velocity distribution along the length of the tube becomes linear. The gas density, on the other hand, has always a drooping characteristic from the breech end to the piston base end (Figure 9 and 13). The same characteristic is observed for the volume fraction of solids, ν_s (Figure 14).

2) The gas pressure varies considerably along the length of the tube, and at the peak pressure, the difference between the pressures at the two ends is as high as 20 per cent of the breech pressure (Figures 8 and 11). The heat transfer to the tube wall reduces the pressure at all points, whereas the skin friction reduces the piston base pressure as the piston reaches the end of the tube. These two effects together reduce the final piston velocity to some extent.

3) The gas temperatures at the breech and the piston base are of the same value all the time except for a short period in the beginning (Figure 9). There is, however, a sag in between the two end points due to the heat loss to the tube wall (Figure 12).

Case II. Similar results for Case II have been presented in Figures 15 through 21. A comparison with Case I reveals that the final values of piston velocity and total time of travel do not differ much from those in Case I. But the peak breech pressure can be 10-15 per cent higher than the corresponding pressure in Case I. This causes the propellant to burn faster. The piston base pressure, however, remains very close to the corresponding pressure in Case I except for a short period towards the end. This accounts for the slight variation in the final piston velocity between the two cases.

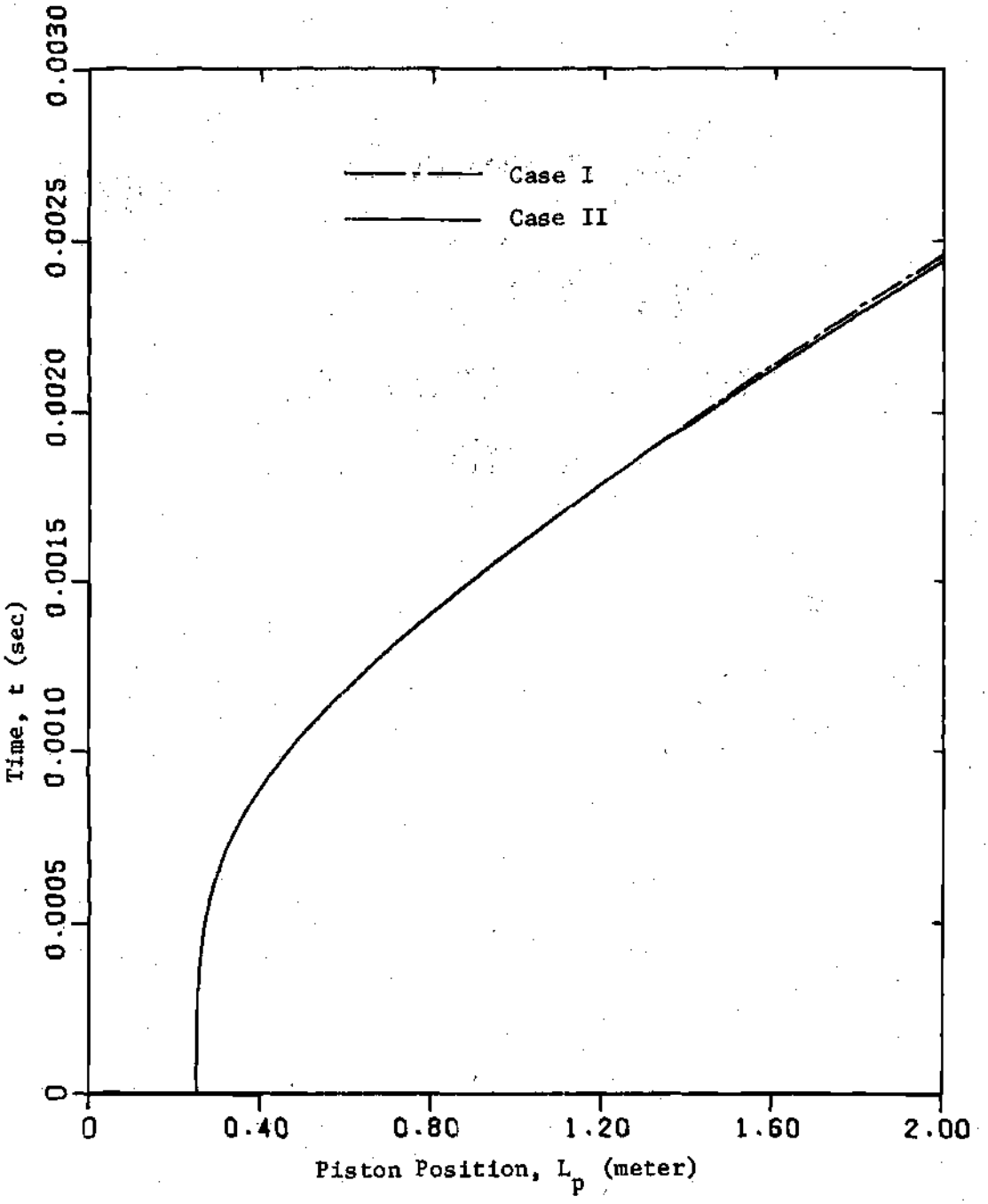

Figure 15. Comparison of Piston Paths in Case I and Case II.

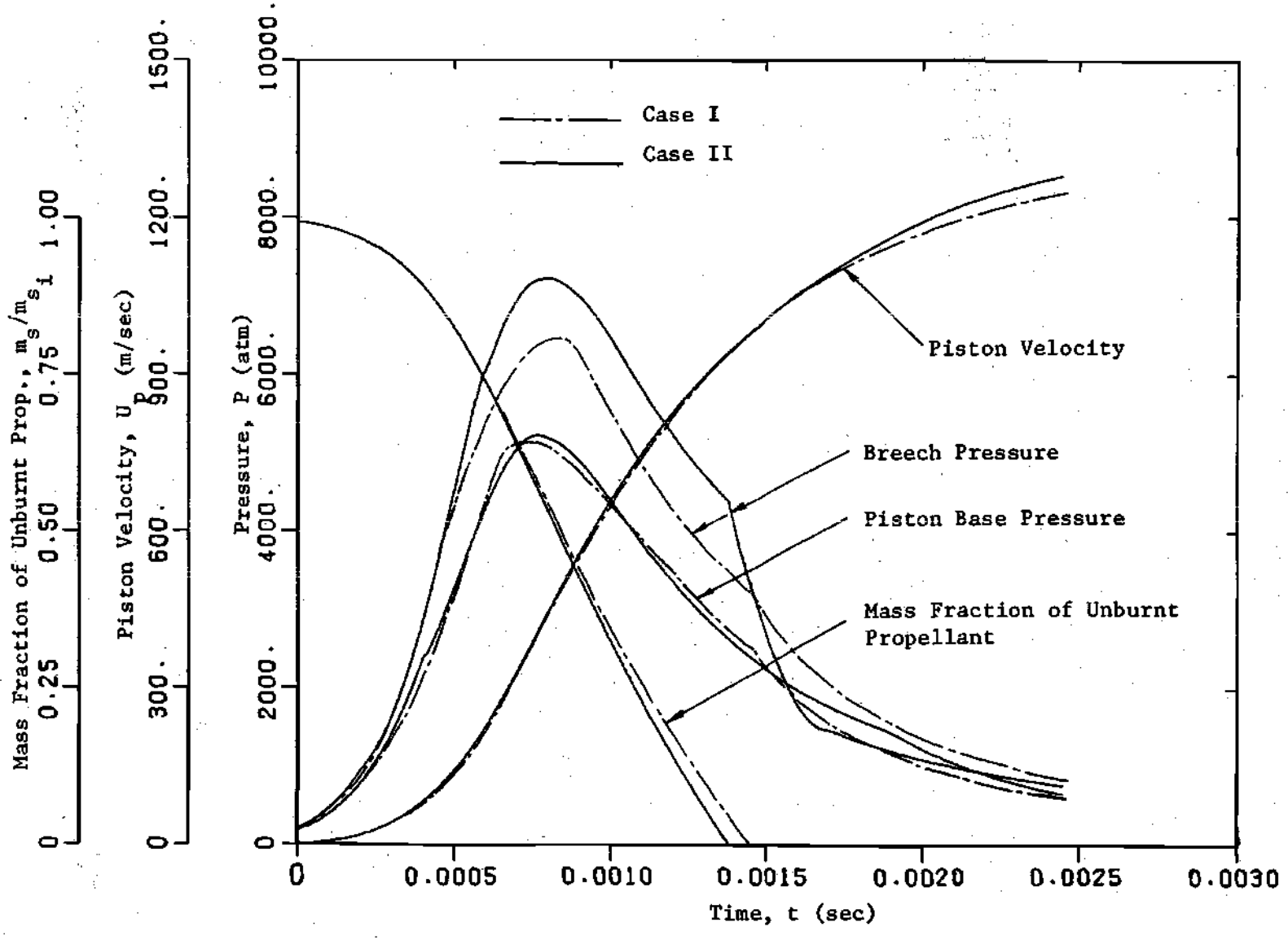

Figure 16. Comparison of End Pressures, Piston Velocities and Mass Fractions of Solids in Case I and Case II.

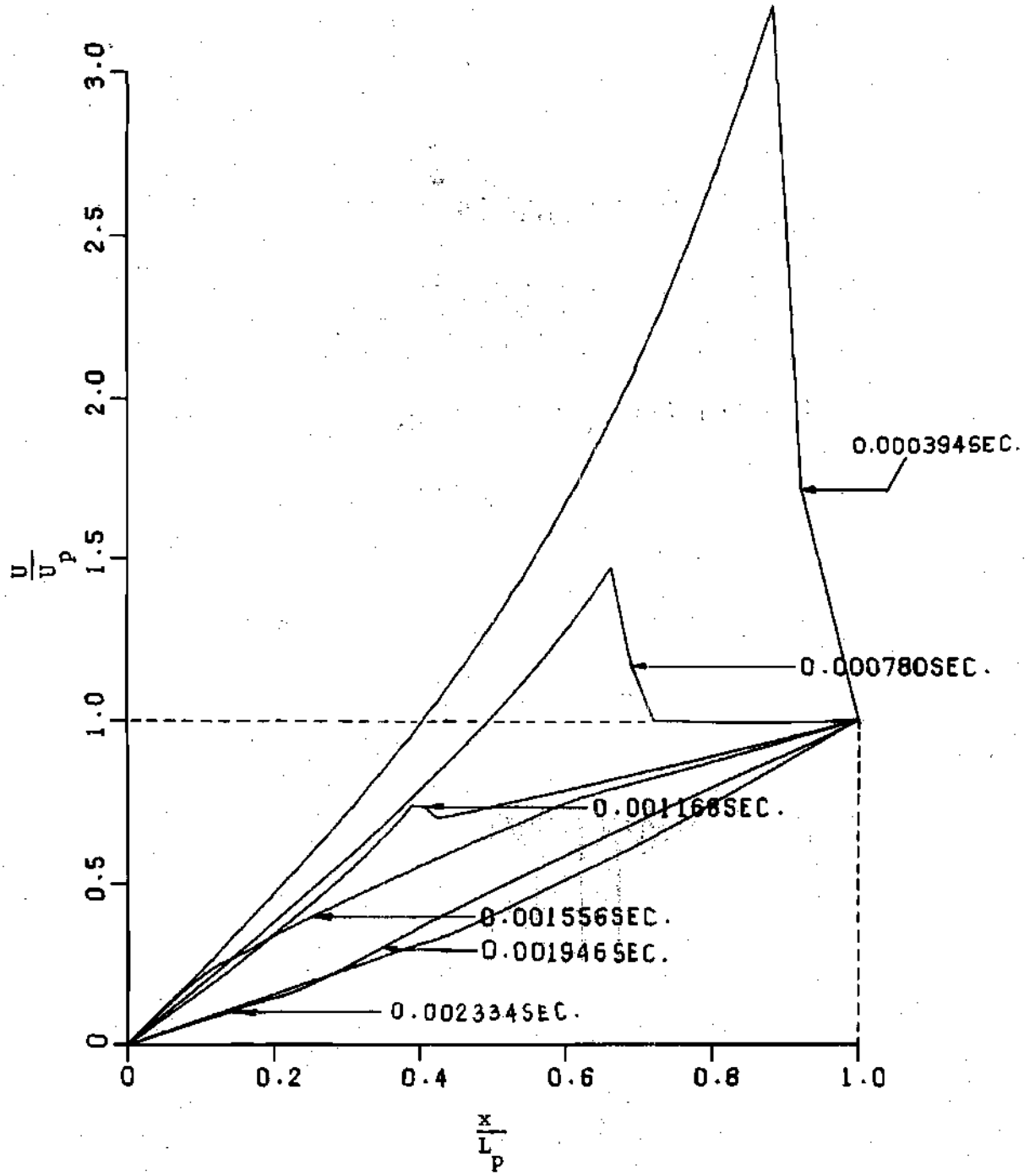

Figure 17. Spacewise Distribution of Gas Velocity at Various Times (Case II).

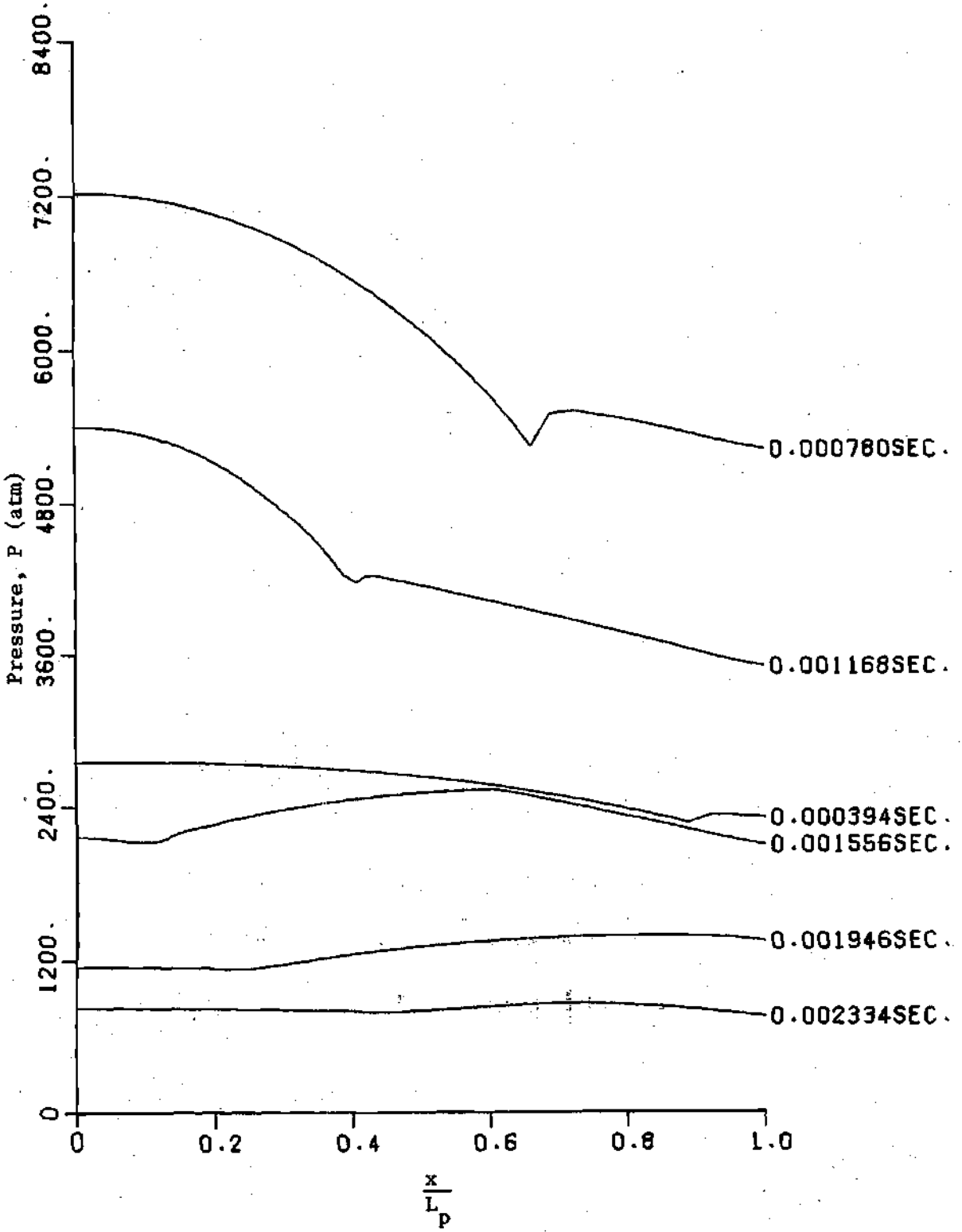

Figure 18. Spacewise Distribution of Pressure at Various Times (Case II).

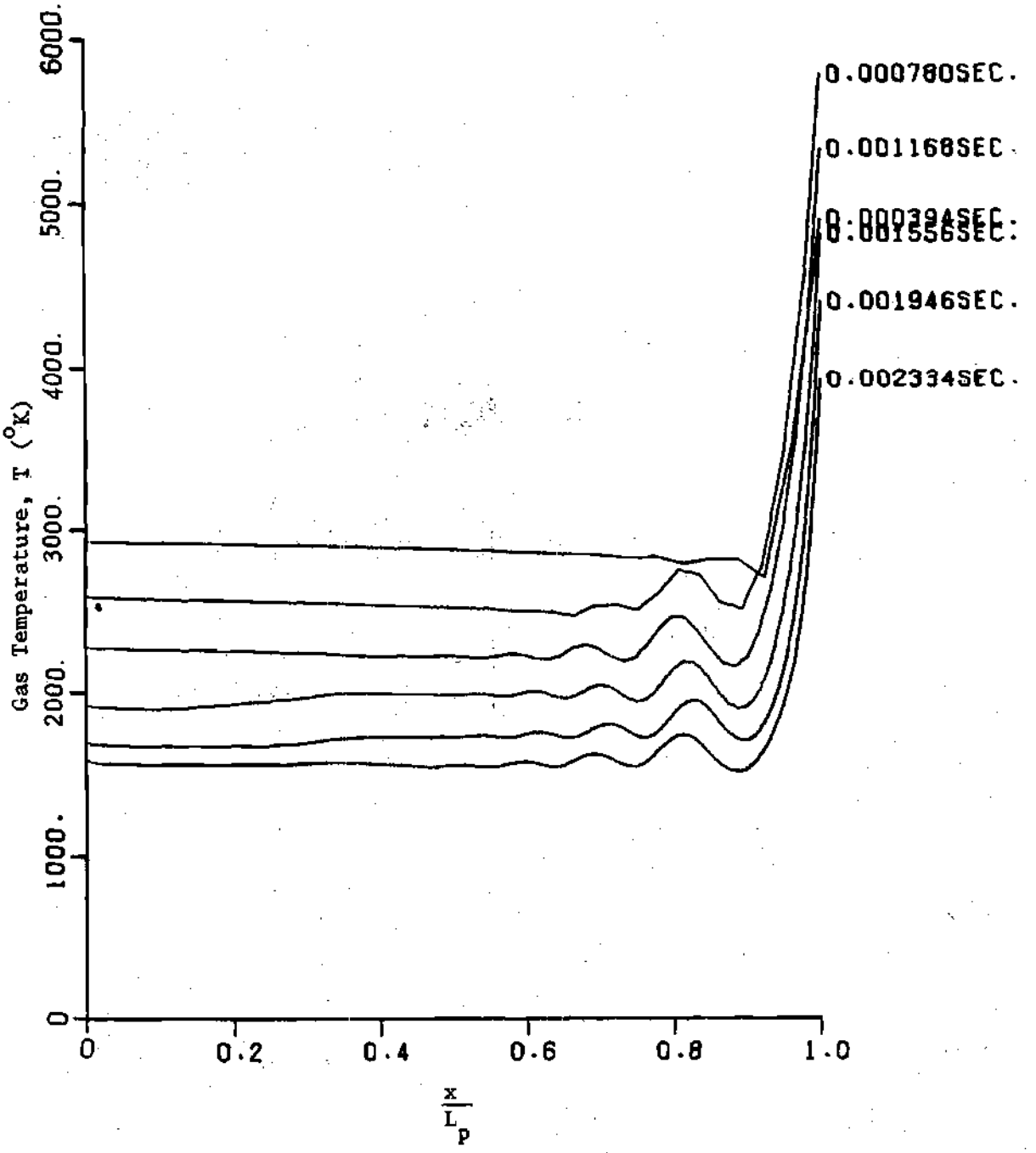

Figure 19. Spacewise Distribution of Gas Temperature at Various Times (Case II).

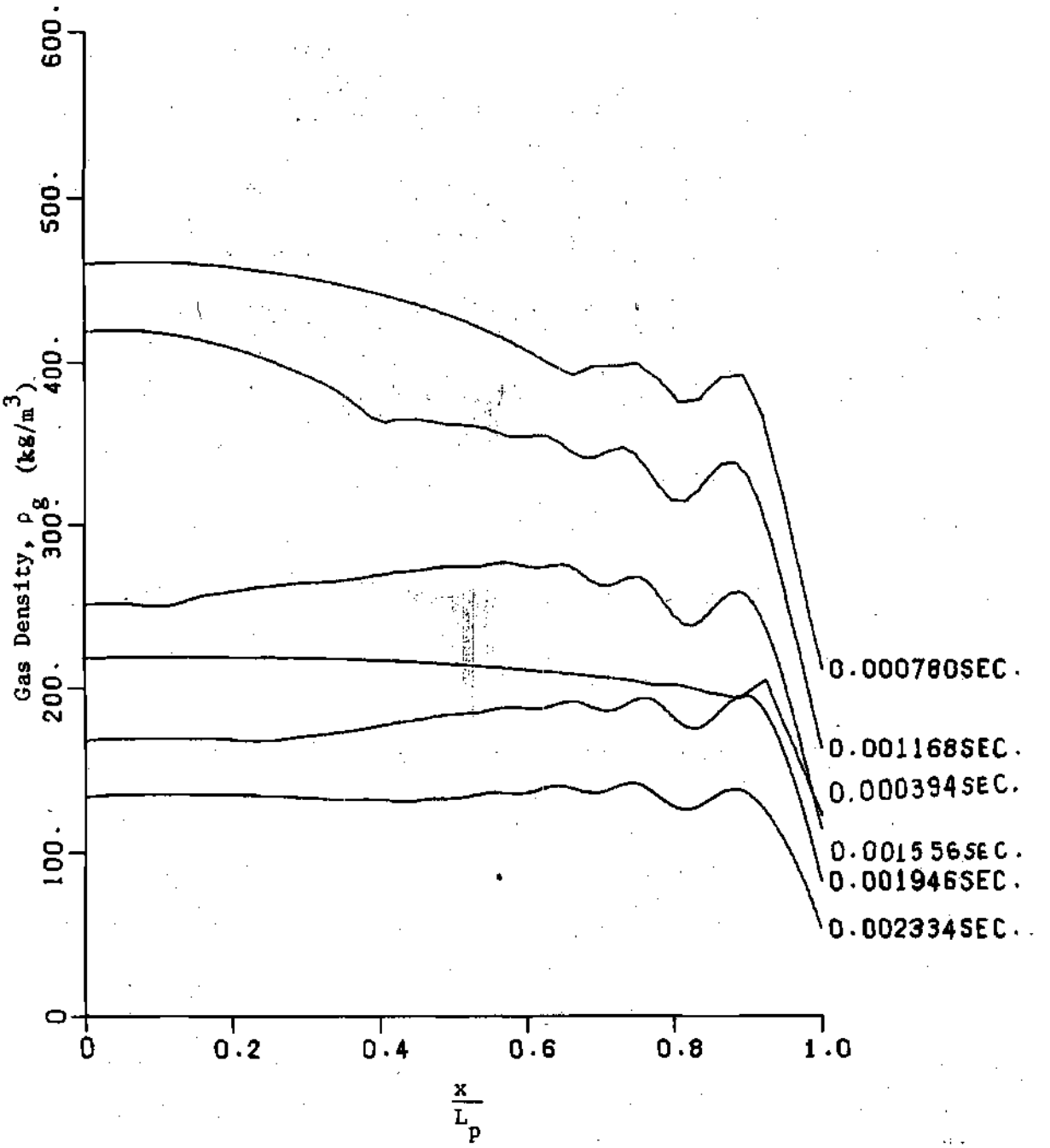

Figure 20. Spacewise Distribution of Gas Density at Various Times (Case II).

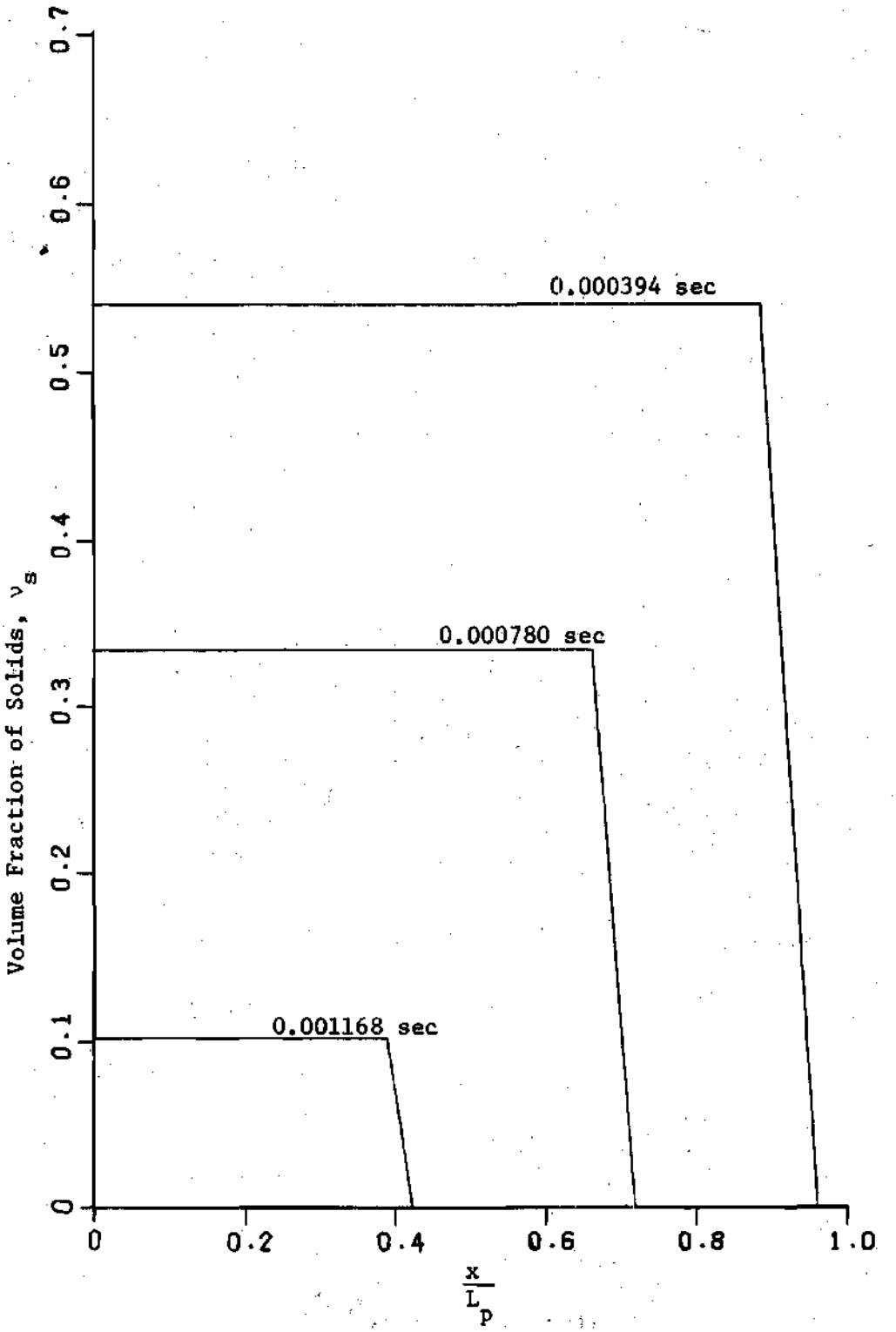

Figure 21. Spacewise Distribution of Volume Fraction of Solids at Various Times (Case II).

A couple of interesting phenomena are observed in this case of stationary solids:

1) Just after the propellant is completely burnt, the breech pressure falls rapidly and finally becomes less than the piston base pressure. The same phenomenon was also observed by Carriere [5]. This happens because of the fact that all the solid particles are assumed to stay near the breech end all the time, whereas there are no solids at the piston base. Therefore, when the solids are completely burnt, no sudden change in the pressure slope occurs at the piston base as it is observed at the breech.

2) Due to the rapid change in the volume fraction of solids ν_s near x equal to L_o, a pressure difference sufficient to produce a local gas velocity higher than the piston velocity is created (Figure 17). The gas having higher velocity slams at the back of the piston and thus increases the temperature (Figure 19). But this large temperature rise is confined within a thin layer at the piston base and does not affect the rest of the gas. The oscillations observed in Figures 19 and 20 are not due to the numerical instability, but most probably due to the sudden area change near x equal to L_o.

Boundary Layer and Heat Transfer Solution

The results showing the boundary layer thickness, heat transfer coefficient, and the wall temperature for moving solids, i.e. Case I, are presented in Figures 22 through 27. As the time increases, the boundary layer thickness increases to a maximum value of approximately 20 per cent of the tube radius when the piston reaches the end of the tube. This implies that the maximum value of the displacement thickness

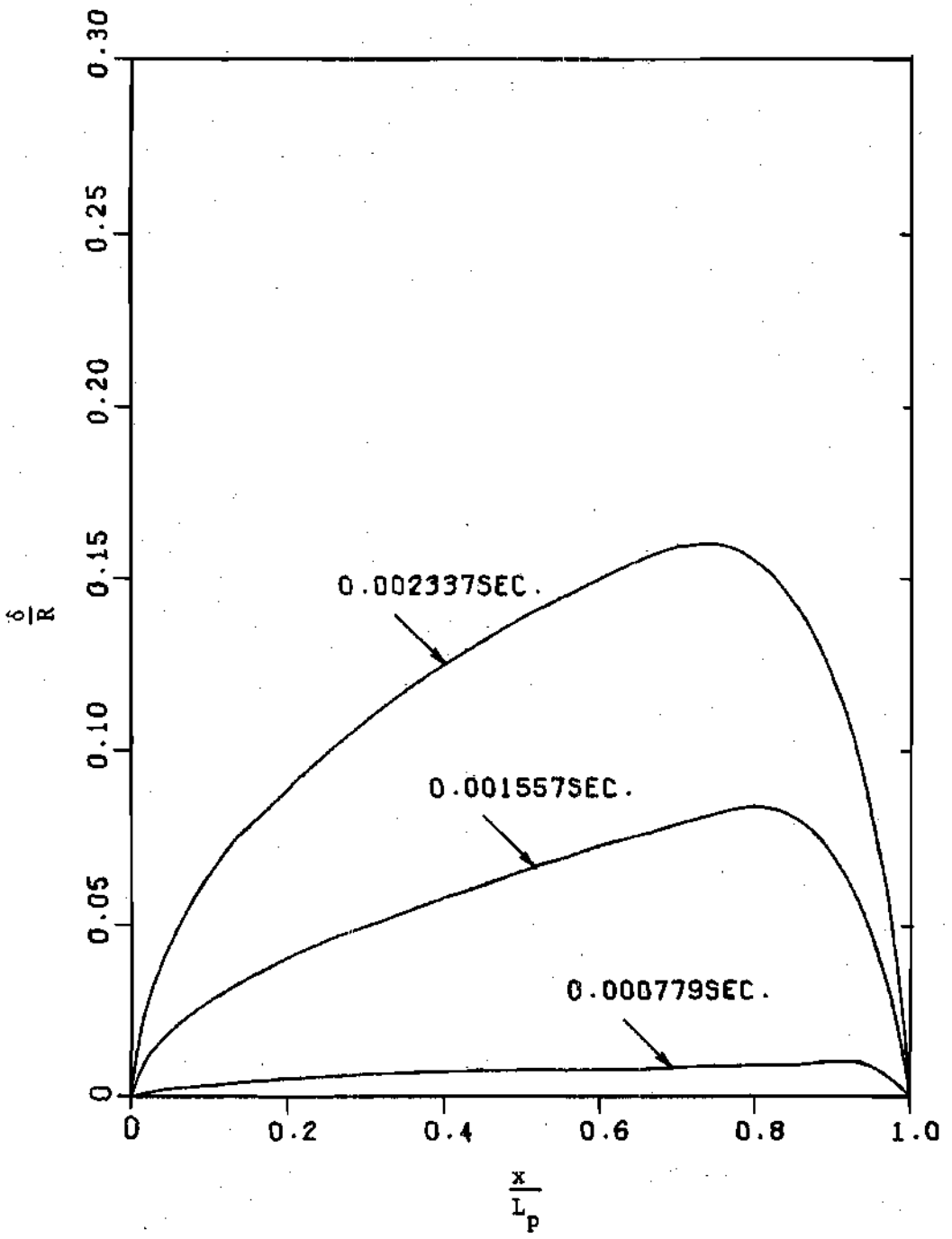

Figure 22. Boundary Layer Growth with Time (Case I).

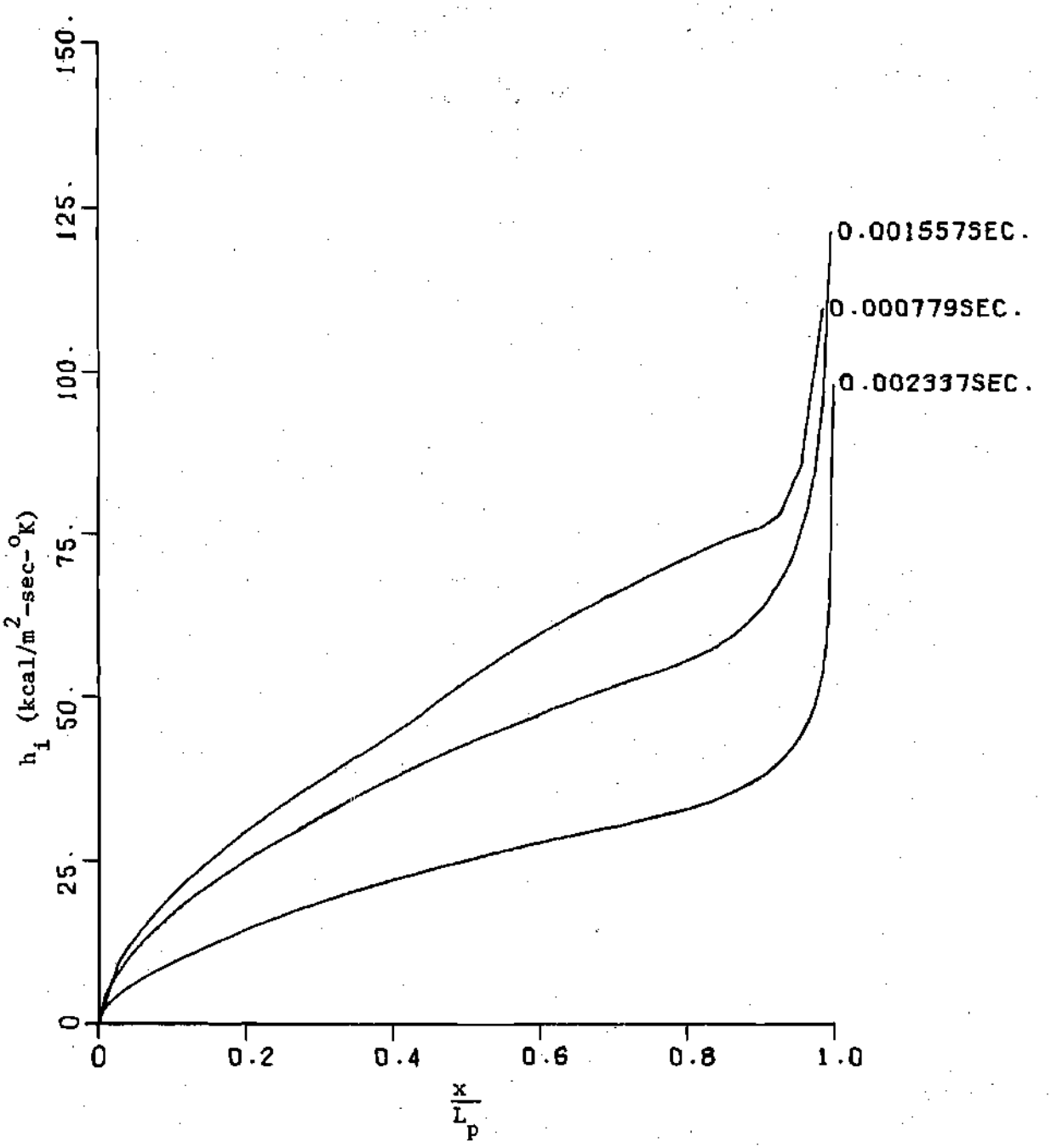

Figure 23. Spacewise Distribution of Heat Transfer Coefficient at Various Times (Case I).

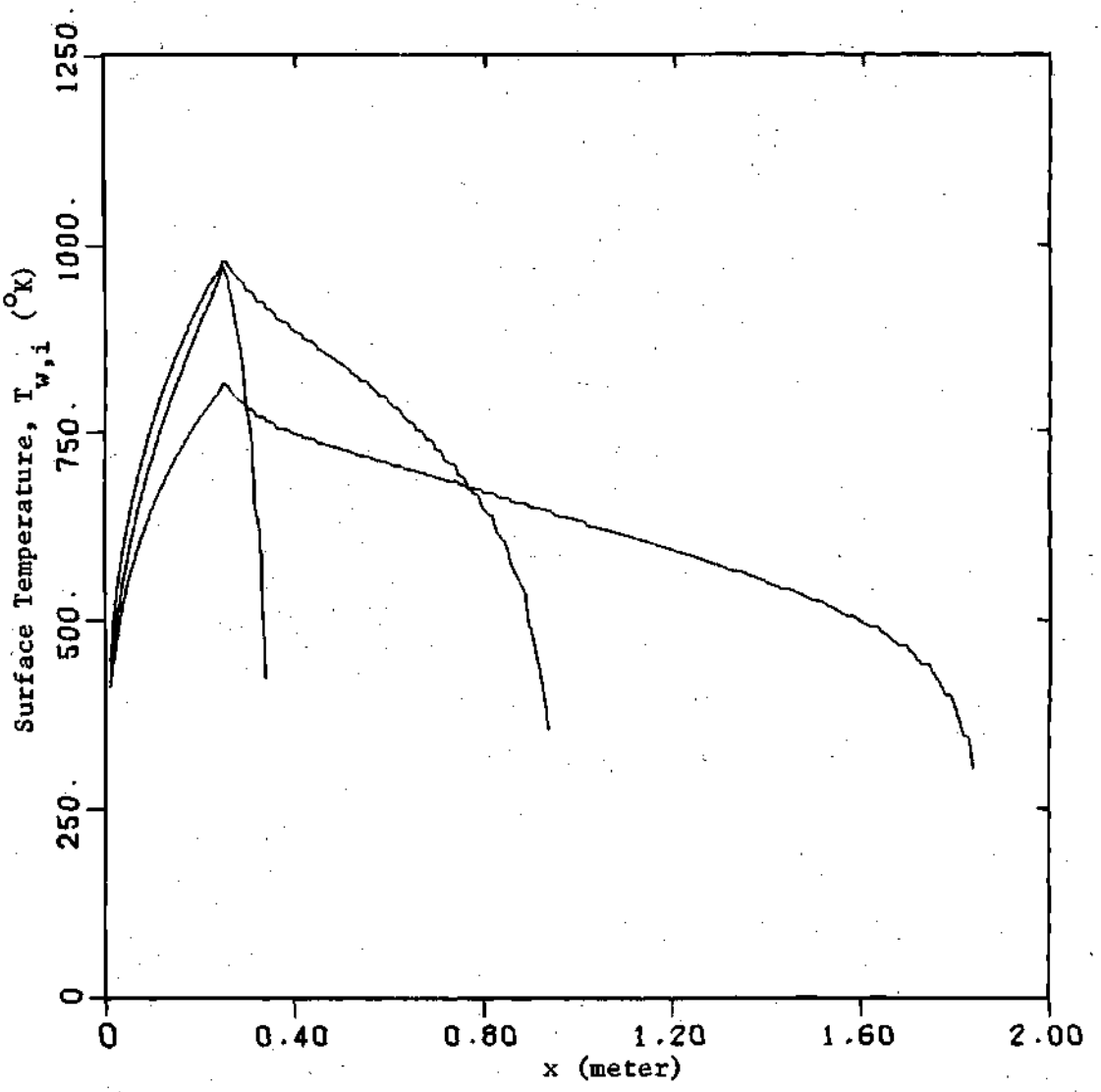

Figure 24. Spacewise Distribution of Wall Surface Temperature at Various Times (Case I)

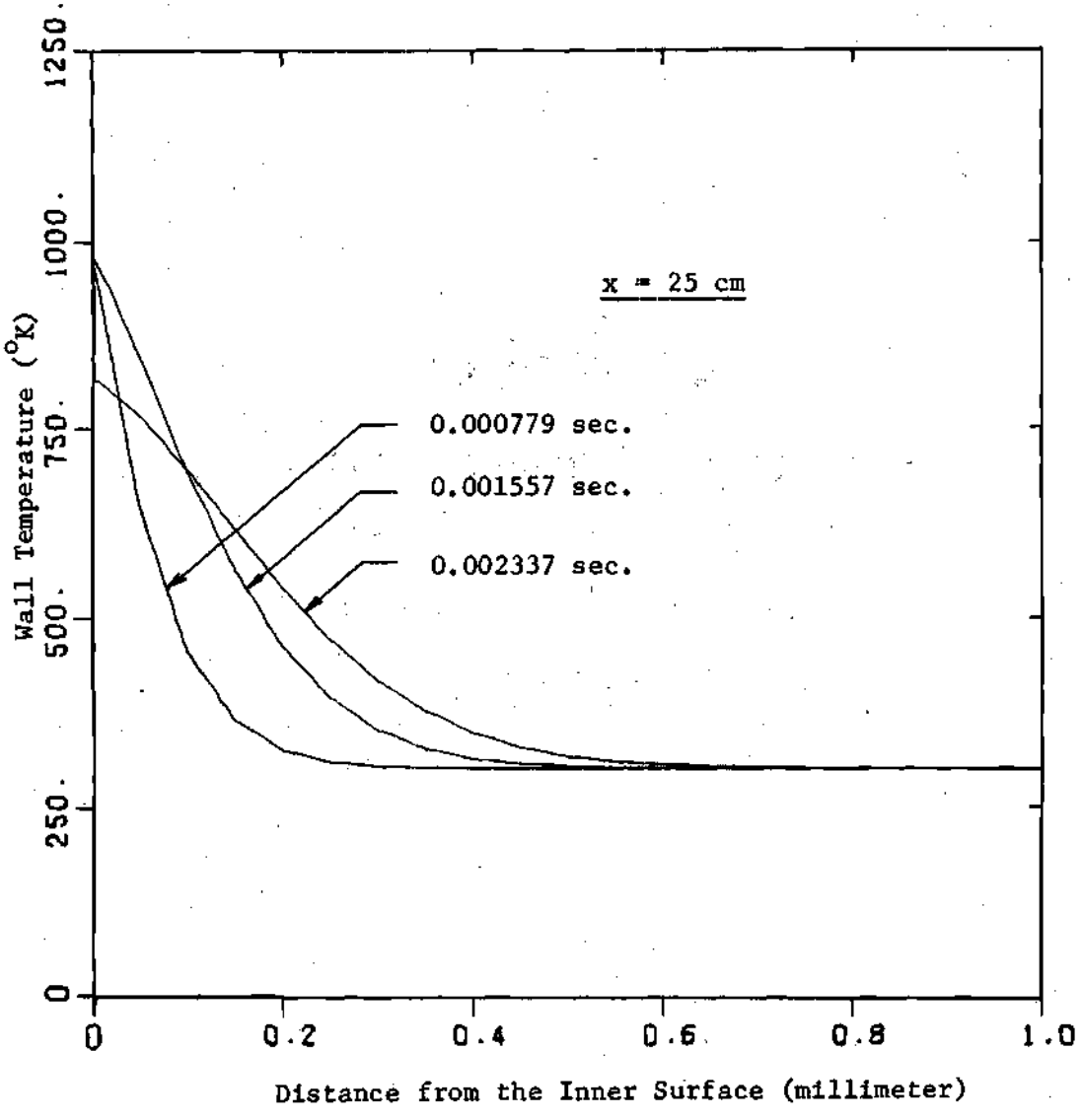

Figure 25. Variation of Wall Temperature at a Particular Position with Depth at Various Times (Case I).

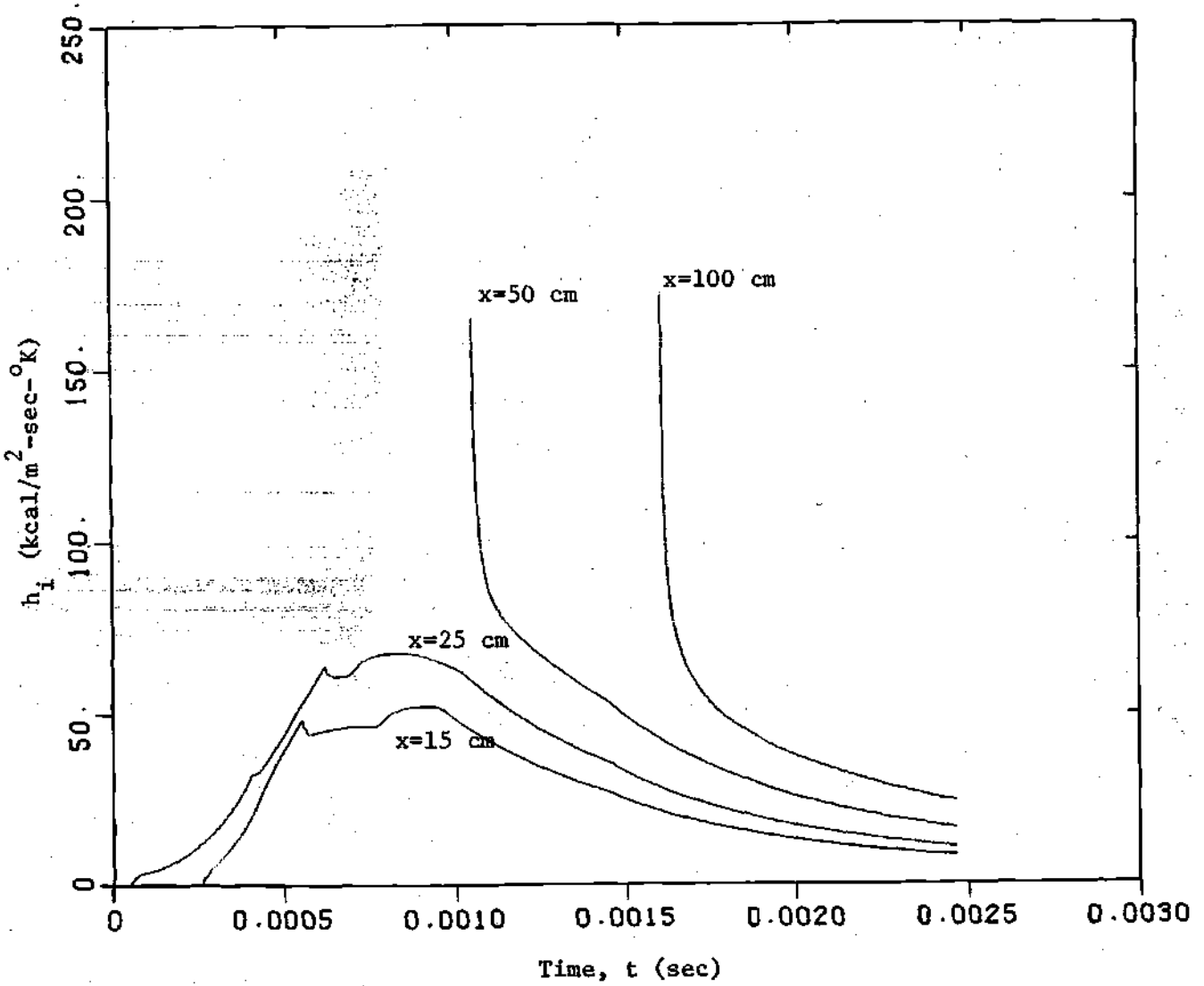

Figure 26. Variation of Heat Transfer Coefficients at Certain Fixed Locations with Time (Case I).

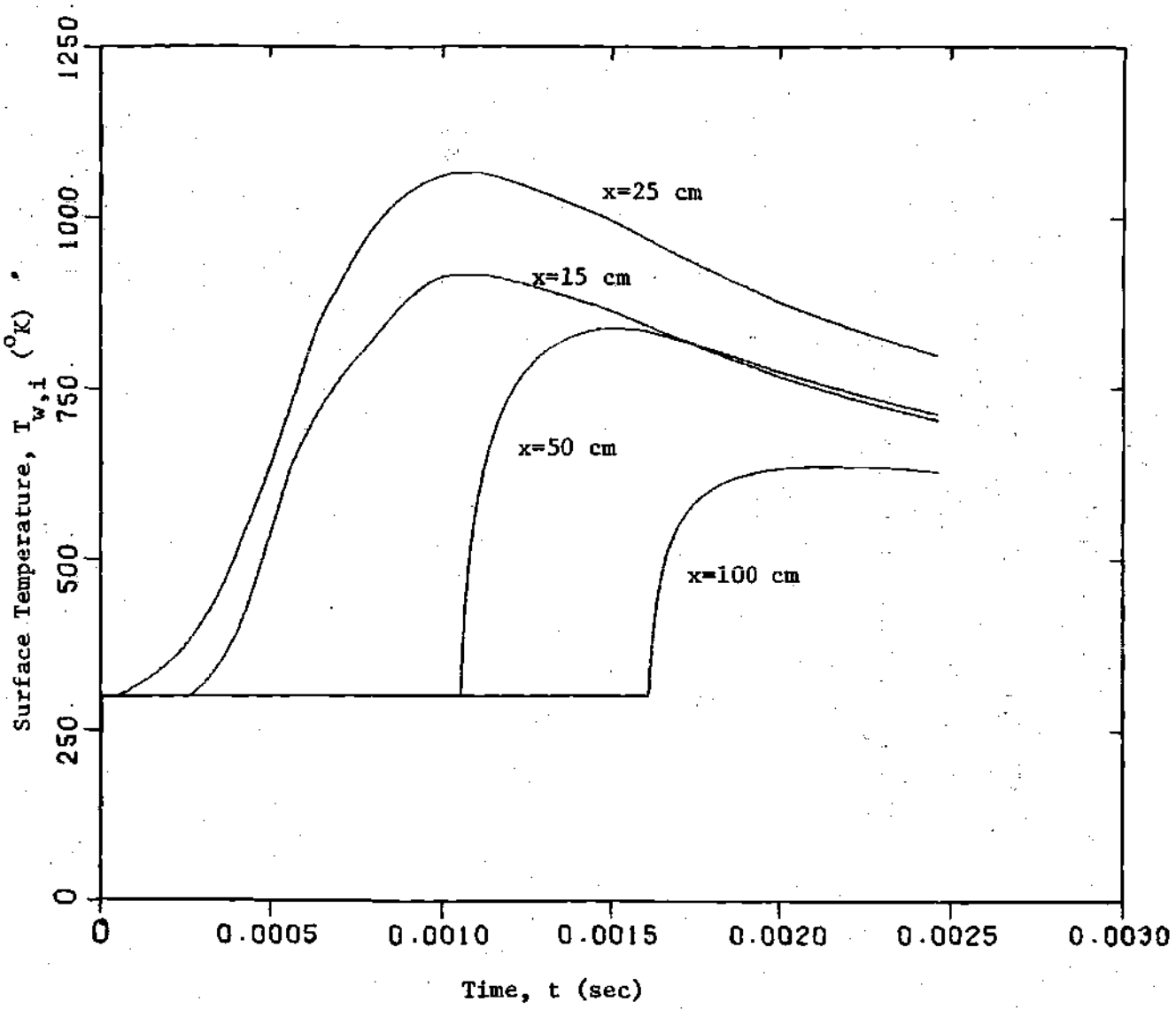

Figure 27. Variation of Wall Surface Temperatures at Certain Fixed Locations with Time (Case I).

is less than three per cent of the tube radius and, therefore, the assumption of a thin boundary layer is valid.

The order of magnitude of the heat transfer coefficient is extremely high due to high gas density and velocity (Figures 23 and 26). The surface temperature of the tube wall reaches as high as $1100^{o}K$ and it occurs at the initial piston position (Figures 24 and 27). The total time is so short that in spite of a very steep radial temperature gradient and high thermal diffusivity of the tube material, the temperature wave cannot penetrate more than one millimeter into the tube wall (Figure 25). This justifies the exclusion of equation (3.43) from the computer program.

The heat flux, $h_i(T-T_{w,i})$ at certain fixed positions along the length of the tube are shown in Figure 28. Although the maximum value of heat flux could be as high as 350,000 $kcal/m^2$-sec, these type of fantastically high values last only for one or two microseconds. The average value of heat flux would be around 50,000 $kcal/m^2$-sec.

The same type of results were also obtained for Case II, and the total heat losses for both the cases are compared in Figure 29. It shows that the heat loss in Case II is about ten per cent higher than that in Case I. This is mainly due to the higher gas velocity in the initial period of Case II. After this initial period, the heat transfer coefficients in the two cases are quite close.

The important results of both the cases are tabulated in Table 2. A mass and energy balance detailed in Table 3 shows that the computation error is less than 0.5 per cent. The ballistic efficiency, i.e. the ratio of final kinetic energy of the piston and the propellant energy,

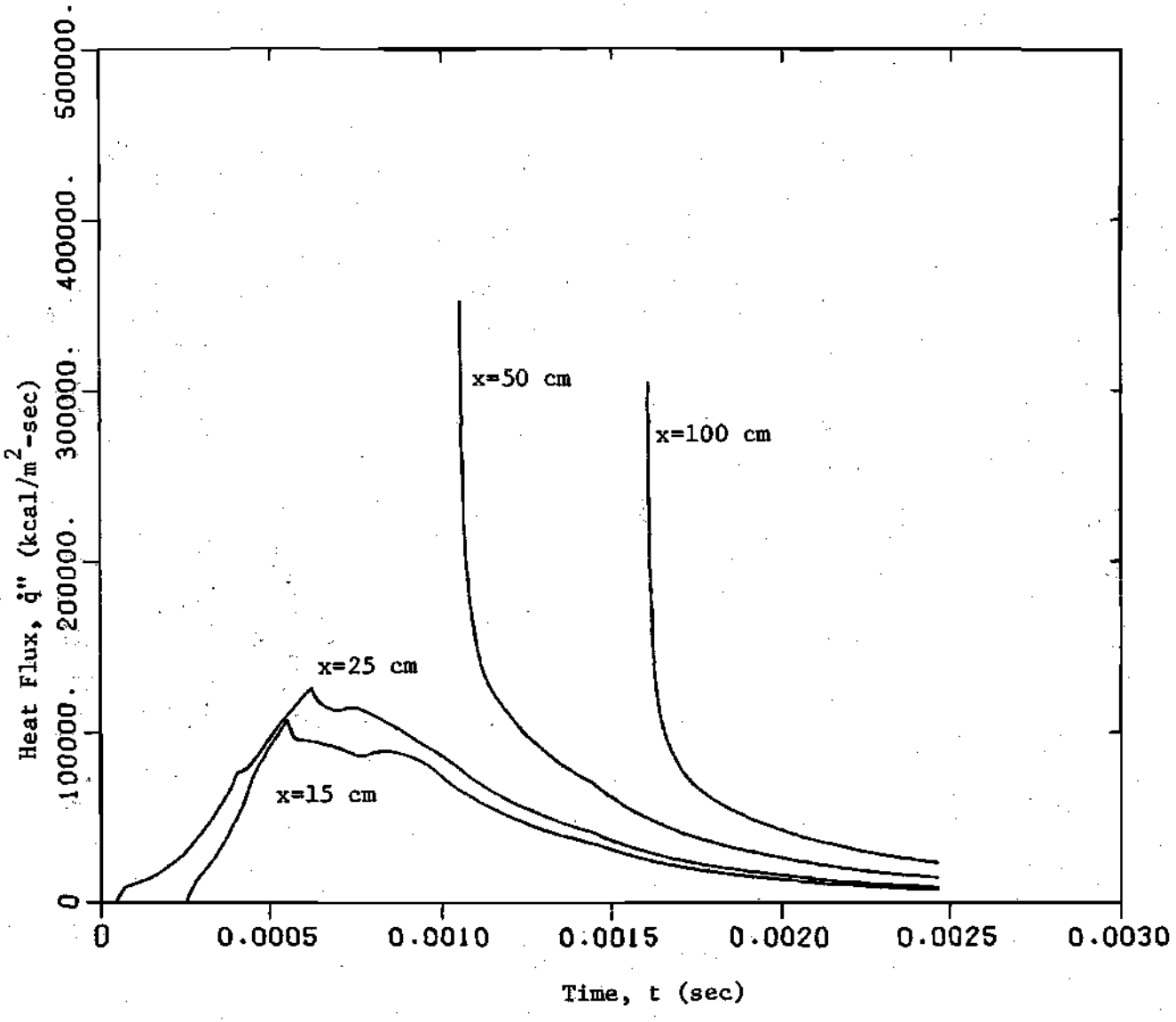

Figure 28. Variation of Heat Fluxes at Certain Fixed Locations with Time (Case I).

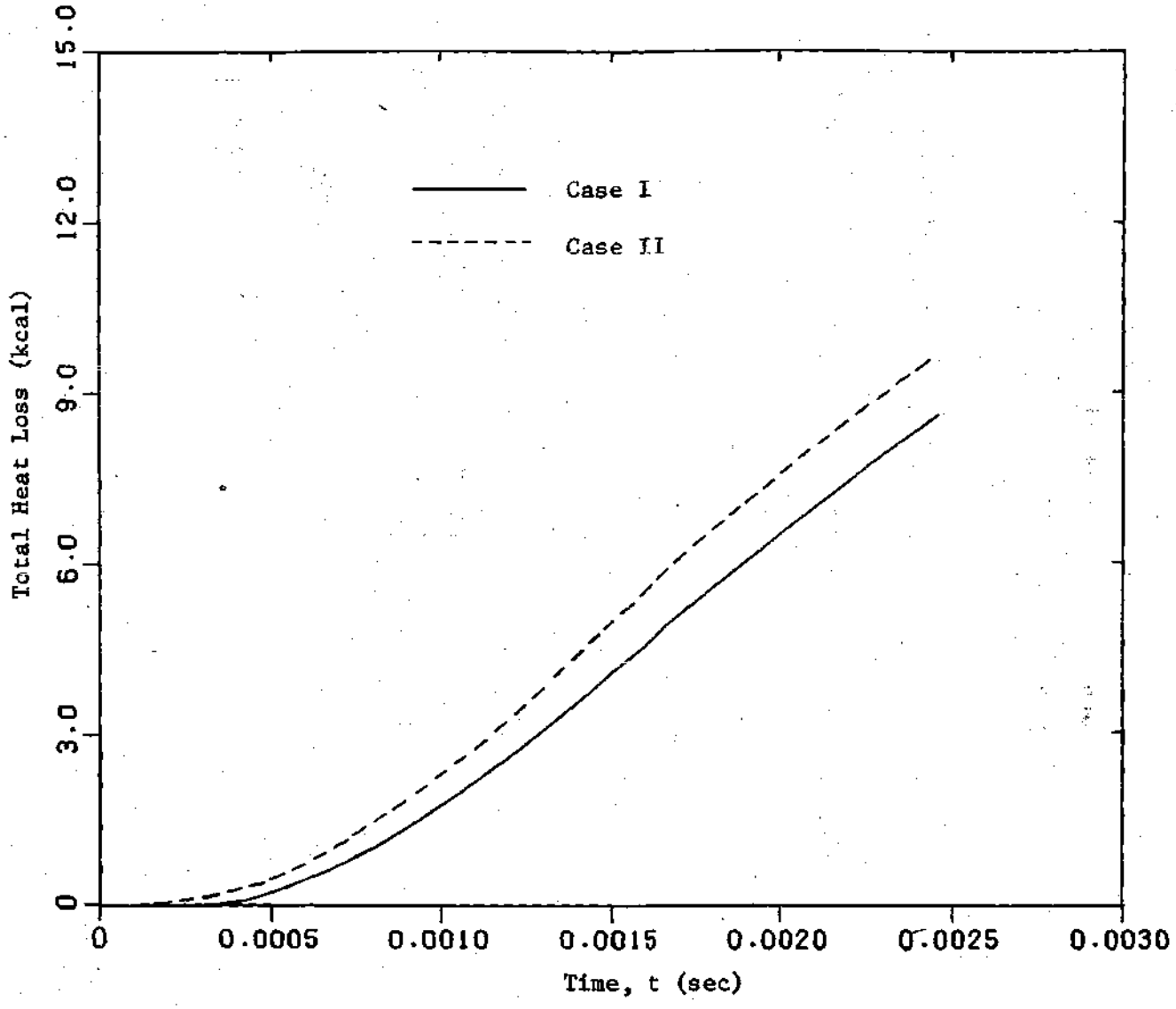

Figure 29. Comparison of Total Heat Losses to the Tube Wall in Case I and Case II.

Table 2. Comparison of Results for Two Limiting Cases of Solids Velocity

	Case I (solids moving)	Case II (solids stationary)
Time of travel (second)	0.002465	0.002448
Final piston velocity (m/sec)	1242.3	1271.3
Peak breech pressure (atmosphere)	6450	7200
Peak surface temperature (^{o}K)	1067	1270
Ballistic efficiency (%)	35.47	37.14
Total heat loss (kcal)	8.64	9.60
Heat loss in percentage of input energy (%)	5.10	5.66

Table 3. Mass and Energy Balance for Case I and Case II.

	Case I	Case II
Initial Conditions:		
Propellant charge (kg)	0.172	0.172
Propellant energy (kcal)	169.53	169.53
Final Conditions:		
Total gas mass (kg)	0.1716	0.1713
Gas internal energy (kcal)	90.10	87.63
Gas kinetic energy (kcal)	9.90	8.56
Piston kinetic energy (kcal)	60.13	62.96
Heat loss (kcal)	8.64	9.60
Total energy (kcal)	168.77	168.75
Error in Mass Balance (%)	-0.233	-0.407
Error in Energy Balance (%)	-0.450	-0.460

has also been presented. The total heat loss to the tube wall is found to be five to six per cent of the input energy and about 15 per cent of the final piston kinetic energy.

Parameter Variation

Because of the large number of independent design parameters, no general correlation is attempted here. Only a few important parameters are varied for Case I to study their effect on the ballistic as well as heat transfer solution, and the important results are presented in Table 4.

Initial Chamber Pressure, P_o

The selection of initial chamber pressure, i.e. "piston start pressure" is quite arbitrary as it is very difficult in practice to determine the exact pressure at which the piston starts to move. Therefore, two different initial chamber pressures, 100 atmosphere and 300 atmosphere, other than the "standard" 200 atmosphere are considered and the solution neglecting the heat transfer and skin friction is presented in Figure 30. The peak breech pressure and the final piston velocity are very much the same for all the three cases of different piston start pressures. Only the time of travel is prolonged as the initial pressure decreases. It is obvious that the heat transfer solution would be very close for all the three initial pressures because of close ballistic properties. This implies that the piston start pressure has insignificant effect on the overall performance of the device.

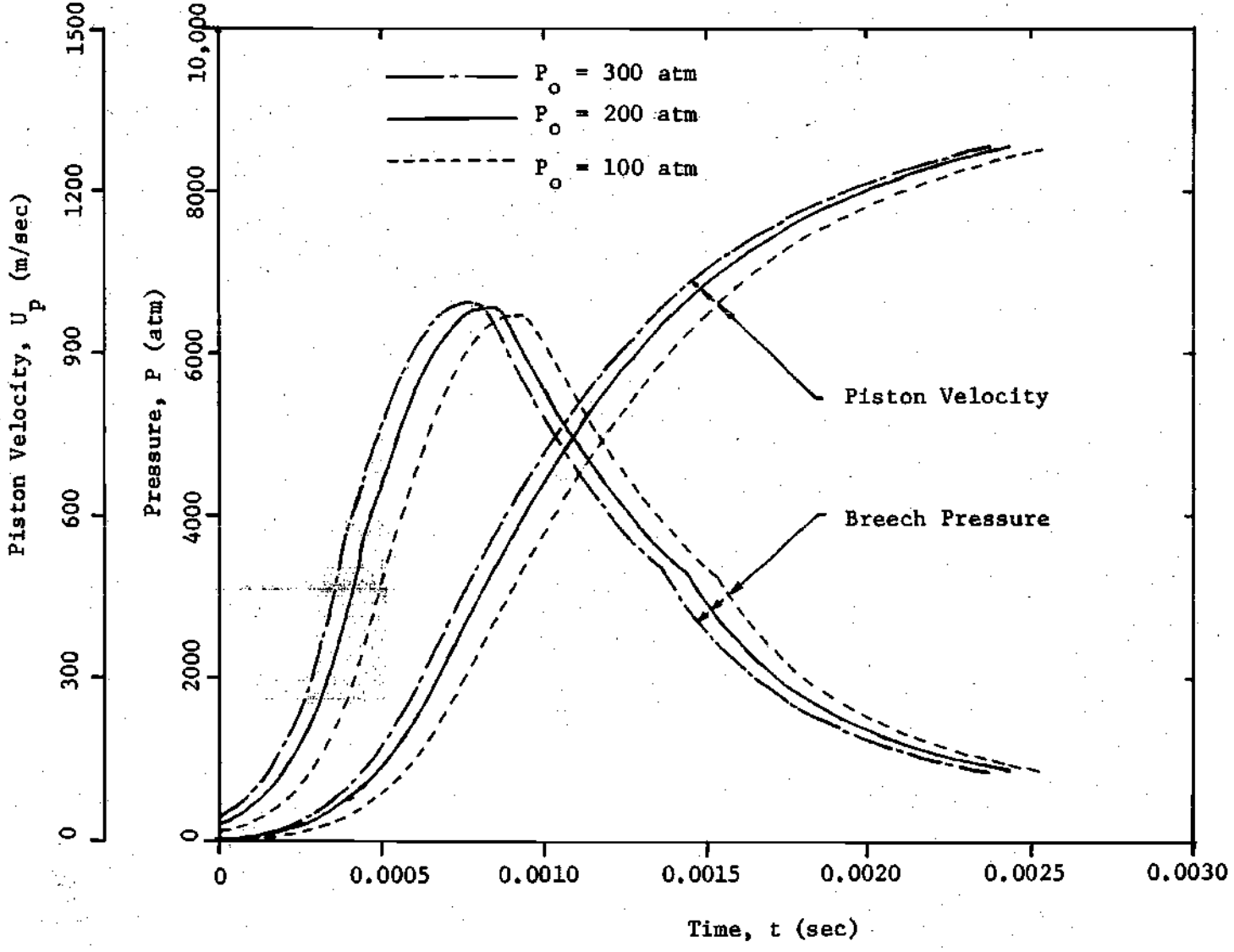

Figure 30. Variation of Breech Pressure and Piston Velocity with Time for Various Piston Start Pressures (Case I).

Profile Shape Factor, H

In the present work the profile shape factor, H, is assumed to be a constant throughout the entire solution; however, this may not be true in the real situation. For non-uniform steady flow, a favorable pressure gradient lowers the value of H [24] whereas in uniform steady flow an increase in flow Mach number increases H [13]. In the present case, however, it is difficult to predict its probable variation. Therefore, two different values of shape factor, 1.4 and 1.2222, corresponding to the one-fifth and the one-ninth velocity profile, are taken and the results are compared with those for H equal to 1.2857. It is clear from Figure 31 that lower values of H cause higher values of boundary layer thickness and heat transfer coefficient, i.e. the viscous effect of the fluid is higher. Because of this, the total heat loss to the tube wall and the peak inner surface temperature go up as the shape factor decreases. However, at H equal to 1.2222, these values do not exceed the corresponding values for the "standard conditions" by more than ten per cent. The total heat losses to the tube wall for the three different values of shape factor are compared in Figure 32.

Tube Inside Diameter, D

The tube inside diameter is varied keeping the loading density (m_{s_i}/V_o), and the piston mass per unit area (M_p/A_p) constant. Two tube diameters, namely 2 cm and 4 cm, are selected with appropriate propellant charge m_{s_i} and piston mass M_p. The results are shown in Figure 33. It can be noted from Table 4 that although an increase in tube diameter means an increase in the total heat loss, the heat loss per unit input energy decreases with larger tube diameter. This is due to decrease in

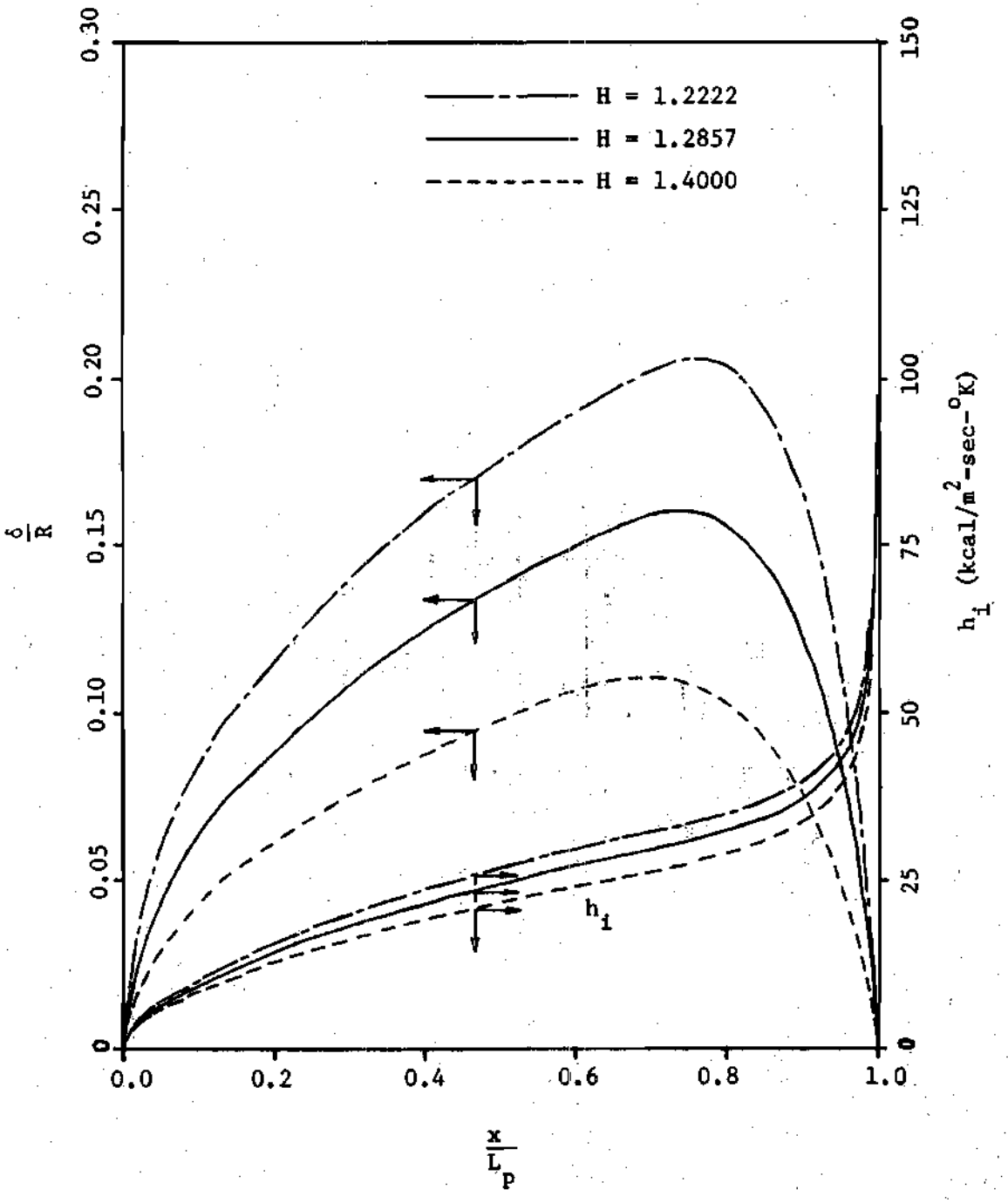

Figure 31. Comparison of Boundary Layer Thickness and Heat Transfer Coefficient for Various Profile Shape Factors at 0.002337 sec (Case I).

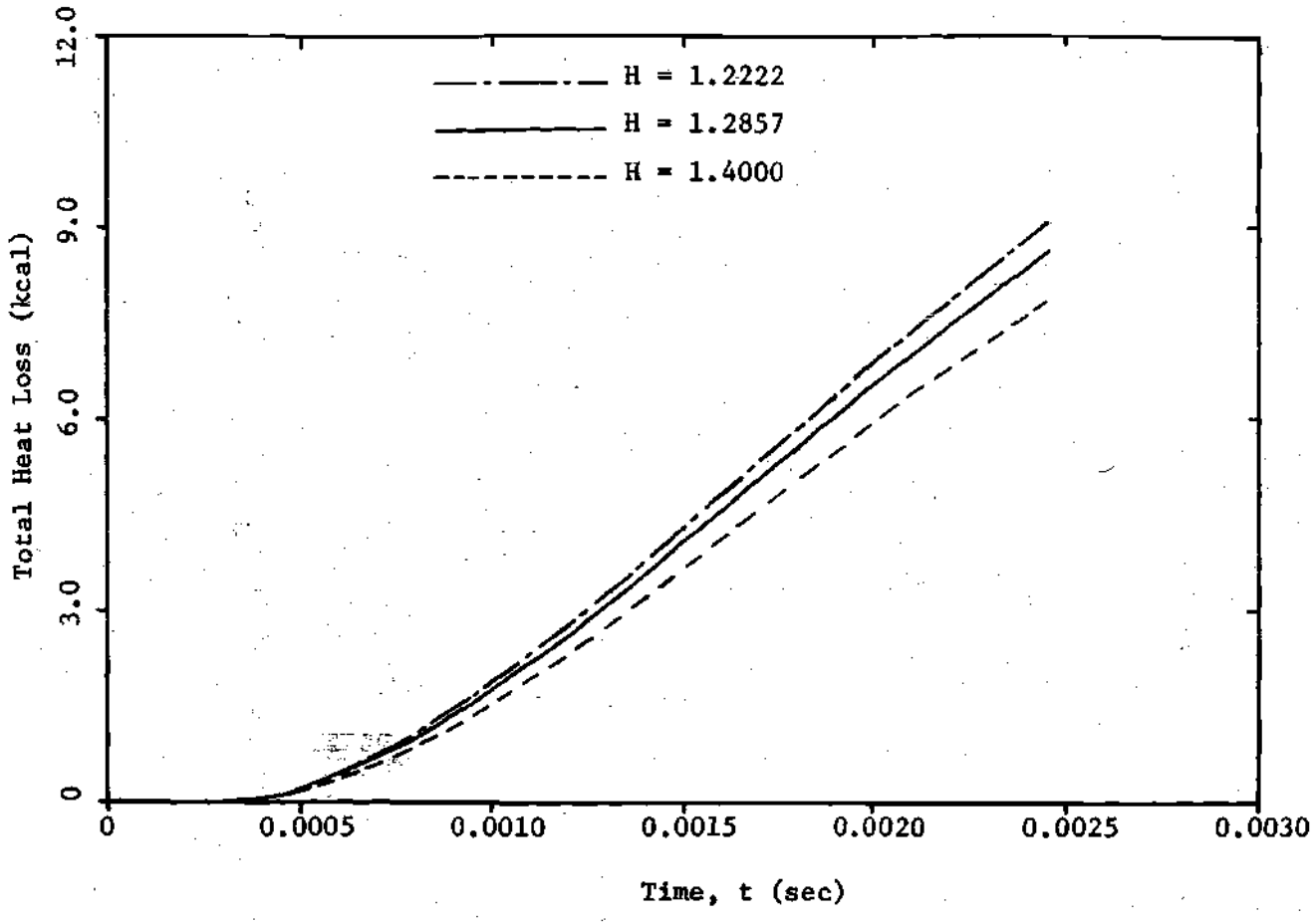

Figure 32. Comparison of Total Heat Loss to the Tube Wall for Various Profile Shape Factors (Case I).

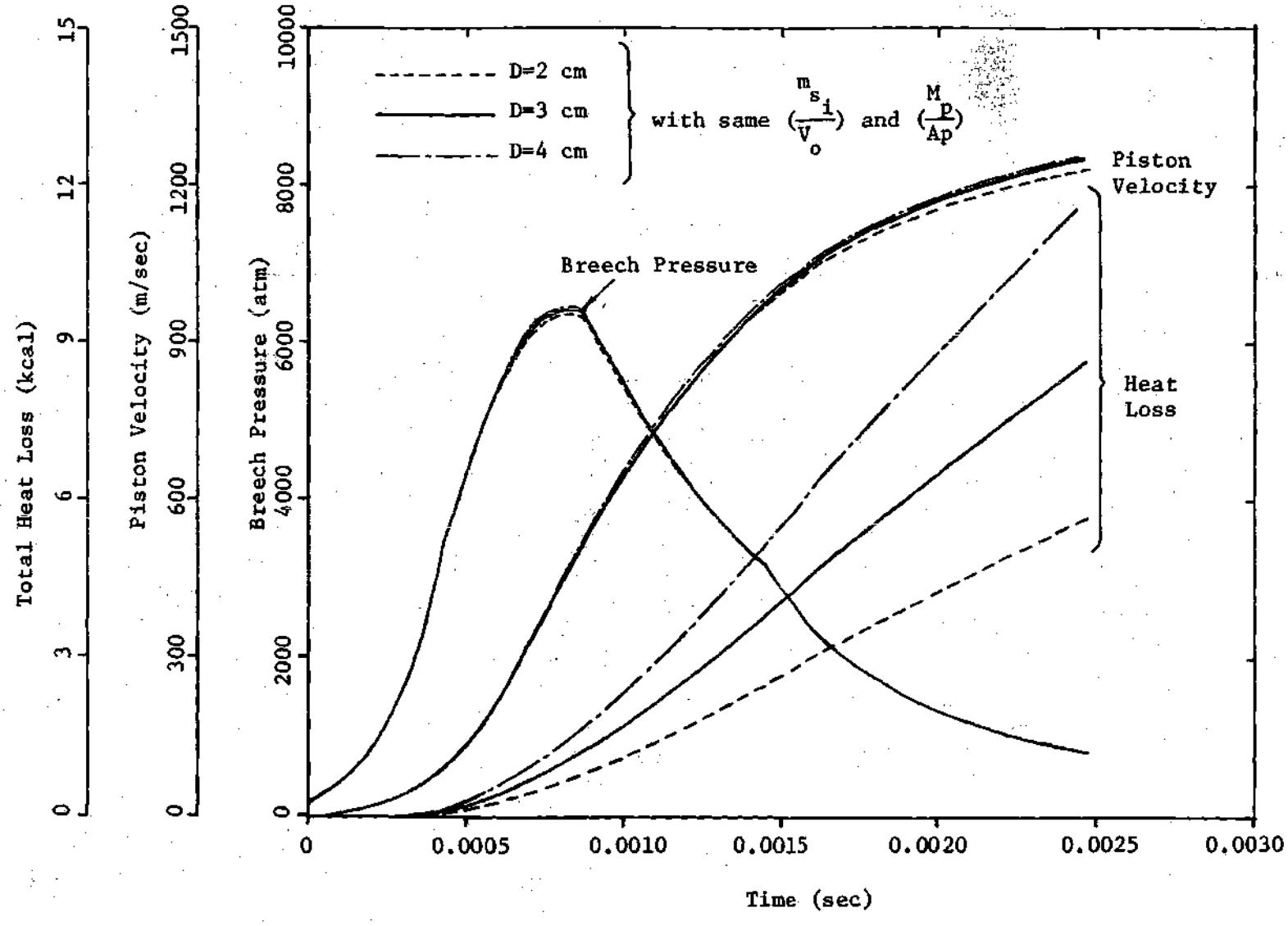

Figure 33. Comparison of Breech Pressure, Piston Velocity and Total Heat Loss to the Tube Wall for Various Tube Diameters with same Loading Density and same Piston Mass per Unit Area (Case I).

the surface to volume ratio. In other words, for ballistically similar devices, the increase in tube diameter reduces the heat loss per unit mass of gas and this accounts for the slightly better ballistic results obtained for the 4 cm diameter tube.

Propellant Charge, m_{s_i}

Two different values of the propellant charge, namely 0.15 kg and 0.19 kg are chosen apart from the "standard" value of 0.172 kg and the results are presented in Figure 34. It is obvious that an increase in propellant charge improves the ballistic efficiency of the device. But at the same time this increases the peak pressure, heat transfer coefficient and the peak surface temperature which put a limit on the propellant charge.

Piston Mass, M_p

Piston mass plays an important role in the problem of internal ballistics. Therefore, besides the standard mass of 0.326 kg two other pistons having masses equal to 0.2 kg and 0.5 kg are considered. The results are shown in Figure 35. The heavier the piston, the slower it moves thereby leaving less room for the combustion gas to expand, which causes an increase in the peak pressure. Although the heavier piston moves slower, the ballistic efficiency of the device is improved and therefore suitable for the application where energy conversion is of prime interest. But if higher velocity is desired a lighter piston would be chosen. The surface temperature is also lower in the case of a lighter piston due to lower pressures which lead to lower heat transfer coefficients.

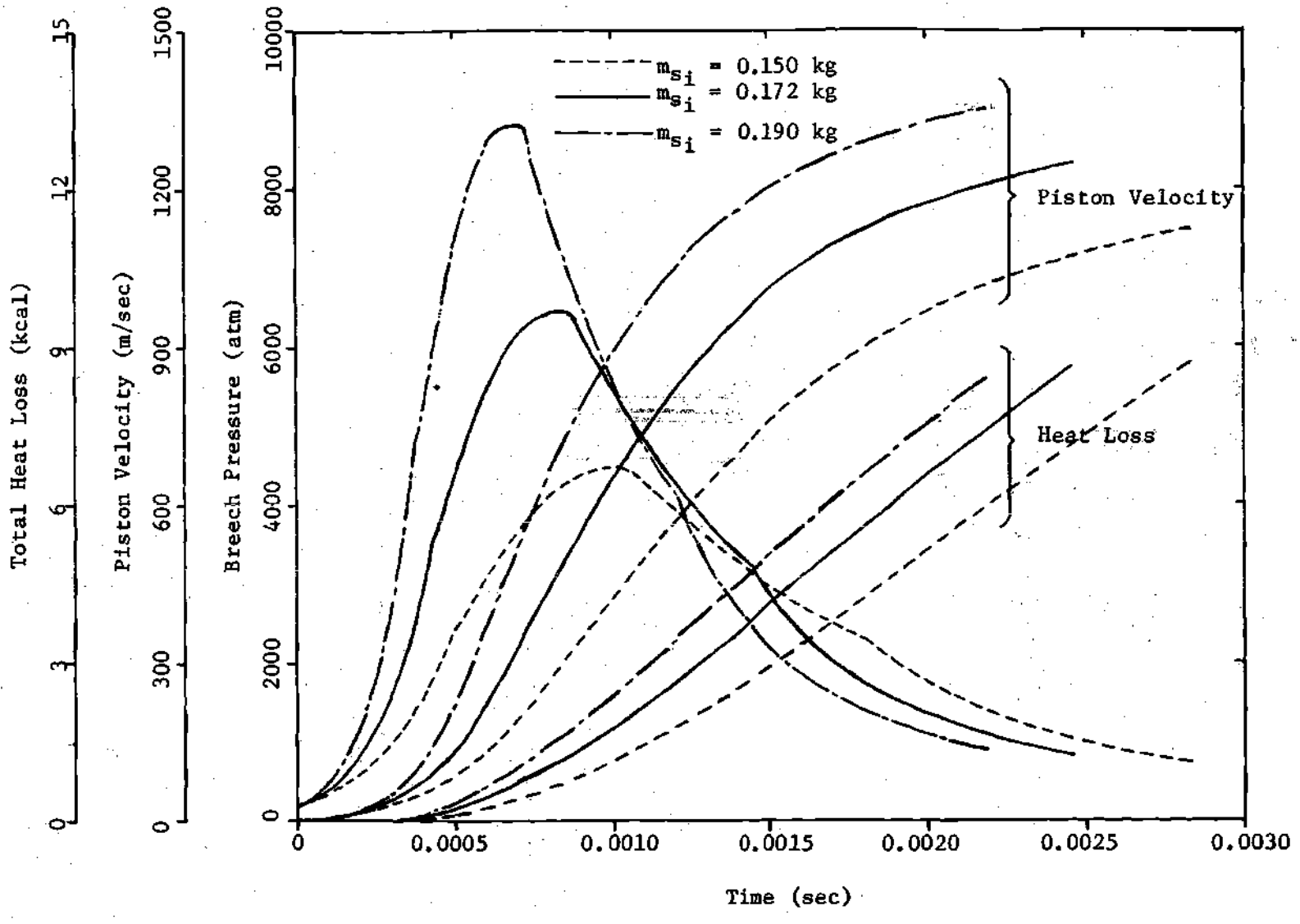

Figure 34. Comparison of Breech Pressure, Piston Velocity and Total Heat Loss to the Tube Wall for Various Propellant Charges (Case I).

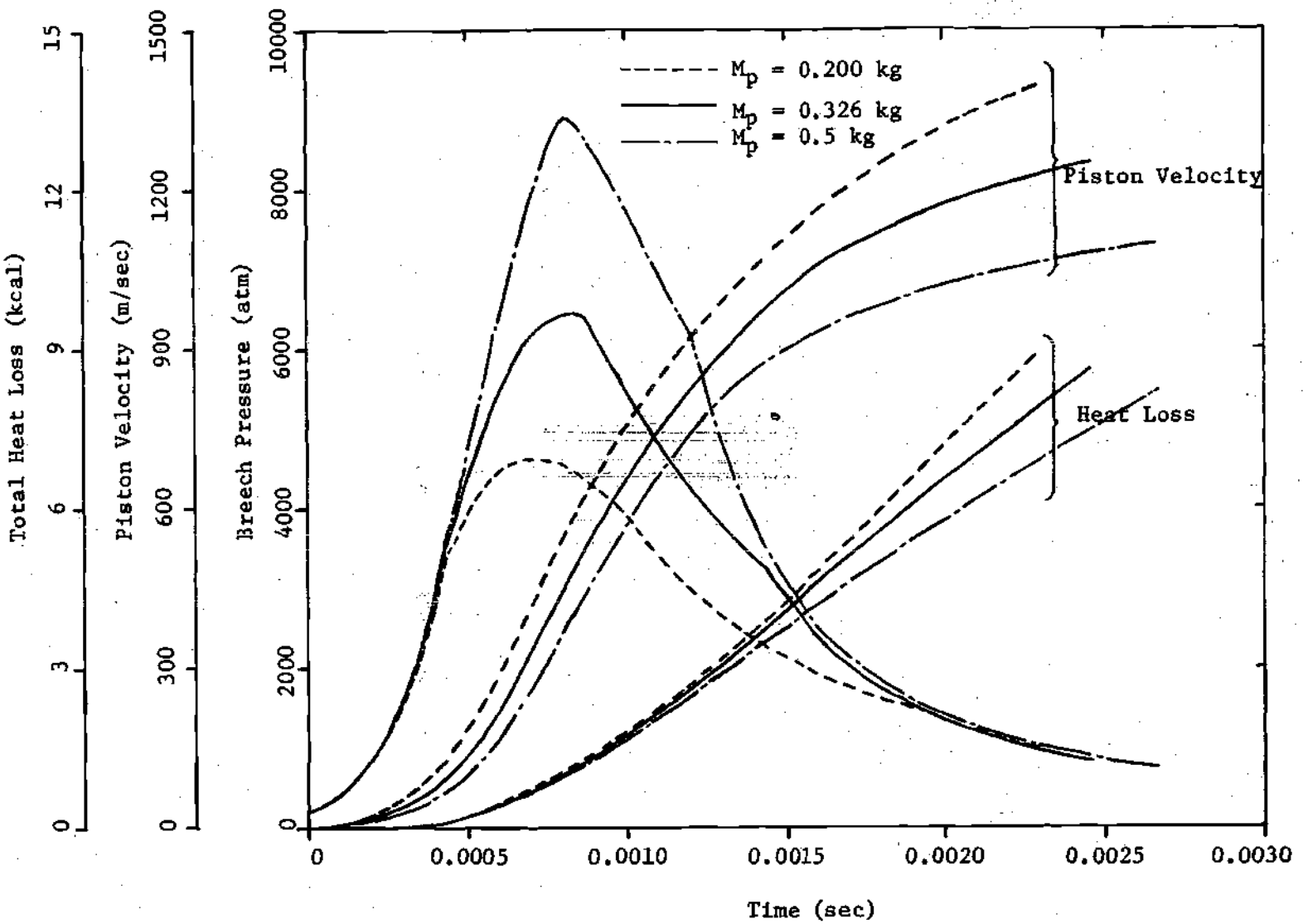

Figure 35. Comparison of Breech Pressure, Piston Velocity and Total Heat Loss to the Tube Wall for Various Piston Masses (Case I).

Web Thickness, w_{s_i}

Although the web thickness is only a geometrical property of the solid particles, it is important because it determines the total burning surface for a given propellant charge. For thinner webs more surface is available for burning and consequently the pressure rise is more rapid. This aspect is clear from Figure 36 where results of three different web thicknesses, namely 0.5mm, 0.711 mm (standard), and 0.9 mm are presented. A rapid pressure rise naturally accelerates the piston faster and thus improves the ballistic efficiency. But this gain is neutralized by a much higher peak pressure and wall surface temperature.

Comparison with Other Work

No analytical work in the past considered the movement of the solid particles in the one-dimensional ballistic solution. Although Carriere [5] studied the problem of internal ballistics assuming the solids to be stationary, it was not possible to determine the input data and final results from his publication. Therefore, a quantitative comparison could not be made. However, an excellent qualitative agreement is observed between his results showing the piston path, piston velocity and end pressures, and the results obtained from the present analysis for the case of stationary solids. Unfortunately, no work until now shows the spacewise distribution of the ballistic properties and, therefore no comparison can be made.

The boundary layer and heat transfer analysis of Hicks and Thornhill [2] assumed the "Lagrange approximation" and omitted the zero boundary layer thickness condition at the piston base. The values of

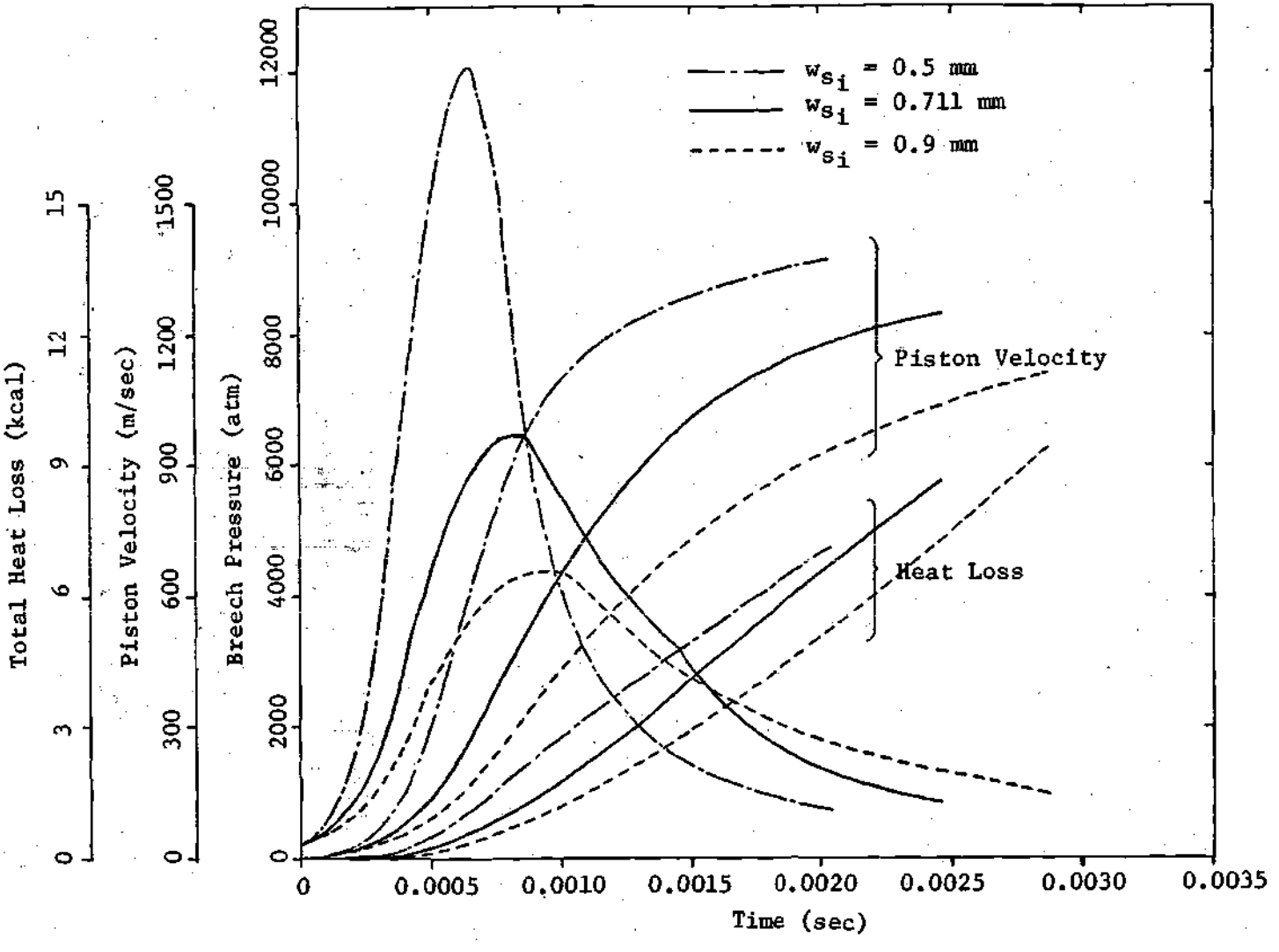

Figure 36. Comparison of Breech Pressure, Piston Velocity and Total Heat Loss to the Tube Wall for Various Web Thicknesses (Case I).

Table 4. Results for Various Input Parameters.

Parameter / Item	H		D		m_{s_i}		M_p		w_{s_i}	
	1.2222	1.40	2.0cm	4.0cm	0.15kg	0.19kg	0.2kg	0.5kg	0.5mm	0.9mm
Time of travel (millisecond)	2.467	2.462	2.484	2.456	2.840	2.196	2.292	2.680	2.047	2.876
Peak breech pressure (atmosphere)	6440	6460	6400	6500	4470	8840	4660	8900	12000	4380
Peak surface temperature (^{O}K)	1114	991	1059	1071	985	1127	1008	1099	1180	984
Ballistic efficiency (%)	35.37	35.63	34.52	35.94	32.86	37.68	27.11	41.85	42.83	28.10
Total heat loss (kcal)	9.09	7.87	5.70	11.60	8.69	8.44	8.85	8.24	7.13	9.43
Heat loss in percentage of input energy (%)	5.36	4.65	7.58	3.85	5.88	4.5	5.21	4.86	4.21	5.56

heat transfer coefficient for a typical case (input data not indicated) presented in reference [2], are lower than the values obtained for the typical case in the present study, roughly by a factor of two. The reason could be due to entirely different input data and different boundary layer thickness condition at the piston base. However, the value of peak surface temperature and the location where it occurs, are in good agreement with the study of Hicks and Thornhill.

A very recent analysis on convective heat transfer in gun barrels [25], which is also based on the "Lagrange approximation," indicates that the heat flux at the inside surface of the barrel can be as high as 2.7×10^5 kcal/m^2-sec. This value is quite close to the expected maxima shown in Figure 28 for the typical case.

CHAPTER V

CONCLUSIONS

The following conclusions can be drawn in the context of the results presented in the previous chapter:

1. The "Lagrange approximation" of linear velocity distribution and uniform gas density along the length of the tube is not a good representation of the real case. It takes a considerable amount of total time before the velocity distribution can be linear. Furthermore, the gas density cannot be called "uniform" at any time.

2. There is a large pressure gradient along the length of the tube and at the peak condition the difference between the pressures at the two ends can be as high as 20 to 30 per cent of the maximum pressure.

3. As the piston moves, the gas temperature continuously decreases with almost a uniform spacewise distribution. For the case of stationary solids, however, a steep spacewise temperature rise is observed at the back of the piston.

4. While the final ballistic results are more or less the same for the two extreme cases of solids velocity, the peak pressure in the case of stationary solids is about 10 to 15 per cent higher than in the case of moving solids.

5. The maximum boundary layer thickness can be on the order of 20 per cent of the tube radius in typical cases. For ballistically similar devices the ratio of the maximum boundary layer thickness to the tube radius increases as the tube diameter is reduced. Therefore

the assumption of a thin boundary layer may not hold good for very small diameter tubes.

6. The order of magnitude of the heat transfer coefficient and the heat flux at the inner surface of the tube is extremely high. Average values of 50 kcal/m^2-sec-^oK and 50,000 kcal/m^2-sec for the heat transfer coefficient and the heat flux, respectively, can be expected for typical cases. The maximum values can be five to six times higher than the average values; but the maxima do not last for more than a few microseconds.

7. The tube inner surface temperature can reach 1000^oC for typical cases and it occurs near the initial piston position. The time of travel is so short that even with the extremely high values of heat fluxes and high thermal properties of tube material the temperature wave cannot penetrate more than one millimeter into the tube wall.

8. The total heat loss to the tube wall is five to six per cent of the input energy for typical cases and has only a minor effect on the final ballistic results. The same conclusion is valid for the skin fraction.

9. The piston start pressure, although difficult to determine in practice, does not pose any real problem due to its insignificant effect on the ballistic solution.

10. Improvement in ballistic efficiency can be brought about by increasing the propellant charge, the piston mass, or by reducing the web thickness. But in each of these cases, there exists an adverse effect of higher peak pressure and higher wall temperature. Therefore,

a great care should be taken in order to obtain the optimum design conditions.

CHAPTER VI

RECOMMENDATIONS

1. Since considerable differences in peak pressure and tube wall temperature are observed in two limiting cases of solids velocity, a rigorous analysis including the correct solids velocity would be of help in predicting peak pressure and wall temperature.

2. The assumption of constant burning surface and uniform burning rate for all the solid particles at any instance of time can be relaxed to make the analysis more general. Relaxation of the latter assumption would increase the difference between the end pressures, as the burning rate at the tube head end would be higher than that at the piston base end.

3. More experimental as well as theoretical studies on the wall shear stress and shape factor should be carried out for non-steady turbulent flow with favorable pressure gradient to improve the present boundary layer analysis. One immediate step, however, would be to include an auxiliary equation for $\frac{\partial H}{\partial t}$.

4. The analogy between heat and momentum transfer can be replaced by the boundary layer energy equation for more accurate evaluation of the heat transfer coefficient.

5. The present analysis only provides a way to determine the tube wall temperature during the first operation of the device. This should further be extended to evaluate the maximum wall temperature when

the device is operated repetitively at high frequency as practical devices.

APPENDIX

APPENDIX A

Derivation of Conservation Equations

A control volume approach has been taken for the derivation of the conservation equations. In Figure 37 a control volume having a cross-sectional area A_p and length Δx has been shown. The volume fraction of solids per unit length is ν_s, or in the other words, ν_s is the fraction of the total cross-sectional area A_p occupied by the solids. Therefore, $(1-\nu_s)$ is the fractional area occupied by the gases at any position and time.

Due to the assumptions regarding the burning rate of the solids (same for all the particles at a particular instant) and the constant total burning surface S_{b_t}, it is easy to estimate the burning surface available in the chosen control volume,

$$S_L = S_{b_t} \frac{\nu_s A_p \Delta x}{\int_0^{L_p} \nu_s A_p \, dx} \tag{A.1}$$

Therefore, the rate of gas produced (by mass) from the solids (or, rate of decrease of solids by mass) within the control volume is given by,

$$\rho_s S_L r_b$$

$$= \rho_s S_{b_t} \frac{\nu_s \Delta x \, r_b}{\int_0^{L_p} \nu_s \, dx} \tag{A.2}$$

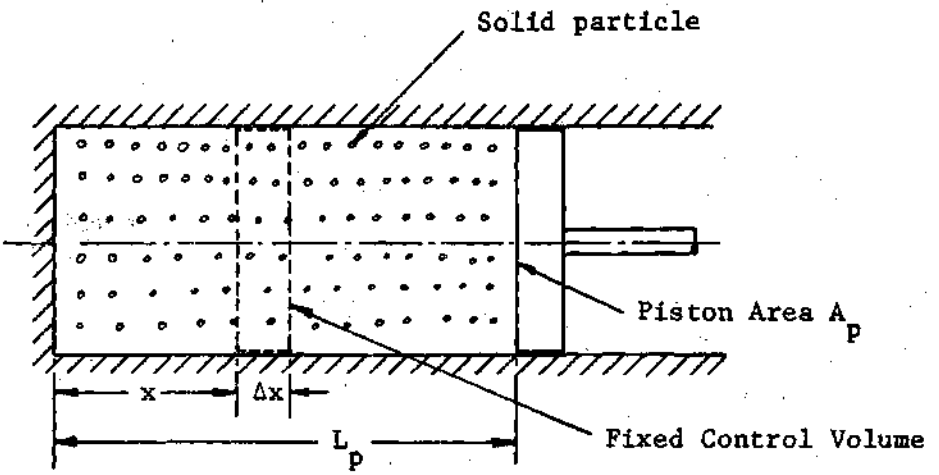

Figure 37. Schematic of Control Volume Chosen for the Derivation of Conservation Equations.

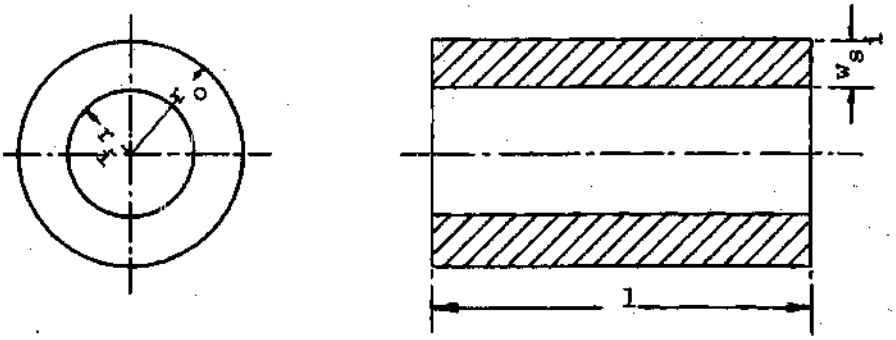

Figure 38. A Typical Solid Particle Assumed in the Present Study.

Case I (Solid particles moving at gas velocity)

Continuity of solids.

Rate of increase of solid mass in c.v. = Rate of solid flowing in − Rate of solid flowing out − Rate of gas produced in c.v.

$$\frac{\partial}{\partial t}(\rho_s A_p \nu_s \Delta x) = (\rho_s U_s A_p \nu_s)\Big|_x - (\rho_s U_s A_p \nu_s)\Big|_{x+dx} - \rho_s S_{b_t} \frac{\nu_s r_b \Delta x}{\int_0^{L_p} \nu_s dx}$$

or,

$$A_p \rho_s \left[\frac{\partial \nu_s}{\partial t} + \frac{\partial}{\partial x}(\nu_s U_s)\right] + \rho_s S_{b_t} \frac{\nu_s r_b}{\int_0^{L_p} \nu_s dx} = 0$$

with $U_s = U_g = U$,

$$\frac{\partial \nu_s}{\partial t} + U \frac{\partial \nu_s}{\partial x} + \nu_s \frac{\partial U}{\partial x} + \left(\frac{S_{b_t}}{A_p}\right) \frac{\nu_s r_b}{\int_0^{L_p} \nu_s dx} = 0$$

or,

$$\frac{\partial \nu_s}{\partial t} + U \frac{\partial \nu_s}{\partial x} + \nu_s \frac{\partial U}{\partial x} + \dot{v}_{d_s} = 0 \qquad (A.3)$$

Continuity of Gases.

Rate of increase of mass of gas in c.v. = Rate of gas flowing in − Rate of gas flowing out + Rate of gas produced in c.v.

$$\frac{\partial}{\partial t}\left[(1-\nu_s)\rho_g A_p \Delta x\right] = \left[(1-\nu_s)\rho_g A_p U_g\right]\Big|_x - \left[(1-\nu_s)\rho_g A_p U_g\right]\Big|_{x+dx} + \rho_s S_{b_t} \frac{\nu_s r_b \Delta x}{\int_0^{L_p} \nu_s dx}$$

or,

$$\frac{\partial}{\partial t}\left[(1-\nu_s)\rho_g\right] + \frac{\partial}{\partial x}\left[(1-\nu_s)\rho_g U_g\right] = \rho_s \left(\frac{S_{b_t}}{A_p}\right) \frac{\nu_s r_b}{\int_0^{L_p} \nu_s dx}$$

Using equation (A.3) and $U_s = U_g = U$:

$$(1-\nu_s)\frac{\partial \rho_g}{\partial t} + (1-\nu_s)\, U \frac{\partial \rho_g}{\partial x} + \rho_g \frac{\partial U}{\partial x} = (\rho_s - \rho_g)\, \dot{v}_{d_s}$$

or,

$$\frac{\partial \rho_g}{\partial t} + U \frac{\partial \rho_g}{\partial x} + \frac{\rho_g}{(1-\nu_s)} \frac{\partial U}{\partial x} = \frac{(\rho_s - \rho_g)}{(1-\nu_s)}\, \dot{v}_{d_s} \qquad (A.4)$$

A general equation of continuity can be obtained by considering the gas-solid mixture as a whole which gives,

Rate of increase of mass of gas-solid mixture in c.v.	=	Rate of gas-solid mixture flowing in	-	Rate of gas-solid mixture flowing out

$$\frac{\partial}{\partial t}\left[\nu_s \rho_s A_p \Delta x + (1-\nu_s)\rho_g A_p \Delta x\right] = \left[\nu_s \rho_s U A_p + (1-\nu_s)\rho_g U A_p\right]\Big|_x - \left[\nu_s \rho_s U A_p + (1-\nu_s)\rho_g U A_p\right]\Big|_{x+dx}$$

or,

$$\frac{\partial}{\partial t}\left[\nu_s \rho_s + (1-\nu_s)\rho_g\right] + \frac{\partial}{\partial x}\left[\nu_s \rho_s U + (1-\nu_s)\rho_g U\right] = 0 \qquad (A.5)$$

Momentum Equation.

Rate of increase of momentum in c.v.	+	Momentum flux out	-	Momentum flux in	=	Σ External forces

$$\frac{\partial}{\partial t}\left[\nu_s\rho_s U + (1-\nu_s)\rho_g U\right] A_p\,\Delta x + \left[\nu_s\rho_s U^2 + (1-\nu_s)\rho_g U^2\right] A_p\Big|_{x+dx}$$

$$- \left[\nu_s\rho_s U^2 + (1-\nu_s)\rho_g U^2\right] A_p\Big|_{x}$$

$$= P\,A_p\Big|_x - P\,A_p\Big|_{x+dx} - 2\pi R\,\Delta x\,\tau_w$$

or,

$$\frac{\partial}{\partial t}\left[\{\nu_s\rho_s + (1-\nu_s)\rho_g\}U\right] + \frac{\partial}{\partial x}\left[\{\nu_s\rho_s U + (1-\nu_s)\rho_g U\}U\right] = -\frac{\partial P}{\partial x} - \frac{2\tau_w}{R}$$

Using equation (A.5):

$$\left[\nu_s\rho_s + (1-\nu_s)\rho_g\right]\left[\frac{\partial U}{\partial t} + U\frac{\partial U}{\partial x}\right] = -\frac{\partial P}{\partial x} - \frac{2\tau_w}{R}$$

Now, mixture density $\rho_m = \nu_s\rho_s + (1-\nu_s)\rho_g$

$$\therefore \quad \frac{\partial U}{\partial t} + U\frac{\partial U}{\partial x} = -\frac{1}{\rho_m}\frac{\partial P}{\partial x} - \frac{2\tau_w}{\rho_m R} \qquad (A.6)$$

Energy Equation.

Rate of increase of energy in c.v. = Energy flux flowing in − Energy flux flowing out + Rate of increase of energy due to conversion of solids into gases in c.v.

− Rate of work done by the gas-solid mixture − Rate of heat loss to the tube wall

or,

$$\frac{\partial}{\partial t}\left[\{\nu_s\rho_s(e_s+\frac{U_s^2}{2})+(1-\nu_s)\rho_g(e_g+\frac{U_g^2}{2})\}A_p\,\Delta x\right]$$

$$=\left[\{\nu_s\rho_s(e_s+\frac{U_s^2}{2})U_s+(1-\nu_s)\rho_g(e_g+\frac{U_g^2}{2})U_g\}A_p\right]\Big|_x$$

$$-\left[\{\nu_s\rho_s(e_s+\frac{U_s^2}{2})U_s+(1-\nu_s)\rho_g(e_g+\frac{U_g^2}{2})U_g\}A_p\right]\Big|_{x+dx}$$

$$+\rho_s\,S_{b_t}\frac{\nu_s r_b\Delta x}{\int_o^{L_p}\nu_s dx}\,\Delta E-\left[A_p\left\{\nu_s\rho_s U_s(\frac{P}{\rho_s})+(1-\nu_s)\rho_g U_g(\frac{P}{\rho_g})\right\}\Big|_{x+dx}\right.$$

$$\left.-A_p\left\{\nu_s\rho_s U_s(\frac{P}{\rho_s})+(1-\nu_s)\rho_g U_g(\frac{P}{\rho_g})\right\}\Big|_x\right]-2\pi R\,\Delta x\,h_i(T-T_{w,i})$$

where, ΔE = Additional energy release per unit mass due to conversion of solids into gases,

$$= c_v T_o - c_s T_s \quad = W - c_s T_s \tag{A.7}$$

Using the definition of enthalpy for solids and gas, i.e.

$$h_s = e_s + \frac{P}{\rho_s} \quad ; \qquad h_g = e_g + \frac{P}{\rho_g} \quad :$$

$$\frac{\partial}{\partial t}\left[\nu_s\rho_s(h_s-\frac{P}{\rho_s})+(1-\nu_s)\rho_g(h_g-\frac{P}{\rho_g})\right]+\frac{\partial}{\partial x}\left[\nu_s\rho_s h_s U_s+(1-\nu_s)\rho_g h_g U_g\right]$$

$$+\frac{\partial}{\partial t}\left[\nu_s\rho_s\frac{U_s^2}{2}+(1-\nu_s)\rho_g\frac{U_g^2}{2}\right]$$

$$+\frac{\partial}{\partial x}\left[\nu_s\rho_s\frac{U_s^2}{2}U_s+(1-\nu_s)\rho_g\frac{U_g^2}{2}U_g\right]=\rho_s(\frac{S_{b_t}}{A_p})\frac{\nu_s r_b\Delta E}{\int_o^{L_p}\nu_s dx}$$

$$-\frac{2h_i}{R}(T-T_{w,i})$$

Using $U_s = U_g = U$,

$$\frac{\partial}{\partial t}\left[\nu_s\rho_s h_s + (1-\nu_s)\rho_g h_g\right] - \frac{\partial P}{\partial t} + \frac{\partial}{\partial x}\left[\nu_s\rho_s h_s U + (1-\nu_s)\rho_g h_g U\right]$$

$$+ \frac{U^2}{2}\frac{\partial}{\partial t}\left[\nu_s\rho_s + (1-\nu_s)\rho_g\right] + \left[\nu_s\rho_s + (1-\nu_s)\rho_g\right] U\frac{\partial U}{\partial t}$$

$$+ \frac{U^2}{2}\frac{\partial}{\partial x}\left[\nu_s\rho_s U + (1-\nu_s)\rho_g U\right] + \left[\nu_s\rho_s + (1-\nu_s)\rho_g\right] U^2\frac{\partial U}{\partial x}$$

$$= \rho_s \dot{v}_{d_s} \Delta E - \frac{2h_i}{R}(T-T_{w,i})$$

Using the general equation of continuity (A.5) and the momentum equation (A.6):

$$\frac{\partial}{\partial t}\left[\nu_s\rho_s h_s + (1-\nu_s)\rho_g h_g\right] + \frac{\partial}{\partial x}\left[\nu_s\rho_s h_s U + (1-\nu_s)\rho_g h_g U\right] - \frac{\partial P}{\partial t} + U\frac{\partial P}{\partial x}$$

$$= \rho_s \dot{v}_{d_s} \Delta E - \frac{2h_i}{R}(T-T_{w,i}) + \frac{2\tau_w U}{R}$$

On differentiation and by use of continuity of solids (A.3) and continuity of gases (A.4):

$$\nu_s\rho_s\left[\frac{\partial h_s}{\partial t} + U\frac{\partial h_s}{\partial x}\right] + (1-\nu_s)\rho_g\left[\frac{\partial h_g}{\partial t} + U\frac{\partial h_g}{\partial x}\right] - \frac{\partial P}{\partial t} + U\frac{\partial P}{\partial x}$$

$$= \rho_s \dot{v}_{d_s}(\Delta E + h_s - h_g) - \frac{2h_i}{R}(T-T_{w,i}) + \frac{2\tau_w U}{R}$$

Using the notation $\frac{D}{Dt} = \frac{\partial}{\partial t} + U\frac{\partial}{\partial x}$

and $h_s = c_s T_s + \frac{P}{\rho_s}$, finally:

$$\nu_s \rho_s \frac{Dh_s}{Dt} + (1-\nu_s)\rho_g \frac{Dh_g}{Dt} - \frac{DP}{Dt} = \rho_s \dot{v}_{d_s} \left(W + \frac{P}{\rho_s} - h_g\right) - \frac{2h_i}{R}(T-T_{w,i}) + \frac{2\tau_w U}{R} \qquad (A.8)$$

Case II (Solid particles stationary at their initial positions)

Continuity of Solids.

Rate of increase of solid mass in c.v. = Rate of solids flowing in − Rate of solids flowing out − Rate of gas produced in c.v.

$$\frac{\partial}{\partial t}(\rho_s A_p \nu_s \Delta x) = 0 - 0 - \rho_s S_{b_t} \frac{\nu_s r_b \Delta x}{\int_0^{L_p} \nu_s dx}$$

or,

$$\frac{\partial \nu_s}{\partial t} = -\left(\frac{S_{b_t}}{A_p}\right) \frac{\nu_s r_b}{\int_0^{L_p} \nu_s dx} = -\dot{v}_{d_s} \qquad (A.9)$$

Continuity of Gases.

Rate of increase of mass of gas in c.v. = Rate of gas flowing in − Rate of gas flowing out + Rate of gas produced in c.v.

$$\frac{\partial}{\partial t}\left[(1-\nu_s)A_p \rho_g \Delta x\right] = \left[(1-\nu_s)A_p \rho_g U_g\right]\Big|_x - \left[(1-\nu_s)A_p \rho_g U_g\right]\Big|_{x+dx} + \rho_s S_{b_t} \frac{\nu_s r_b \Delta x}{\int_0^{L_p} \nu_s dx}$$

or,

$$\frac{\partial}{\partial t}\left[(1-\nu_s)\rho_g\right] + \frac{\partial}{\partial x}\left[(1-\nu_s)\rho_g U_g\right] = \rho_s\left(\frac{S_{b_t}}{A_p}\right)\frac{\nu_s r_b}{\int_0^{L_p}\nu_x dx} = \rho_s \dot{v}_{d_s} \quad (A.10)$$

Putting $U_g = U$ and using equation (A.9):

$$(1-\nu_s)\left[\frac{\partial \rho_g}{\partial x} + U\frac{\partial \rho_g}{\partial x} + \rho_g\frac{\partial U}{\partial x}\right] + \rho_g \dot{v}_{d_s} - \rho_g U\frac{\partial \nu_s}{\partial x} = \rho_s \dot{v}_{d_s}$$

or,

$$\frac{\partial \rho_g}{\partial t} + U\frac{\partial \rho_g}{\partial x} + \rho_g\frac{\partial U}{\partial x} = \frac{(\rho_s-\rho_g)}{(1-\nu_s)}\dot{v}_{d_s} + \frac{\rho_g U}{(1-\nu_s)}\frac{\partial \nu_s}{\partial x} \quad (A.11)$$

Momentum Equation. As the solids are at rest, the free gas volume in the control volume shown in Figure 37 is taken as the new control volume in the following derivation. It is assumed that the solids are at the core of the flow and the skin friction at the surface of the solid particles is negligible.

Rate of increase of momentum in c.v. + Momentum flux out − Momentum flux in = $\sum$ External forces

$$\frac{\partial}{\partial t}\left[(1-\nu_s)A_p\rho_g U_g \Delta x\right] + \left[(1-\nu_s)A_p\rho_g U_g^2\right]\Big|_{x+dx} - \left[(1-\nu_s)A_p\rho_g U_g^2\right]\Big|_x$$

$$= \left[(1-\nu_s)A_p P\right]\Big|_x - \left[(1-\nu_s)A_p P\right]\Big|_{x+dx}$$

$$+ P A_p \Delta x \frac{\partial(1-\nu_s)}{\partial x} - 2\pi R \Delta x \tau_w$$

or,

$$\frac{\partial}{\partial t}\left[\{(1-\nu_s)\rho_g\}U_g\right] + \frac{\partial}{\partial x}\left[\{(1-\nu_s)\rho_g U_g\}U_g\right] = -\frac{\partial}{\partial x}\left[(1-\nu_s)P\right] + P\frac{\partial(1-\nu_s)}{\partial x} - \frac{2\tau_w}{R}$$

Using equation (A.10) and putting $U_g = U$,

$$(1-\nu_s)\rho_g\left[\frac{\partial U}{\partial t} + U\frac{\partial U}{\partial x}\right] + \rho_s \dot{v}_{d_s} U = -(1-\nu_s)\frac{\partial P}{\partial x} - \frac{2\tau_w}{R}$$

or,

$$\frac{\partial U}{\partial t} + U\frac{\partial U}{\partial x} = -\frac{1}{\rho_g}\frac{\partial P}{\partial x} - \frac{\rho_s U}{(1-\nu_s)\rho_g}\dot{v}_{d_s} - \frac{2\tau_w}{(1-\nu_s)\rho_g R} \qquad \text{(A.12)}$$

Energy Equation. The same control volume as used in the derivation of momentum equation is taken.

Rate of energy increase in c.v. = Energy flux flowing in − Energy flux flowing out + Rate of energy increase due to gas coming into the c.v. from the solids − Rate of work done by the flowing gas − Rate of heat loss to the tube wall

or,

$$\frac{\partial}{\partial t}\left[(1-\nu_s)A_p\rho_g(e_g+\frac{U_g^2}{2})\Delta x\right] = \left[(1-\nu_s)A_p\rho_g U_g(e_g+\frac{U_g^2}{2})\right]\Big|_x$$

$$- \left[(1-\nu_s)A_p\rho_g U_g(e_g+\frac{U_g^2}{2})\right]\Big|_{x+dx}$$

$$+\rho_s S_{b_t}\int_0^{L_p}\frac{\nu_s\Delta x\, r_b}{\nu_s dx} W$$

$$- \left[\left\{(1-\nu_s)A_p\rho_g U_g(\frac{P}{\rho_g})\right\}\Big|_{x+dx}\right.$$

$$\left. - \left\{(1-\nu_s)A_p\rho_g U_g(\frac{P}{\rho_g})\right\}\Big|_x\right] - 2\pi R\,\Delta x\, h_i(T-T_{w,i})$$

or,

$$\frac{\partial}{\partial t}\left[(1-\nu_s)\rho_g(e_g+\frac{U_g^2}{2})\right] + \frac{\partial}{\partial x}\left[(1-\nu_s)\rho_g U_g(e_g+\frac{P}{\rho_g}+\frac{U_g^2}{2})\right]$$

$$= \rho_s(\frac{S_{b_t}}{A_p})\frac{\nu_s r_b}{\int_0^{L_p}\nu_s dx} W - \frac{2h_i}{R}(T-T_{w,i})$$

Put $U_g = U$ and $h_g = e_g + \frac{P}{\rho_g}$,

$$\frac{\partial}{\partial t}\left[(1-\nu_s)\rho_g(h_g-\frac{P}{\rho_g})\right] + \frac{\partial}{\partial x}\left[(1-\nu_s)\rho_g h_g U\right] + \tfrac{1}{2}\frac{\partial}{\partial t}\left[(1-\nu_s)\rho_g U^2\right]$$

$$+ \tfrac{1}{2}\frac{\partial}{\partial x}\left[\{(1-\nu_s)\rho_g U\}U^2\right] = \rho_s \dot{v}_{d_s} W$$

$$- \frac{2h_i}{R}(T-T_{w,i})$$

Using equations (A.10) and (A.12):

$$\frac{\partial}{\partial t}\left[(1-\nu_s)\rho_g h_g\right] + \frac{\partial}{\partial x}\left[(1-\nu_s)\rho_g h_g U\right] - \frac{\partial}{\partial t}\left[(1-\nu_s)P\right] + \rho_s \dot{v}_{d_s}\frac{U^2}{2}$$

$$+ U\left[-\rho_s \dot{v}_{d_s} U - (1-\nu_s)\frac{\partial P}{\partial x} - \frac{2\tau_w}{R}\right] = \rho_s \dot{v}_{d_s} W$$

$$- \frac{2h_i}{R}(T-T_{w,i})$$

Using equation (A.9):

$$\frac{\partial}{\partial t}\left[(1-\nu_s)\rho_g h_g\right] + \frac{\partial}{\partial x}\left[(1-\nu_s)\rho_g h_g U\right] - (1-\nu_s)\left[\frac{\partial P}{\partial t} + U\frac{\partial P}{\partial x}\right]$$

$$= \rho_s \dot{v}_{d_s}\left(W + \frac{P}{\rho_s} + \frac{U^2}{2}\right) - \frac{2h_i}{R}(T-T_{w,i}) + \frac{2\tau_w U}{R}$$

or,

$$(1-\nu_s)\rho_g\left[\frac{\partial h_g}{\partial t} + U\frac{\partial h_g}{\partial x}\right] + h_g\left[\frac{\partial}{\partial t}\left\{(1-\nu_s)\rho_g\right\} + \frac{\partial}{\partial x}\left\{(1-\nu_s)\rho_g U\right\}\right]$$

$$- (1-\nu_s)\left[\frac{\partial P}{\partial t} + U\frac{\partial P}{\partial x}\right] = \rho_s \dot{v}_{d_s}\left(W + \frac{P}{\rho_s} + \frac{U^2}{2}\right)$$

$$- \frac{2h_i}{R}(T-T_{w,i}) + \frac{2\tau_w}{R}U$$

Using equation (A.10) and notation $\frac{D}{Dt} = \frac{\partial}{\partial t} + U\frac{\partial}{\partial x}$, finally :

$$(1-\nu_s)\rho_g \frac{Dh_g}{Dt} - (1-\nu_s)\frac{DP}{Dt} = \rho_s \dot{v}_{d_s} \left(W + \frac{P}{\rho_s} + \frac{U^2}{2} - h_g\right)$$

$$- \frac{2h_i}{R}(T-T_{w,i}) + \frac{2\tau_w}{R} U \qquad (A.13)$$

Computation of Burning Surface

A typical solid particle, a single perforated cylinder in shape, is shown in Figure 38.

Let,

r_i = initial inner radius of the particle

r_o = initial outer radius of the particle

l = length of the particle

n = total number of the particles in the chamber

Therefore, total initial burning surface = $2\pi(r_i+r_o)\, l\, n$. It is assumed that combustion gas is produced from both inner and outer cylindrical surfaces of a particle but not from two ends. If r_b is the linear speed of burning, which is assumed to be same for all the particles at a particular instant, the total burning surface after time Δt is

$$2\pi \left[(r_i+r_b\,\Delta t) + (r_o-r_b\,\Delta t)\right] \; l\, n$$

$$= 2\pi\,(r_i+r_o) l\, n$$

Therefore, it is clear that for hollow cylindrical particles the total burning surface is constant and can be given by :

$$S_{b_t} = \frac{2\pi(r_o^2 - r_i^2) l \, n \, \rho_s}{\rho_s (r_o - r_i)}$$

$$= \frac{2m_{s_i}}{\rho_s w_{s_i}} \qquad (A.14)$$

where

m_{s_i} = initial mass of solids

ρ_s = solid mass density

w_{s_i} = initial web thickness of a solid particle

Expressions for Enthalpies of Solids and Gases

For any pure substance, $h = h(P,T)$

$$dh = \left(\frac{\partial h}{\partial P}\right)_T dP + \left(\frac{\partial h}{\partial T}\right)_P dT \qquad (A.15)$$

From thermodynamics, $dh = Tds + vdP$

$$\left(\frac{\partial h}{\partial P}\right)_T = T\left(\frac{\partial s}{\partial P}\right)_T + v \qquad (A.16)$$

Again from Gibb's form of first law of thermodynamics,

$$dG = - s \, dT + v \, dP \qquad (A.17)$$

As Gibb's function G is a property of the system, dG must be an exact differential

$$\therefore \quad \left(\frac{\partial s}{\partial P}\right)_T = -\left(\frac{\partial v}{\partial T}\right)_P \tag{A.18}$$

Now, coefficient of thermal expansion, $\beta = \frac{1}{v}\left(\frac{\partial v}{\partial T}\right)_P$

$\therefore$ Equation (A.16) becomes,

$$\left(\frac{\partial h}{\partial P}\right)_T = -T\beta v + v = v(1-T\beta)$$

$\therefore$ Equation (A.15) becomes,

$$dh = v(1-T\beta)\, dP + c_p\, dT \tag{A.19}$$

Solids

For solids, c_p is equal to c_s and it has been assumed that the temperature of the solids T_s remains constant throughout the period of burning

$$\therefore \quad dh_s = \frac{1}{\rho_s}(1-T_s\beta_s)\, dP$$

It has also been assumed that the coefficient of expansion for solids β_s is negligible.

$$\therefore \quad dh_s = \frac{dP}{\rho_s} \tag{A.20}$$

$$\text{and} \quad h_s = c_s T_s + \frac{P}{\rho_s} \tag{A.21}$$

Gases

The equation of state for the combustion gas at high pressure can be taken as,

$$P(v_g - \eta) = R_g T \tag{A.22}$$

where, the covolume η is a constant.

Now,

$$P\left(\frac{\partial v_g}{\partial T}\right)_P = R_g$$

$$\therefore \beta_g = \frac{1}{v_g}\left(\frac{\partial v_g}{\partial T}\right)_P = \frac{R_g}{v_g P}$$

From equation (A.19):

$$dh_g = v_g\left[1 - \frac{R_g T}{v_g P}\right] dP + c_p\, dT$$

or,

$$dh_g = \eta\, dP + c_p\, dT \tag{A.23}$$

Now, the specific heat at constant pressure, $c_p = \frac{\gamma}{\gamma-1} R_g$

$$\therefore dh_g = \eta\, dP + \frac{\gamma}{\gamma-1} R_g\, dT \tag{A.24}$$

Differentiating equation (A.22) and using $v_g = 1/\rho_g$:

$$R_g\, dT = \left(\frac{1}{\rho_g} - \eta\right) dP - \frac{P}{\rho_g^2}\, d\rho_g$$

Equation (A.24) becomes,

$$dh_g = \frac{(\gamma-\eta\rho_g)}{\rho_g(\gamma-1)}\ dP - \frac{\gamma P}{(\gamma-1)\rho_g^2}\ d\rho_g \qquad (A.25)$$

From equation (A.23),

$$h_g = \eta\ P + c_p\ T$$

$$= \eta\ P + \frac{\gamma}{(\gamma-1)}\ P\ (\frac{1}{\rho_g} - \eta)$$

$$= \frac{(\gamma-\eta\rho_g)}{(\gamma-1)\rho_g}\ P \qquad (A.26)$$

APPENDIX B

Derivation of Boundary Layer Momentum Equation

With reference to Figure 39, the boundary layer momentum integral equation is derived as follows:

Equation of Continuity

Rate of increase of mass in c.v. = Rate of mass flow into the c.v. through surface AB − Rate of mass flow out through surface CD + Rate of mass flow into the c.v. through surface BC

$$\frac{\partial}{\partial t}\int_{R-\delta}^{R} 2\pi r\,\Delta x\,\rho\,dr = \left[\int_{R-\delta}^{R} 2\pi r\,\rho\,u\,dr\right]\Bigg|_{x} - \left[\int_{R-\delta}^{R} 2\pi r\,\rho\,u\,dr\right]\Bigg|_{x+dx} + \dot{m}_{BC} \tag{B.1}$$

Momentum Equation (x-directional)

Rate of increase of momentum in c.v. − Momentum flux in + Momentum flux out = $\sum$ External forces

$$\frac{\partial}{\partial t}\int_{R-\delta}^{R} 2\pi r\,\Delta x\,\rho\,u\,dr - \dot{m}_{BC}\,U_{\infty} - \left[\int_{R-\delta}^{R} 2\pi r\,\rho\,u^{2}\,dr\right]\Bigg|_{x} + \left[\int_{R-\delta}^{R} 2\pi r\,\rho\,u^{2}dr\right]\Bigg|_{x+dx}$$

$$= \left[\int_{R-\delta}^{R} 2\pi r\,P\,dr\right]\Bigg|_{x} - \left[\int_{R-\delta}^{R} 2\pi r\,P\,dr\right]\Bigg|_{x+dx}$$

$$+ 2\pi(R-\delta)\left(\frac{\partial\delta}{\partial x}\Delta x\right)P - 2\pi R\,\Delta x\,\tau_{w} \tag{B.2}$$

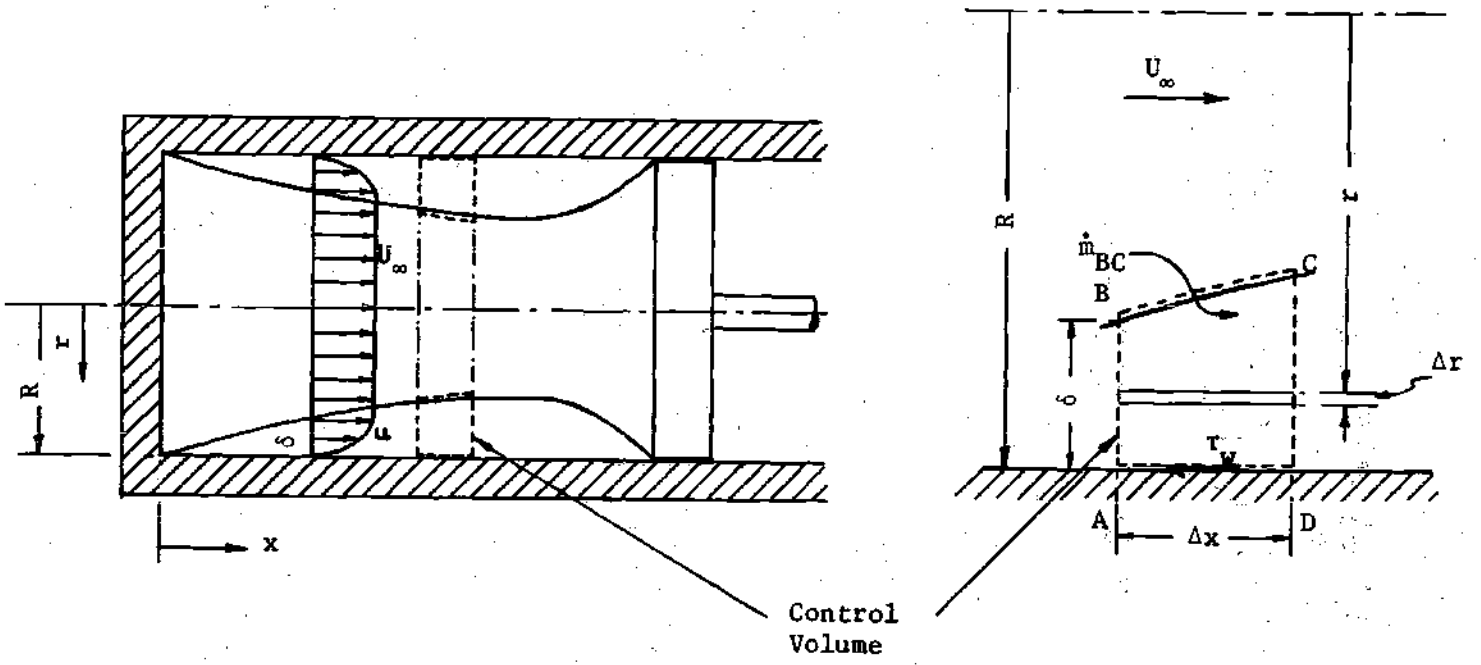

Figure 39. Schematic of Boundary Layer Growth in a Tube With a Sliding Piston at one End.

Using the expression for $\dot{m}_{BC}$ from equation (B.1), equation (B.2) becomes,

$$\frac{\partial}{\partial t}\int_{R-\delta}^{R}(\rho u\, r)dr - U_\infty \frac{\partial}{\partial t}\int_{R-\delta}^{R}(\rho r)dr - U_\infty \frac{\partial}{\partial x}\int_{R-\delta}^{R}(\rho u\, r)dr + \int_{R-\delta}^{R}(\rho u^2 r)dr$$
$$= -\frac{\partial}{\partial x}\int_{R-\delta}^{R}(P\, r)dr + (R-\delta)P\frac{\partial \delta}{\partial x} - \tau_w R \qquad (B.3)$$

Now, for thin boundary layer, radial component of velocity is very small and consequently,

$$\frac{\partial P}{\partial r} \simeq 0 \qquad (B.4)$$

Also, as $U_\infty \neq f(r)$,

$$\frac{\partial}{\partial t}\int_{R-\delta}^{R} U_\infty \rho r\, dr = U_\infty \frac{\partial}{\partial t}\int_{R-\delta}^{R}\rho r\, dr + \left[\int_{R-\delta}^{R}\rho r\, dr\right]\frac{\partial U_\infty}{\partial t} \qquad (B.5)$$

and

$$\frac{\partial}{\partial x}\int_{R-\delta}^{R} U_\infty(\rho u r)dr = U_\infty \frac{\partial}{\partial x}\int_{R-\delta}^{R}\rho u r\, dr + \left[\int_{R-\delta}^{R}\rho u r\, dr\right]\frac{\partial U_\infty}{\partial x} \qquad (B.6)$$

Using relations (B.4), (B.5), (B.6) finally:

$$\frac{\partial}{\partial t}\int_{R-\delta}^{R}\rho(U_\infty - u)r\, dr + \frac{\partial}{\partial x}\int_{R-\delta}^{R}\rho u(U_\infty - u)r\, dr - \left[\int_{R-\delta}^{R}\rho r\, dr\right]\frac{\partial U_\infty}{\partial t}$$
$$-\left[\int_{R-\delta}^{R}\rho u r\, dr\right]\frac{\partial U_\infty}{\partial x} = \left[\int_{R-\delta}^{R} r\, dr\right]\frac{\partial P}{\partial x} + \tau_w R \qquad (B.7)$$

now,

$$\int_{R-\delta}^{R} r\, dr = R\delta - \frac{\delta^2}{2}$$

and using ρ_f, i.e. gas density corresponding to the film temperature, as the average density in the boundary layer, the equation (B.7) becomes,

$$\frac{\partial}{\partial t}\int_{R-\delta}^{R}\rho(U_\infty-u)r\, dr + \frac{\partial}{\partial x}\int_{R-\delta}^{R}\rho u(U_\infty-u)r\, dr + \left[\int_{R-\delta}^{R}\rho(U_\infty-u)r\, dr\right]\frac{\partial U_\infty}{\partial x}$$
$$= (R\delta - \frac{\delta^2}{2})\left[\frac{\partial P}{\partial x} + \rho_f\frac{\partial U_\infty}{\partial t} + \rho_f U_\infty\frac{\partial U_\infty}{\partial x}\right] + \tau_w R \qquad (B.8)$$

The equation (B-8) is the required momentum integral equation for a nonsteady, nonuniform, and developing compressible flow in a tube.

APPENDIX C

Flow Chart for the Computer Program

Main Program

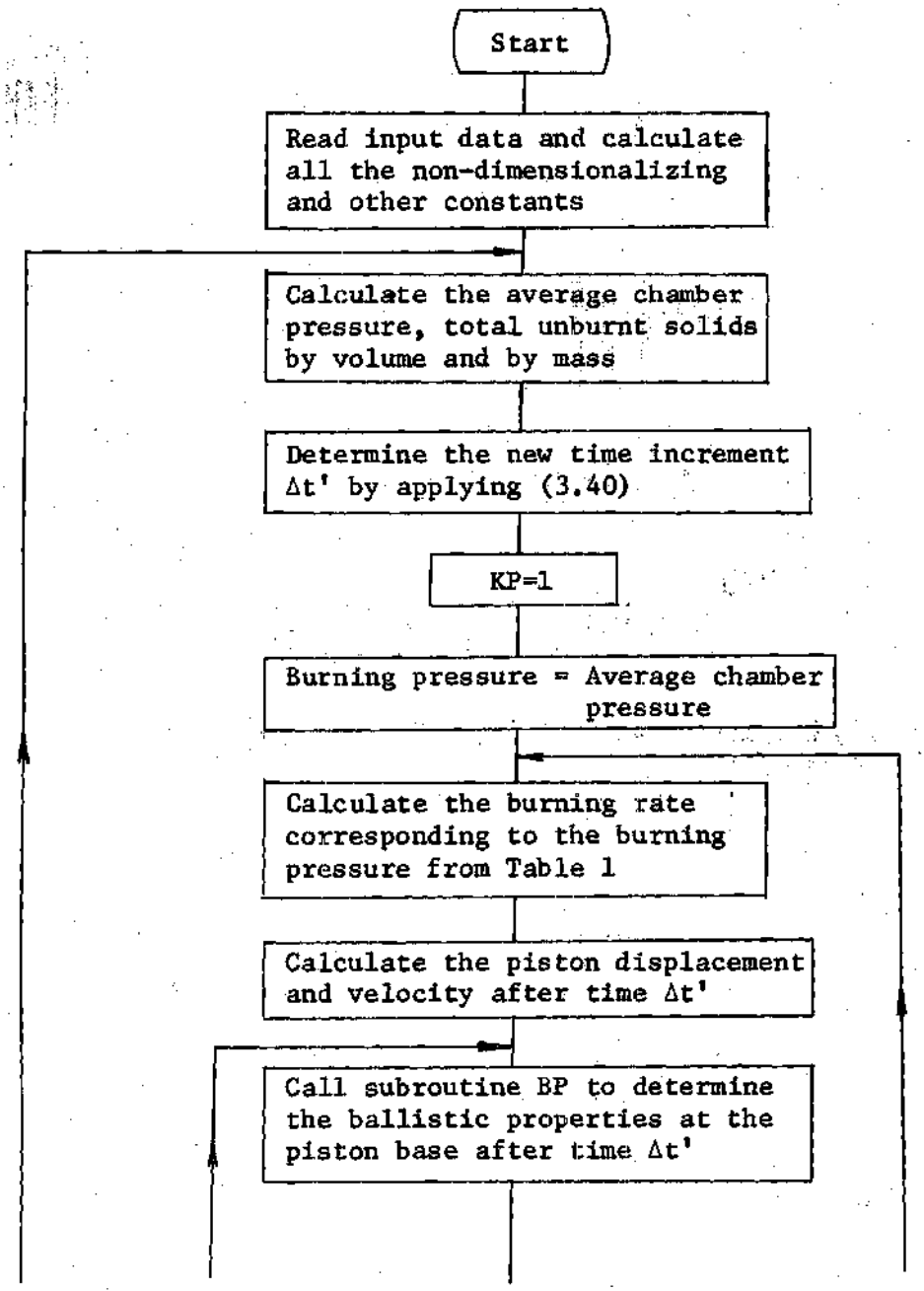

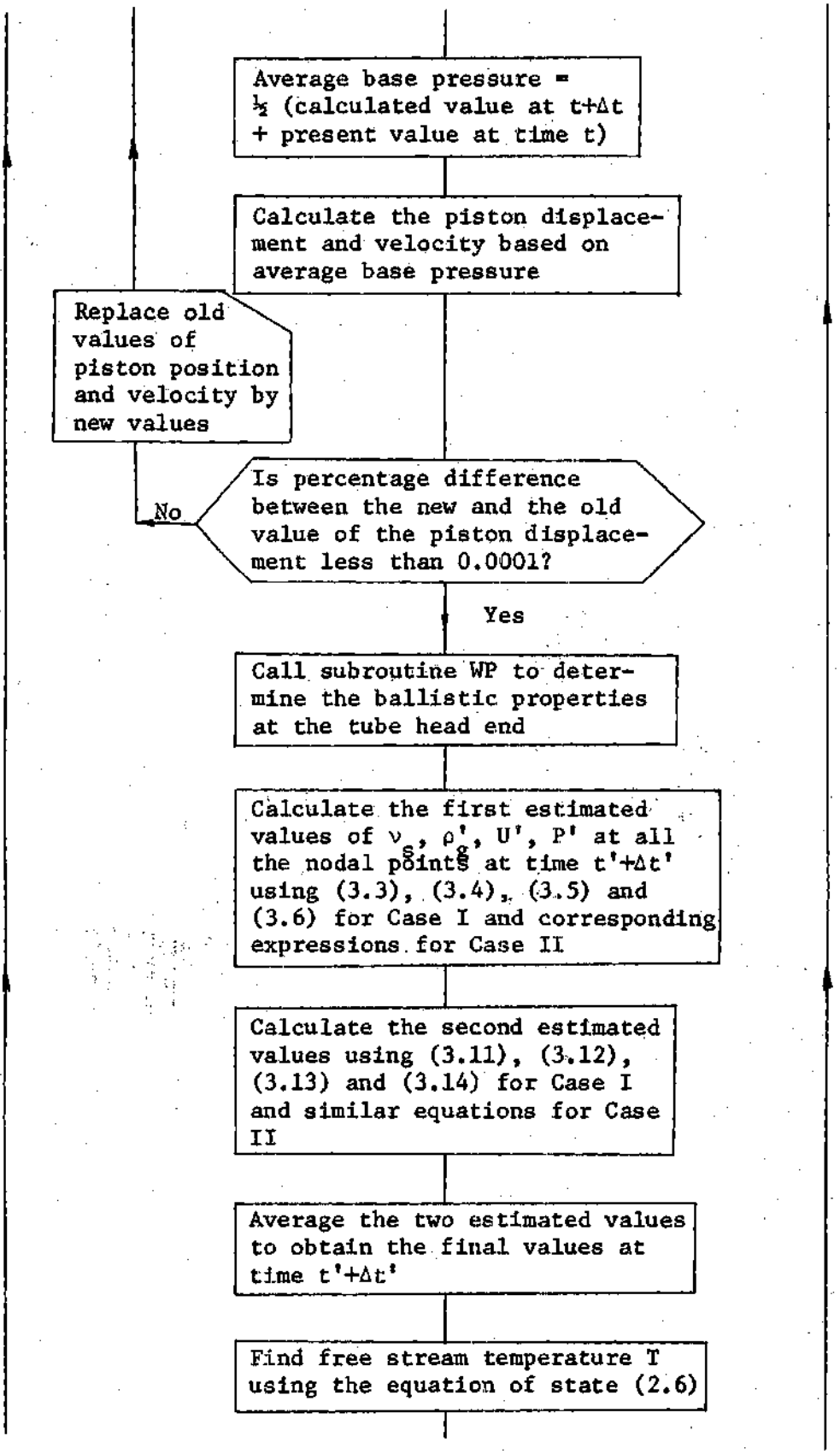
Average base pressure = ½ (calculated value at t+Δt + present value at time t)
Calculate the piston displacement and velocity based on average base pressure
Replace old values of piston position and velocity by new values
No
Is percentage difference between the new and the old value of the piston displacement less than 0.0001?
Yes
Call subroutine WP to determine the ballistic properties at the tube head end
Calculate the first estimated values of ν_g, ρ', U', P' at all the nodal points at time t'+Δt' using (3.3), (3.4), (3.5) and (3.6) for Case I and corresponding expressions for Case II
Calculate the second estimated values using (3.11), (3.12), (3.13) and (3.14) for Case I and similar equations for Case II
Average the two estimated values to obtain the final values at time t'+Δt'
Find free stream temperature T using the equation of state (2.6)

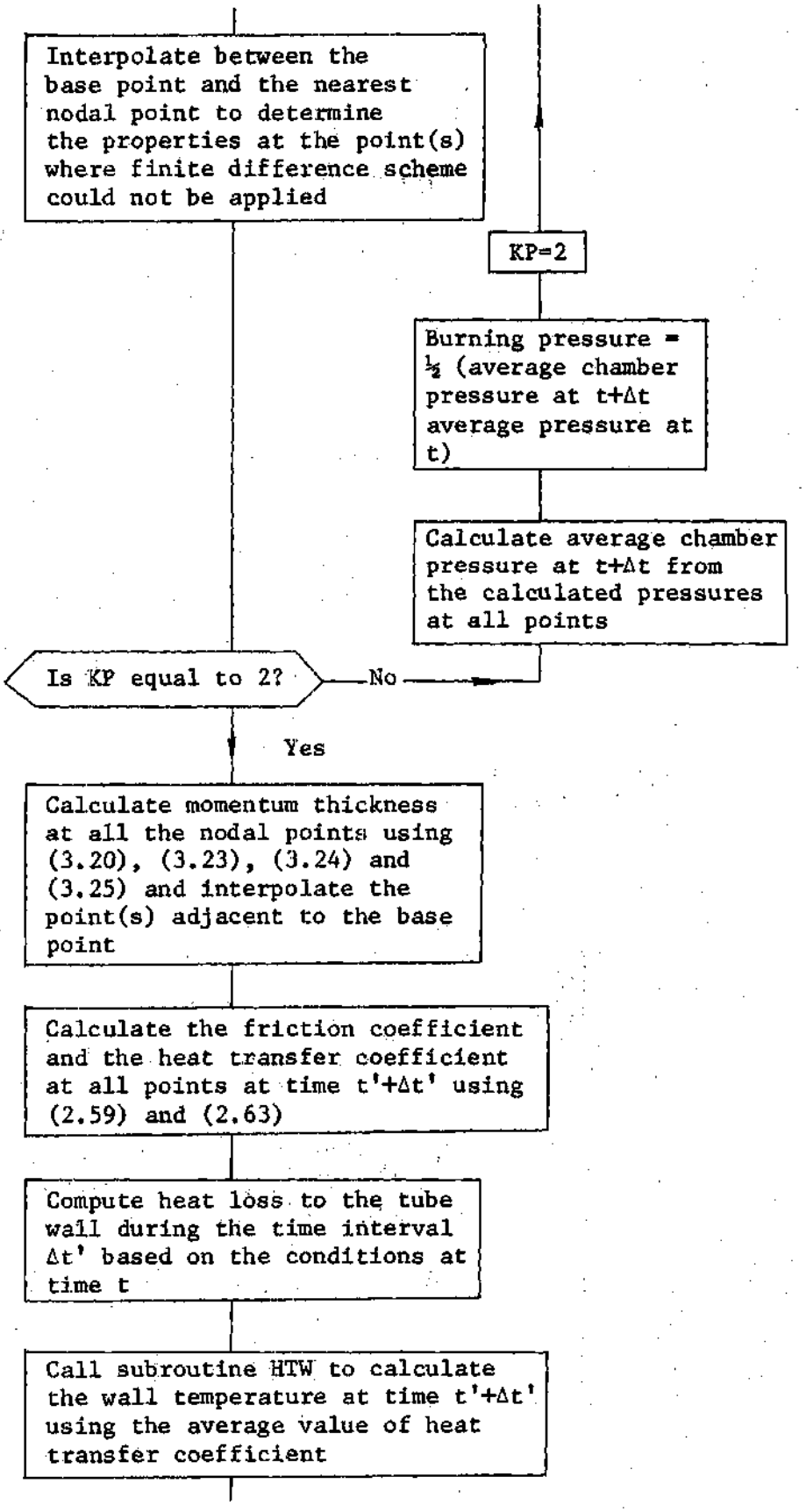
Interpolate between the base point and the nearest nodal point to determine the properties at the point(s) where finite difference scheme could not be applied
KP=2
Burning pressure = ½ (average chamber pressure at t+Δt average pressure at t)
Calculate average chamber pressure at t+Δt from the calculated pressures at all points
Is KP equal to 2?
No
Yes
Calculate momentum thickness at all the nodal points using (3.20), (3.23), (3.24) and (3.25) and interpolate the point(s) adjacent to the base point
Calculate the friction coefficient and the heat transfer coefficient at all points at time t'+Δt' using (2.59) and (2.63)
Compute heat loss to the tube wall during the time interval Δt' based on the conditions at time t
Call subroutine HTW to calculate the wall temperature at time t'+Δt' using the average value of heat transfer coefficient

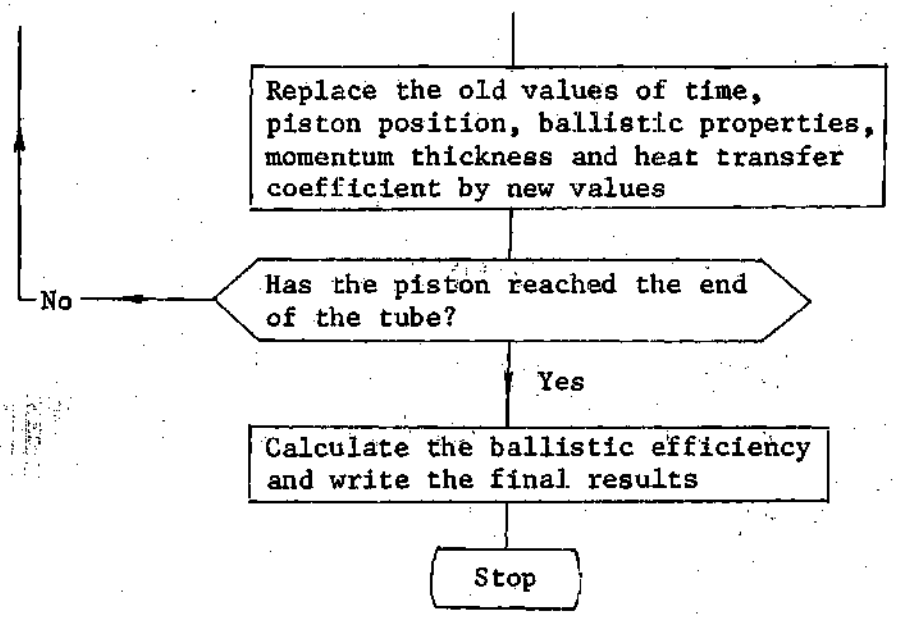
Replace the old values of time, piston position, ballistic properties, momentum thickness and heat transfer coefficient by new values
Has the piston reached the end of the tube?
No
Yes
Calculate the ballistic efficiency and write the final results
Stop

Subroutine BP

The purpose of the subroutine is to calculate the ballistic properties at the piston base at time t'+Δt' knowing the properties at all the points at time t', and the velocity and the position of the piston at time t'+Δt'. The following flow diagram should be read along with Figure 3.

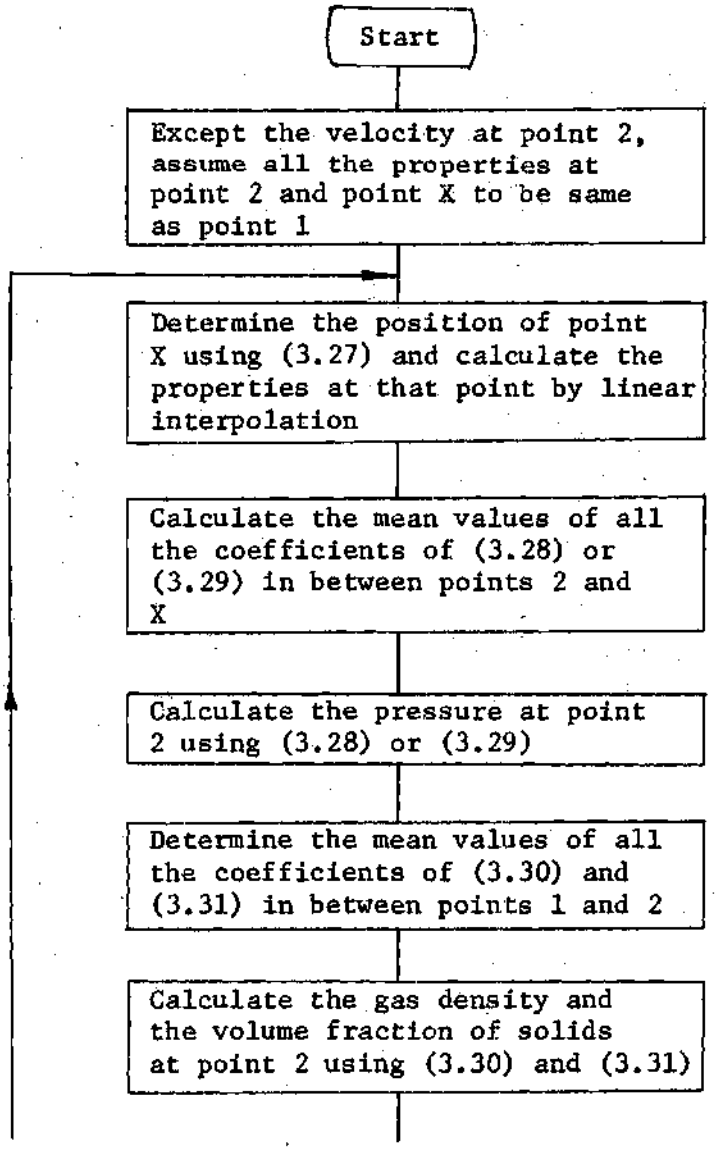

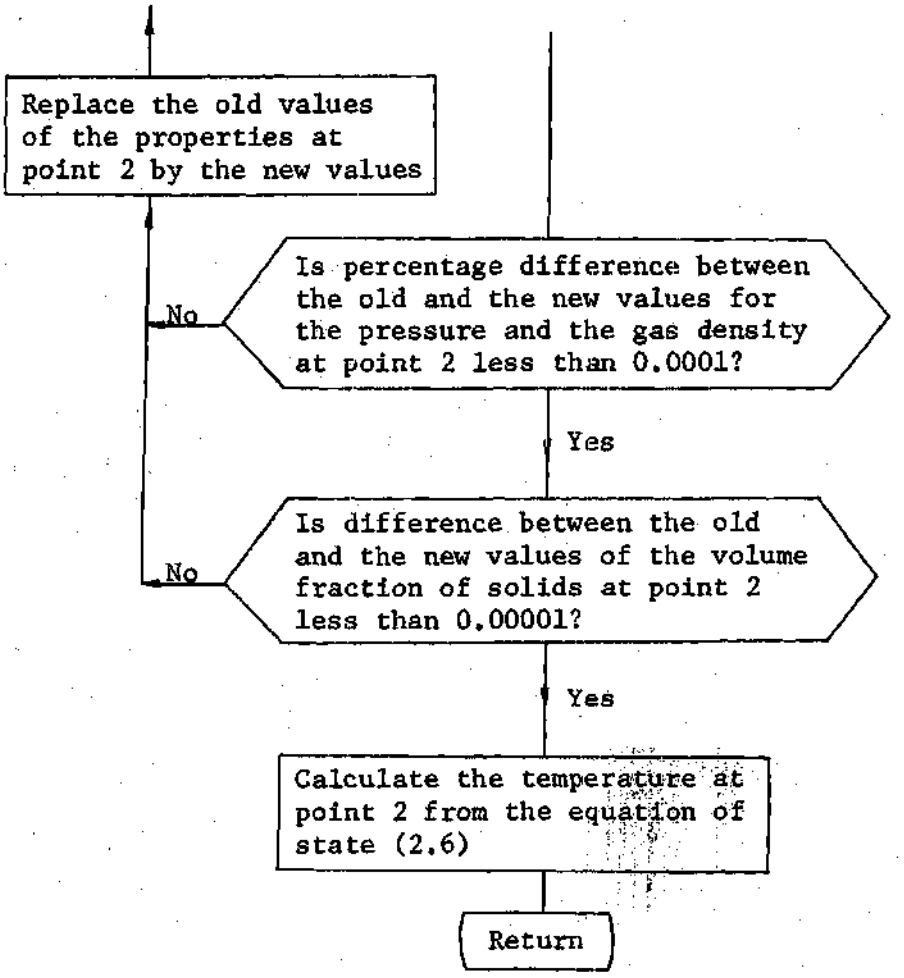
Replace the old values of the properties at point 2 by the new values
Is percentage difference between the old and the new values for the pressure and the gas density at point 2 less than 0.0001?
No
Yes
Is difference between the old and the new values of the volume fraction of solids at point 2 less than 0.00001?
No
Yes
Calculate the temperature at point 2 from the equation of state (2.6)
Return

Subroutine WP

This subroutine is called to calculate the properties at the tube head end at time $t'+\Delta t'$. The logic is same as that for subroutine BP and the flow diagram should also be read along with Figure 3.

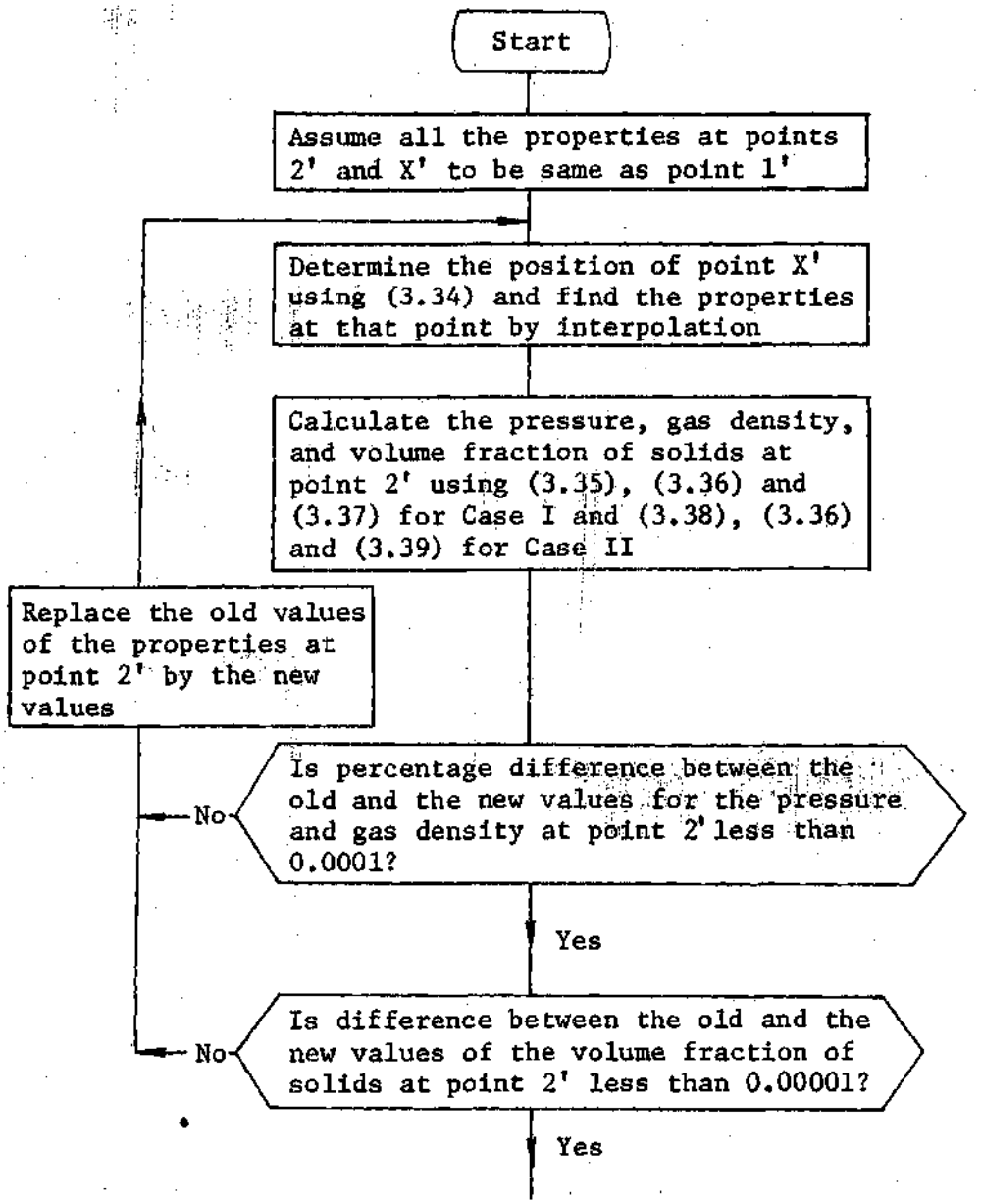

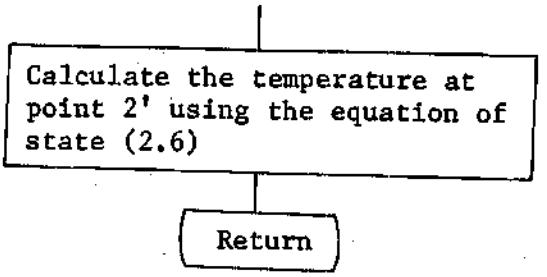
Calculate the temperature at point 2' using the equation of state (2.6)
Return

Subroutine HTW

The purpose of the subroutine is to calculate the wall temperature at a particular station along the length of the tube at time $t+\Delta t$, knowing the temperature distribution at the present time t, and the mean heat transfer coefficient h_m over the time interval Δt. In the following flow diagram, Δt is the time step selected in the main program whereas $\Delta\bar{t}$ is the time step selected in accordance with the stability condition for the temperature calculation.

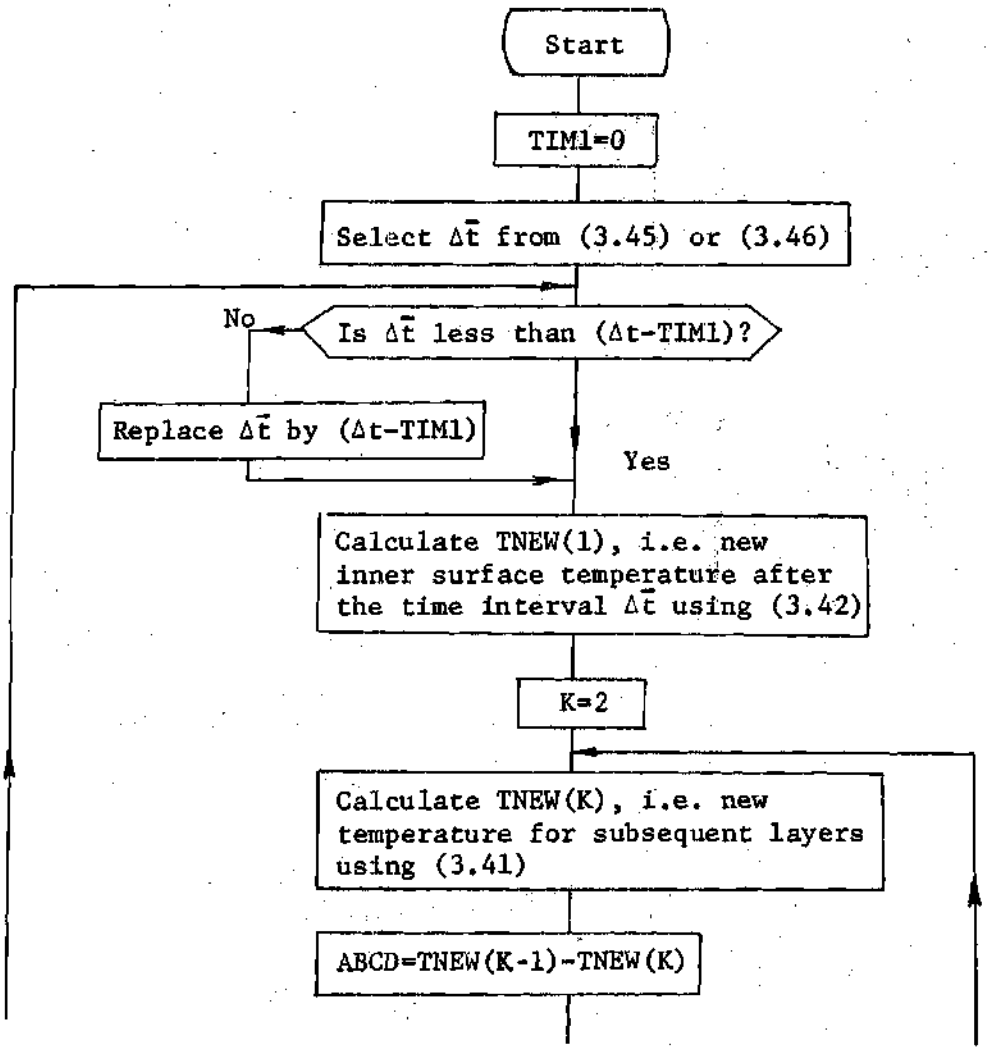

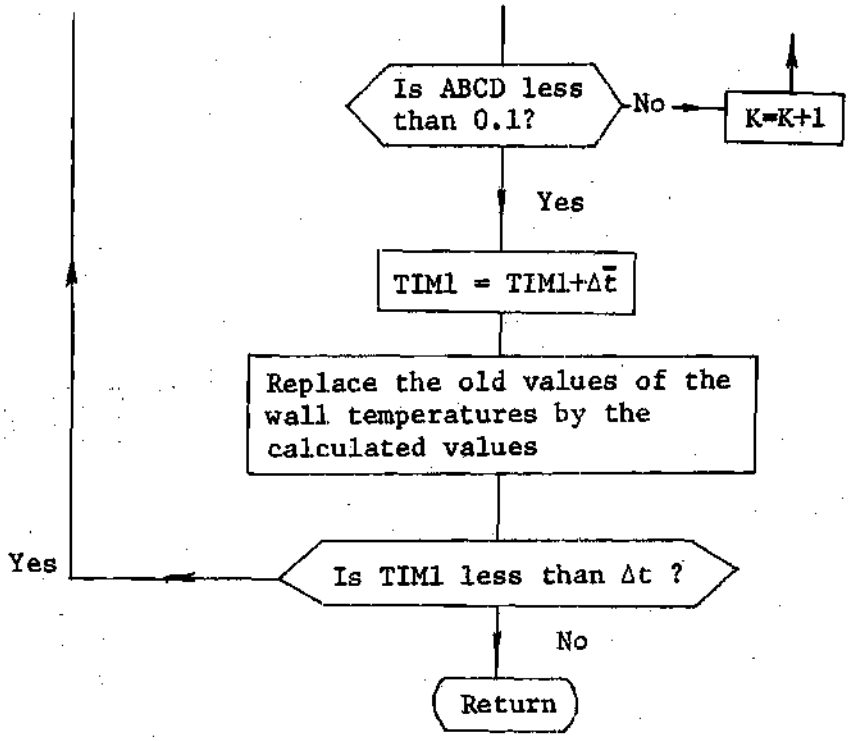
Is ABCD less than 0.1?
No
K=K+1
Yes
TIM1 = TIM1+Δt̄
Replace the old values of the wall temperatures by the calculated values
Yes
Is TIM1 less than Δt ?
No
Return

BIBLIOGRAPHY

1. Hunt, F. R. W. ed., Internal Ballistics, Philosophical Library, New York, 1951.

2. Corner, J. Theory of the Interior Ballistics of Guns, John Wiley & Sons, Inc., New York, 1950.

3. Brode, H. L. and Enstrom, J. E. "A Numerical Method for Calculating Interior Ballistics," AD-712-846, The RAND Corporation, Snata Monica, California, September 1970.

4. Love, A. E. H. and Pidduck, F. B., "The Lagrange Ballistic Problem," Philosophical Transaction of Royal Society (London), 222A, 1921-22, pp. 167.

5. Carriere, P., "The Method of Characteristics Applied to the Problem of Internal Ballistics," Proceedings of 7th International Congress of Applied Mechanics, London, 1948, pp. 139.

6. Ludwieg, H. and Tillmann, W., "Investigations of the Wall Shearing Stress in Turbulent Boundary Layers," NACA Technical Memorandum 1285, 1950.

7. Colburn, A. P., "A Method of Correlating Forced Convection Data and A Comparison with Fluid Friction," Transaction-American Institute of Chemical Engineers, 1933, pp. 174.

8. Vincenti, W. G. and Kruger, C. H., Introduction to Physical Gas Dynamics, John Wiley and Sons, Inc., New York, 1965, pp. 300-305.

9. Bergles, A. E., "Survey and Evaluation of Techniques to Augment Convective Heat and Mass Transfer," Progress in Heat and Mass Transfer, Vol. 1, Pergamon Press, Oxford and New York, 1969, pp. 405-406.

10. Tien, C. L., "Heat Transfer by a Turbulently Flowing Fluid-Solids Mixture in a Pipe," Journal of Heat Transfer, Transaction of the ASME, May 1961, pp. 183-188.

11. Depew, C. A. and Farber, L., "Heat Transfer to Pneumatically Conveyed Glass Particles of Fixed Size," Journal of Heat Transfer, Transaction of the ASME, May 1963, pp. 164-172.

12. Simpson, A. V., et. al., "Heat and Mass Transfer in Dispersed, Two-Phase, Single-Component Flow," International Journal of Heat and Mass Transfer, Vol. 12, Pergamon Press, Oxford, 1969, pp. 1141-1155.

13. Reshotko, E. and Tucker, M., "Approximate Calculation of the Compressible Turbulent Boundary Layer with Heat Transfer and Arbitrary Pressure Gradient," NACA TN-4154, 1957.

14. Reynolds, W. C., "A Morphology of the Prediction Methods," Proceedings-Computation of Turbulent Boundary Layer-1968, AFOSR-IFP-STANFORD Conference, Vol. I, pp. 1-15.

15. Eckert, E. R. G. and Drake, R. M. Jr., Heat and Mass Transfer, 2nd ed., McGraw-Hill Book Company, Inc., 1959, pp. 31-32.

16. Lomax, H., "An Analysis of Finite Difference Technique Applied to Equation Governing Convective Transfer," Analytical Methods in Aircraft Aerodynamics, NASA SP-228, 1970, pp. 245-264.

17. Richtmyer, R. D. and Morton, K. W., Difference Methods for Initial Value Problem; 2nd ed., Chapter 12, Interscience Publishers (a division of John Wiley and Sons, Inc.), New York, 1967.

18. Holman, J. P., Heat Transfer, McGraw-Hill Book Company, Inc., New York, 1968, pp. 98-103.

19. Schneider, P. J., Conduction Heat Transfer, Chapter 12, Addison-Wesley Publishing Company, Inc., Massachusetts, 1955.

20. Private Communication, O. K. Heiney, AFATL (ATDG), Eglin Air Force Base, Florida.

21. Schlichting, H., Boundary Layer Theory, 6th ed., McGraw-Hill Book Company, Inc., New York, 1968.

22. Bartz, D. R., "An Approximate Solution of Compressible Turbulent Boundary Layer Development and Convective Heat Transfer in Convergent Divergent Nozzles," Transaction of the ASME, Vol. 77, No. 8, 1955, pp. 1235-1245.

23. Kays, W. M., Convective Heat and Mass Transfer, McGraw-Hill Book Company, Inc., New York, 1966, pp. 95.

24. Daily, J. W. and Harleman, D. R. F., Fluid Dynamics, Addison-Wesley Publishing Company, Inc., Reading, Massachusetts, 1966, pp. 252.

25. Dahm, T. J. and Anderson, L. W., "Propellant Gas Convective Heat Transfer in Gun Barrels," Aerotherm Project 7028, Aerotherm Corporation, California, August 1970.